Electrical Impedance Tomography of Fast Neural Activity In The Brain

Anthony Ghosh

Supervisors:

Professor David S. Holder

Mr. Andrew McEvoy

Submitted for the degree of MD(Res)

Department of Medical Physics and Bioengineering

University College London

2015

Declaration

I, Anthony Ghosh, confirm that the work presented in this thesis is my own. Where information has been derived from other sources, I confirm that this has been indicated in the thesis.

_____ _____

Signature Date

Acknowledgements

This thesis was possible through the support of a number of people who I would like to express my sincere gratitude to. Firstly I am grateful to my primary supervisor, Professor David Holder, for the opportunity to work on this project and for his support, guidance and optimism, which kept me motivated throughout the entire project. I am grateful to Mr. Andrew McEvoy as my second supervisor for his operative teaching, which helped with the animal preparation I undertook.

I am especially grateful to Dr Dong In Oh, for his expertise and patience in preparing and helping me understand the hardware during the experiments. The experiments would not have been possible without him. I Cannot thank enough Dr. Ori Gilad, for the endless hours of data analysis and helping me understand the sophisticated codes written in Matlab to reconstruct the images. I am also grateful to Dr. Oh and Dr Gilad for their friendship.

I would also like to thank Brett Packham for his work and efforts towards the statistical analysis in this project and for his continuation project thereafter.

Finally I am grateful to my partner, Hayley Rose, my parents and my two daughters, Daisy and Arianna: without their love and support none of this would have been possible.

Abstract

Electrical impedance tomography (EIT) is a recently developed imaging method that can be used to reconstruct the internal conductivity of a body from boundary measurements. A proposed application of EIT within head imaging is functional brain imaging. The work of this thesis was aimed specifically at producing images of fast neuronal depolarisation in the brain.

Chapter 1 is a review of other brain imaging techniques, the principles of EIT and bioimpedance and nerve physiology. Chapter 2 was a study to verify previous work on measuring the impedance change in unmyelinated crab nerves using a DC carrier. Chapter 3 was a study aimed at using a low frequency sinusoidal wave carrier to do the same and in chapter 4 the same carrier was used to measure the impedance change during evoked responses on the anaesthetised rat cerebral cortex and identify the optimum frequency and current to be used to reconstruct images. Chapter 5 details experiments to image fast neuronal activity in rat cerebral cortex of different evoked sensory modalities (vibrissae, forepaw, hindpaw sensation and visual responses) using the above carrier.

Publications and presentations resulting from this thesis

In peer-reviewed journals

Gilad O, **Ghosh A**, Oh D, Holder S. A method for recording resistance changes non-invasively during neuronal depolarization with a view to imaging brain activity with electrical impedance tomography. *J Neurosci Methods (2009),* doi:10.1016/j.jneumeth.2009.03.012

Oh D, Gilad O, **Ghosh A**, Shuettler M, Holder D. A novel method for recording neuronal depolarization with recording at 125–825 Hz: implications for imaging fast neural activity in the brain with electrical impedance tomography. Med Biol Eng Comput (2011) 49:593–604

In Peer-Reviewed conference proceedings

Gilad O, Oh D, **Ghosh A**, McEvoy AW, Akselrod S and Holder DS (2008) Imaging neuronal depolarization in the brain with Electrical or Magnetic Detection Impedance Tomography : a review of experimental studies *Proc. of IX Int. Conf. on Electrical Impedance Tomography, Dartmouth, USA*, pp 9-12. http://engineering.dartmouth.edu/eit2008/EIT_Conference_2008.pdf

Oh D, Gilad O, **Ghosh A** and Holder DS. (2008) Analytic correction for the square wave carrier in low frequency Electrical Impedance Tomography of neuronal depolarization. *Proc. of IX Int. Conf. on Electrical Impedance Tomography, Dartmouth, USA*, pp 5-8. Available: http://engineering.dartmouth.edu/eit2008/EIT_Conference_2008.pdf

Additional conference presentations and posters

Ghosh A, Gilad O, Oh D, Packham B, McEvoy AW, Holder DS (2014). Imaging neuronal activity using intracranial electrodes and electrical impedance tomography (EIT). The British Neurosurgical Research Group Meeting, Liverpool, March 2014.

Oh D, Gilad O, **Ghosh A**, Koo H, Holder DS (2010). Imaging fast neural activity in the brain with Electrical Impedance Tomography using a low frequency applied current : method and validation during the compound action potential in the walking leg nerve of the edible crab, Cancer pagurus. XIV *International Conference on Electrical Bioimpedance & 11th International Conference on Biomedical Applications of Electrical Impedance Tomography, Gainesville, Florida, April 2010.*

Ghosh A, Gilad O, Oh D, Schuettler M, Packham B, Holder DS (2010). Imaging fast neural activity in the brain with Electrical Impedance Tomography using a low frequency sinusoidal applied current : single channel measurements during somatosensory evoked potentials with epicortical electrodes in the rat brain. XIV *International Conference on Electrical Bioimpedance & 11th International*

Conference on Biomedical Applications of Electrical Impedance Tomography, Gainesville, Florida, April 2010.

Gilad O, Oh D, **Ghosh A**, McEvoy A and Holder DS (2007) Towards imaging neuronal activity using intracranial electrodes and low frequency electrical impedance tomography (LFEIT). *Theoretical Neuroscience Network meeting on invasive intracranial electrophysiology of the human brain: "non-clinical" studies in epilepsy patients, KCL, London, UK*

Contents

List of Figures

List of tables

1. Introduction

1.1 Overview

Functional neuroimaging has improved greatly in the past two decades but the 'holy grail' would be to image neuronal activity with a time and spatial resolution of about 1 ms and 1 mm respectively. This has not been achieved yet with any approach. Electrical impedance Tomography (EIT) is a medical imaging method in progress, which has the potential to achieve this goal. The principle is that impedance to electricity changes over milliseconds when neuronal ion channels open during activity. Hence these changes can be imaged with EIT. These changes in the cerebral cortex have previously been estimated to be about 1%, provided they are measures with applied current of under 100Hz, when using Cable theory modeling and previous animal studies. The purpose of this thesis was to determine if such changes could be reproducibly recorded on the cerebral cortex of anaesthetized rats and to image such changes.

This introductory chapter starts with a brief review of functional brain imaging modalities, with an emphasis on those potentially capable of imaging neuronal activity. This is followed by general background on EIT and a review of current knowledge on neuronal activity related impedance changes, previous measurement attempts and identifies important challenges that remain to be addressed.

In chapter 2, I present a study in which I measured the impedance changes to a 2Hz square wave current during action potentials in unmyelinated crab walking leg nerves. In the study I aimed to identify the effects of different current levels and spacing of current injection and recording electrodes on the impedance change, with a view to identifying the ideal current for recording on the anaesthetized rat cerebral cortex. This was attempted with an earlier set of experiments where there were technical issues with the longevity of the nerves and the aquisistion (appendix 1). Thus with an improved method and hardware the experiments were repeated in chapter 2.

Attempts were made to record impedance changes on the human scalp during visual evoked responses (VEP's) using a 2Hz square wave current as the carrier. A reproducible impedance change was unfortunately not seen. This was because the small estimated impedance change was obscured by uncorrelated noise, mainly the Electroencephalogram (EEG)(O Gilad & Holder 2009). Recording with a square wave 2Hz current had been used because modelling showed that this should produce the largest signal. Following this unsuccessful study, physicists in the group suggested that an increased signal-to-noise could be achieved by recording at higher frequencies of a few hundred Hz. Although

the signal was about 10 times lower, the ECoG was about 100 times lower, so this gave a much larger signal-to-noise ratio.

In chapter 3, I repeated the Crab nerve experiments described in chapter 2, using such sine wave currents as the carrier. Here I aimed to identify the ideal frequency, current level and electrode spacing combination for recording the impedance change during compound action potentials, with a view to using this carrier in recording the impedance change during neuronal activity on the cortex of the anaesthetized rat.

In Chapter 4, I repeated the rat experiments described in appendix 1 using the sine wave carriers described in chapter 3 to measure the impedance change during a sommatosensory evoked response (SSEP) on the cortex of anaesthetized rats. In these experiments I use different frequencies and current levels with a view to identify the ideal combination to use for imaging the neuronal depolarization in the brain of anaesthetized rats.

In Chapter 5, I present the experiments and recordings made to construct images of neuronal depolarization in the brain of anaesthetised rats using low frequency EIT.

1.2 Functional brain imaging

1.2.1 Imaging slow physiological changes

Several imaging techniques can be used to measure haemodynamic function of the brain with a time resolution limited by the physiological mechanisms which have a time constant of about 1 second. These methods image metabolic changes associated with the brain function such as blood flow, oxygenation, energy consumption and other metabolic processes. The main methods are tracer enhanced CT, Positron Emission Tomography (PET), Single Photon Emission Computerised Tomography (SPECT), functional Magnetic Resonance Imaging (fMRI), optical methods (Near Infra Red Spectroscopy (NIRS) Diffuse Optical Imaging (DOI) and Diffuse Optical Tomography (DOT)) and Electrical Impedance Tomography (EIT) sensitive to impedance changes related to blood volume changes and cell swelling (Table 1-1).

Table 1-1: Summary of haemodynamic brain imaging techniques

Method (source)	Spatial resolution	Temporal resolution	Limitations
Tracer CT (Konig, 2003)	1 mm	1 s	X-ray radiation + injection of contrast agent
PET (Robinson, 1999)	4 mm	~30 s	Very expensive, radioactive labelling required
SPECT (Brown, 1999)	7 mm	15 min	Radioactive labelling required
fMRI (Belliveau, 1991; Koretsky, 2004)	0.1–1 mm	1-5 s	Very expensive, not suitable for some patients
NIRS/DOI/DOT (Obrig, 2003; Mehta, 2004)	10-20 mm	0.1–60 s	Research only, cortical surface only
EIT (Tidswell, 2001)	10-20 mm	0.3 s	Research only

(Konig, 2003**,** Belliveau et al., 1991; Brown, Smallwood, Lawford, & Hose, 1999; Koretsky, 2004; Mehta, Jung, Flusberg, & Schnitzer, 2004; Obrig & Villringer, 2003; Robinson, Ferrie, Capra, & Maisey, 1999; Tidswell, Gibson, Bayford, & Holder, 2001)

1.2.2 Imaging fast physiological changes

Another family of imaging modalities focuses on non-invasive ways to image the neuronal activity itself with the highest possible spatial and temporal resolutions. At present, a technique producing reliable images with spatial resolution of about 1 mm and time resolution of about 1ms is not yet available.

Partial achievements have been demonstrated using inverse source modelling of recordings made using electro-encephalography (EEG) and magneto-encephalography (MEG) techniques and the multi-modality fusion of these methods with data from haemodynamic fMRI and anatomical MRI constraints.

Recent experimental methods include direct mapping of neuronal activity with MRI, Diffuse Optical Imaging (DOI), and the EIT variants, namely Low Frequency EIT (LF-EIT) and Magnetic Detection EIT (MD-EIT).

Finally, several invasive imaging methods have been developed. These techniques are important for animal models but could be rarely used on humans unless justified by specific clinical conditions such as pre-surgical evaluation. Sub-dural electro- corticography (ECoG), optical imaging with optical dyes and Electron Spin Resonance (ESR) are such examples. ECoG electrodes are what I used to

measure the impedance change during SSEP's on the cortex of anaesthetized rats.

The potential performance of these methods varies from time resolution of 1 to 100 ms and spatial resolution of 0.05 to 10 mm (Table 1-2). The following elaborate on each method.

Table 1-2: Summary of neuronal activity imaging techniques

Method (source)	Spatial resolution	Temporal resolution	Limitations
Non-invasive methods			
EEG (Baillet, 2001a; Baillet, 2001b; Michel, 2004)	~ 10 mm	~ 1ms	Limited for sources close to the surface
MEG (Hamalainen, 1992; Baillet, 2001a)	~ 10 mm	~ 1ms	Expensive, limited to sulci sources
Multi-modality fusion (Dale, 2001)	<10 mm	~ 1ms	Expensive, research only, haemodynamic and neuronal sources not always correlates
Direct MRI mapping (Xiong, 2003; Lin, 2006)	3 mm	100 ms (20 ms)	Research only, needs to be replicated and refined
DOI (Franceschini, 2004)	10 mm	25 ms	Research only, limited to cortical surface
LF-EIT and MD-EIT (Holder, 1987), this thesis	~ 10 mm	~ 1ms	Research only. Limited SNR. The theme of this thesis
Invasive methods			
ECoG	10 mm	~ 1ms	Slightly enhance EEG accuracy
Optic dyes (Shoham, 1999)	0.05 mm	~ 1ms	Limited 2D area on the surface of the cortex
ESR (Holder, 1987)	?	?	Theoretical application , toxic contrast agents

(Baillet et al. 2001; Michel et al. 2004; Hamalainen 1992; Dale et al. 2001; Xiong et al. 2003; Lin et al. 2006; Boas et al. 2004; Holder & Gardner-Medwin 1988)

1.2.2.1 EEG

Electrophysiological methods have long been used to study the function, over milliseconds, of individual neurons. Their depolarisation, or "firing", is well understood, as is the integration of signals

on their cell projections, dendrites, from the synapses of neighbouring neurons. Brain function depends on the spatial and temporal synchrony of large populations of neurons.

EEG, the most widespread monitoring technique, provides information about the electrical activity of neurons near the surface of the cortex by measuring voltage changes on the scalp. Applications of EEG include recording spontaneous activity during normal and abnormal conditions such as epilepsy or encephalitis, monitoring sleep stages and characterizing the response stimuli such as visual, auditory or somatosensory.

The magnitude of the signal depends on the number, location and geometry of synchronously firing neurons. In certain geometries, it is possible for many arrangements to generate currents so that their associated potential distributions cancel. Therefore, EEG is sensitive to the dendritic currents of active pyramidal neurons, oriented parallel to each other so that their potential distributions do not cancel. Temporal resolution is high and data is normally collected at a sampling rate of around 250 Hz, sufficient to describe a 70ms interictal spike, common in epilepsy, with over 17 data points. EEG is non-invasive and safe. It is also inexpensive and widely used as a clinical tool. It is, however, difficult to detect signals from neurons deeper in the brain, and spatial resolution is poor.

EEG can be used as a parametric or an imaging tool in the estimation of EEG sources in the brain (source imaging)(Baillet, 2001a; Baillet, 2001b). It is assumed that the electrical activity in the cortex can be represented by a few equivalent dipole sources. The number, localization, magnitude and orientation of these are estimated, iteratively, until the calculated potential distribution matches best the measured voltages at the scalp electrodes. For parametric modelling, one assumes / guesses a predefined number of sources. Due to the non-uniqueness of the inverse problem, employing this sole priori assumption may result in non-physical solutions where the sources are found outside the head. For source imaging, the number of unknowns is two orders of magnitude higher than the number of electrodes so the problem is severely underdetermined and difficult to solve without some mathematical trickery. Yet, with sufficient prior information (such as combined fMRI data and individual MRI segmentation of grey matter), spacial resolution of <10 mm and time resolution of ~1 ms is achieved for most cortical sources, but not for deep sources (Michel, 2004).

1.2.2.2 MEG

MEG also provides information about the electrical activity of pyramidal neurons, similar to EEG, with high temporal resolution (Hamalainen, 1992). Small inductive coils, instead of electrodes, are arranged on the inside of a helmet about 1-3 cm from the subject's scalp. Tiny currents are induced by the changes in magnetic field associated with dendritic currents and these are measured using sensing

coils and Superconducting Quantum Interference Devices (SQUIDS) (Baillet, 2001a). The typical magnetic field magnitude outside the head are 10^{-13} and 10^{-12} Tesla for evoked responses and spontaneous brain activity respectively (Cohen 1968; Hamalainen et al. 1993). A typical SQUID sensor has a spectral noise density below 5 fT $Hz^{-1/2}$ (1 fT = 10^{-15} Tesla) (Brown, 1999), however the main limiting factor for evoked responses studies is the larger signal generated by the spontaneous brain activity. The problem of contact impedance is avoided, since the sensors do not come into contact with the scalp, and the positions of the electrodes are well defined. However, MEG apparatus is expensive and immobile. It requires a dedicated, shielded room and also high maintenance costs.

In addition, a major difference between EEG and MEG is that EEG is more sensitive to gyral sources as it has limited sensitivity to deep sources while MEG is more sensitive to sulcal sources as the use of sensing coils limit the sensitivity to the radial magnetic field component perpendicular to the coil plane.

1.2.2.3 Direct mapping with MRI

The ability to directly detect neuronal magnetic fields by MRI would help to achieve the "holy grail" of neuroimaging, namely both high spatial and temporal resolution without ambiguous localization. Both positive and negative findings have been reported in the literature, with no clear consensus as to the feasibility of direct detection (Hagberg et al. 2006; Parkes et al. 2006). In theory, the magnetic fields generated by neurons could affect both the magnitude and phase of the NMR signal (Kamei et al. 1999; Bodurka et al. 1999; Bodurka & Bandettini 2002; Kim & Ogawa 2002; Kilner et al. 2004).

The effects of externally applied small (~2 mA) electric current pulses has been shown to be detectable in the human body using MRI (Joy et al. 1989). The challenge of detecting neuronal currents resulting from brain activity is much more difficult, since these currents are approximately three orders of magnitude smaller, much more transient, and perhaps localized to a smaller region in space, than what has been detected previously using MRI.

Much consideration must also be made as to how to separate the fast, neuronal effects changing over tens of milliseconds from slower effects such as the BOLD signal changing over hundreds of milliseconds to seconds.

Several studies have used MRI with visual evoked potentials, however it has not been certain that the changes seen are directly due to neuronal activity as opposed to haemodynamic changes (Konn et al. 2004; Kilner et al. 2004; Chu et al. 2004).

Liston et al. (Liston 2004)(retrospectively analyzed data acquired as part of an fMRI study to assess the possibility of large spiking currents (finite impulse responses (FIRs)) associated with seizures in epilepsy patients. This study showed possible evidence for detection of generalized spike wave discharge (GSWD) complexes which are thought to be at least twenty times larger than evoked responses, based on EEG voltage measurements.

Overall, the controversy and inconsistency between the different studies measuring both phase and magnitude changes demonstrate that the sensitivity for detecting spontaneous and smaller evoked neuronal currents is too low to be of practical use with existing MRI techniques. Recent advances in development of ultra fast fMRI reconstruction methods have allowed an improved time resolution of 20 ms which will be essential if direct MRI mapping of neuronal activity can be convincingly shown (Lin, 2006).

1.2.2.4 Diffuse Optical Imaging (DOI)

Several groups have explored fast changes in optical signals following sensory stimulation (Gratton et al. 2001; Franceschini & Boas 2004; Steinbrink et al. 2005; Low et al. 2006). These effects are believed to arise more directly from neuronal depolarization than from metabolism and result from changes in neuronal volume or refractive index and occur within ~1 ms or less of neuronal activation. These faster phenomena alter light scattering by 0.0001-0.01% and remain poorly understood and hard to detect (Cohen & Keynes 1973; Stepnoski et al. 1991).

The fast neuronal signal was detected in the motor cortex with time resolution of 16 ms, spatial resolution of 8 mm, signal to noise of 3.6 and averaging lasting 5 minutes (Wolf et al. 2002). Fast optical signals were measured over the visual cortex during visual stimulation by Gratton's group (Gratton, 2001; Low, 2006; Gratton, 2006). Recent work by Boas's group (Franceschini, 2004; Boas, 2004) report 2D mapping of fast neuronal activity over the surface of the cortex resulting from motor task and somatosensory stimulation with 25 ms time resolution, spatial resolution of ~10 cm and SNR of ~10. However, the encouraging findings of these groups could not be reproduced by other groups employing similar methods (Syre et al. 2003; Steinbrink et al. 2005).

Applications of non-invasive optical imaging methods to image the fast neuronal signals are still preliminary and require further validations but generally seem to be a promising way of obtaining information from the surface of the cortex. However, the lack of penetration of near infra-red (NIR) light into the highly scattering white matter limit the fast optical imaging methods form detecting

activity in deep structures, providing true 3D imaging.

1.2.2.5 LF-EIT and MD-EIT

EIT has the potential to achieve non-invasive functional imaging of fast neuronal activity in the human brain (Holder 1987; Boone 1995). The principle is that electrical impedance changes over milliseconds when neuronal ion channels open during activity, and this could be imaged by EIT. Imaging neuronal activity using EIT methods is the theme of this thesis and will be described in detail in the following sections and chapters. If successful, this method is expected to achieve a time resolution of about 1 ms, similar to EEG and MEG and spatial resolution of about 1 cm. It is also expected to be more sensitive to deep sources in addition to cortical sources which EEG and MEG methods are mainly sensitive to.

1.2.2.6 Invasive methods

Subdural Electro-corticography (ECoG) and depth electrodes: this is similar to EEG, however the electrodes are placed directly on the surface of the brain or into the brain parenchyma. It is mainly used for pre-surgical localization of epileptic sources and mapping of essential functional regions.
In animal studies, microelectrode arrays have been used such as that described by Petersen and Diamond. This was a 100 contact microelectrode grid-array, commonly known as the Utah array (Petersen & Diamond 2000). It covered 13mm and was used to measure single unit activity and generate prestimulus time histograms (PSTH). The array was implanted in Wistar rats using a pneumatic impulse inserter so that the tips were in layer IV and the bottom of layer III, of the rats cortex. Single vibrissae were stimulated at 1 Hz ant the response measured from the elctrodes to genereate PSTH's.

Depth electrodes such as the Michigan probe (Sun et al. 2006), have also been used to study neuronal activity within the rat's brain. The Michigan probe is a linear microelectrode array with 16 recording contacts spaced 150 μm apart, inserted perpendicularly into the rat's cortex. This was used to measure local field potentials to assess noxious and innocuous stimuli within different layers of the cortex.

Optic dyes: optical imaging method using voltage sensitive dyes applied to the exposed cortex in vivo (Grinvald et al. 1992). This method is only used in animal models for brain research but was shown to produce images of neuronal activity with a time resolution of ~1 ms and excellent spatial resolution of 50 μm (Shoham et al. 1999; Seidemann et al. 2002). The main limitations of this method are the need for exposure of the brain and that mapping could be achieved only for the outermost layers of the cortex with a depth of less then 1 mm.

Electron Spin Resonance (ESR): this method is based on the electromagnetic field produced by an unpaired electron. Depolarization was previously recorded using potential-sensitive spin label (Cafiso & Hubbell 1978). This method was suggested by Holder (Holder, 1987) as an alternative method for imaging neuronal activity but has hitherto not been investigated as a result of the possible toxicity of the labelling contrast agent which requires free radicals.

1.3 Electrical Impedance Tomography (EIT)

1.3.1 Introduction to bioimpedance

1.3.1.1 Relevant physics

Bioimpedance is the impedance that is measured when an electrical current is applied to a sample of biological tissue. Bioimpedance varies with frequency and temperature, and different tissue types have characteristic impedances that relate to their histology.

The resistance (R) and capacitance (C) of tissue are the two basic components of bioimpedance. Ohm's law defines the resistance of a sample as the ratio of the potential difference across it to the current flowing through it.

$R = V/I$

Where V = potential difference in Volts and I = current in Amperes.

Resistance has units in Ohms (Ω).
The definition of capacitance of a sample is defined as the ratio of the electrical charge to the potential difference:
$C = Q/V$

Where Q = charge in Coulombs and V = potential difference in Volts.

Capacitance has units in Farads.

In a biological context, resistance can be thought of as a measure of the extent to which a tissue opposes the movement of charged particles (electrons or ions) either through or around its constituent cells. The capacitance is an expression of the extent to which tissue stores and releases energy.

EIT involves the application of both direct current (DC) and alternating current voltages to biological tissues. When an alternating current is passed through a purely resistive sample, the output voltage measured will be in phase with the input. When a capacitive element is added, the output voltage will be shifted out of phase with the input (Figure 1-1). This shift is known as phase angle of the tissue.

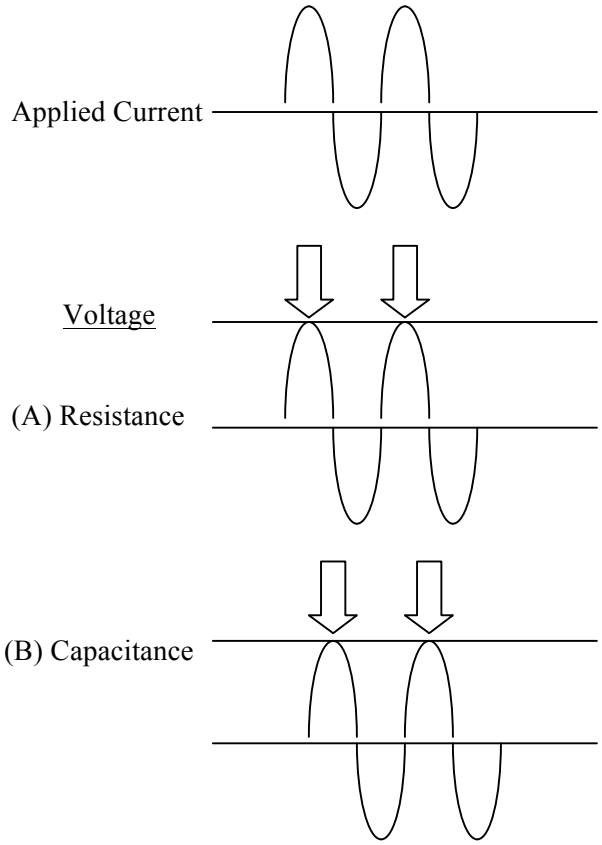

Figure 1-1: Applied current, voltage, resistance and capacitance
The voltage that results from an applied current is in phase for a resistor (A) and 90° out of phase for a capacitor (B).

Bioimpedance is a complex quantity made up of two components, resistance and reactance. The resistance can be thought of as the part that impedes the flow of direct current, and the reactance as the part that impedes the flow of alternating current.

Reactance (X) is related to capacitance by the following formula:

$$X = 1/j\omega C$$

Where $\omega = 2\pi f$ (f = frequency of alternating current) and C = capacitance.

Therefore as the frequency of the applied current increases, the reactance of the sample will decrease. Similarly if the capacitance increases, the reactance will also decrease. Resistance is known as the real part of the impedance, and reactance is known as the imaginary part of the impedance. Resistance is given the notation *real* Z', while reactance is given the notation *imaginary* Z'' ($-jZ$). These components both have units of ohms (Ω).

A simple model of tissue consists of a resistance and a capacitance in series. The total iimpedance of this model is given by:

$$Z = R + 1/j\omega C$$

A diagram helps to clarify the relationship between various quantities (Figure 1-2):

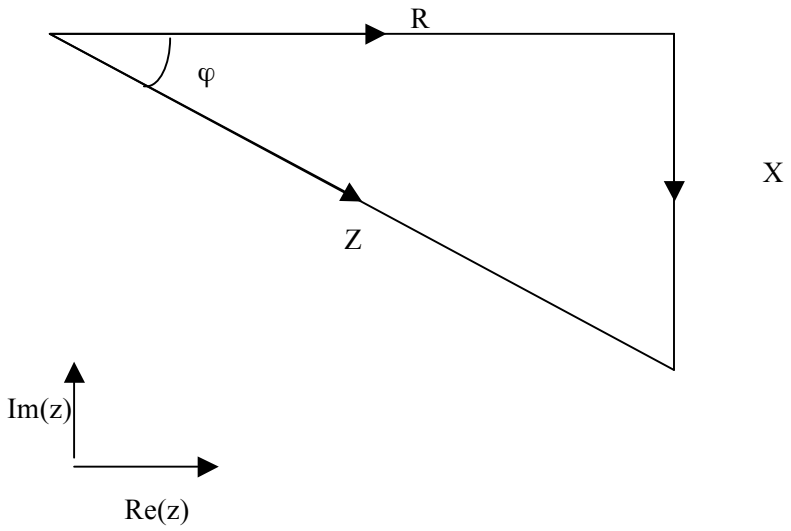

Figure 1-2: Impedance, resistance and reactance
The relationship between the impedance of a series model and its two component parts – resistance and reactance.

So the magnitude of the impedance can be found from the resistance and reactance by Pythagoras theorem:

$$Z = (R^2 + X^{1/2})^{1/2}$$

And the phase angle can be found by trigonometry:

$$\mathrm{Tan}(\varphi) = X/R$$

The resistance and capacitance of a sample are dependant on its length and cross-sectional area. The longer the sample, the greater the resistance whereas the greater the cross-sectional area, the lower the resistance. Thus, to compare different sized samples, we need to look at the resistance for a defined unit area and length. This is known as the resistivity (ρ) and is defined by the formula

$$\rho = R.A/l$$

Where R = resistance in ohms, A = cross-sectional area of a sample in m^2 and l = lenghth of sample in m.

Resistivity has units of Ωm (often quoted as Ωcm). It can be thought of as the intrinsic availability of a material to resist the passage of an electrical current. The resistivity can be calculated resistance and the size of the tissue sample are known.

Reciprocal quantities often arise. *Conductance* is the reciprocal of resistance, and has units of Siemens (S). *Susceptance* is the inverse of reactance and also has units of Siemens.

Conductivity (σ) is the inverse of resistivity, and the conductance of a unit cube of any material and is given in S/m. The *permittivity* of a tissue is the property of a dielectric material (i.e. essentially non-conducting) that determines how much electrostatic energy can be stored per unit of volume when unit voltage is applied and measured in Farads per metre (F/m).

1.3.1.2 Modelling Tissue

Tissue can be modelled as an electronic circuit, with increasing levels of complexity. In the simplest model, the extracellular space is represented as a resistor (R_e), and the intracellular space is modelled as a resistor (R_i) and a capacitor (C_m) (Figure 1-3). The membrane is modelled as a capacitor because of its lipid nature, which allows charge to be stored and released.

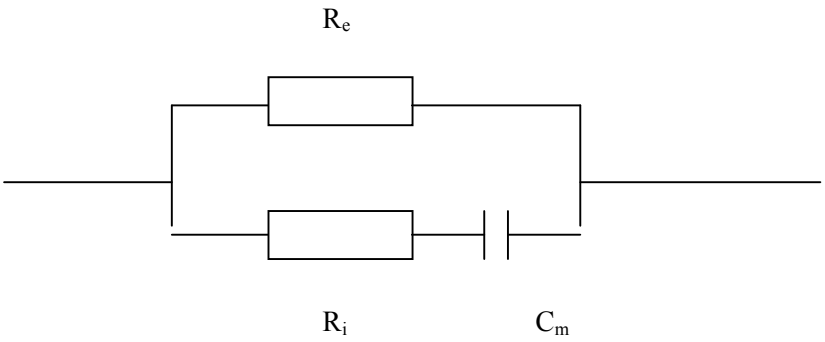

Figure 1-3: The cell model as a basic circuit
R_i, and R_e are the resistances of the intracellular and extracellular space, and C_m is the membrane capacitance.

It is considered easier for current to flow through the extracellular space of the cell than through the intracellular space. At the lowest frequency the majority of the current flows through the extracellular space resulting in a higher resistance and lower reactance. At higher frequencies, the current can move through the intracellular space and through the cell membrane (Figure 1-4), so the resistance decreases and the reactance increases due to the cell membrane now being included in the path the current takes. The frequency at which the measured reactance is greatest is known as the centre frequency (F_c).

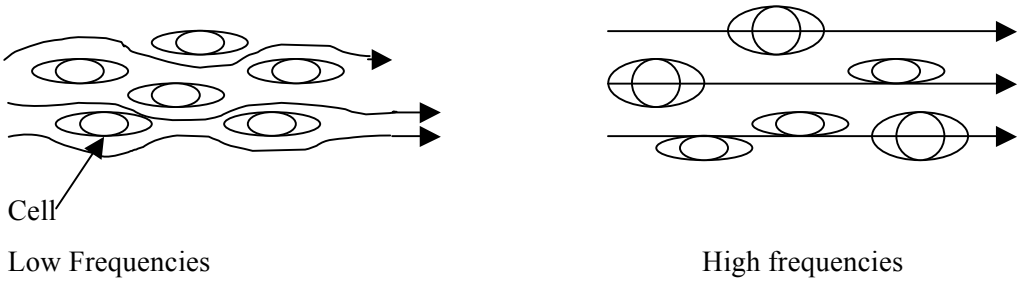

Figure 1-4:The movement of current through cells
The movement of current through cells at low and high frequencies.

1.3.1.3 Measurement of Tissue Impedance

The impedance of tissue or a solution can be measured both in vitro and in vivo. For in vivo the electrodes are placed directly on the tissue, whereas for in vitro experiments, the tissue sample is packed into a measuring cell, or placed between plate electrodes.

Tissue impedance can be measured by a two-electrode arrangement or a four polar arrangement. For the two-electrode arrangement (figure 1-5), the current is injected and the voltage is measured via the same two electrodes. The disadvantage of this arrangement is that the recorded resistance also

includes the resistance of the electrodes. Therefore measurements should be made on a number of different length samples. The impedance measurement for each should then be plotted against length, and the graph extrapolated back to find the impedance of the tissue sample.

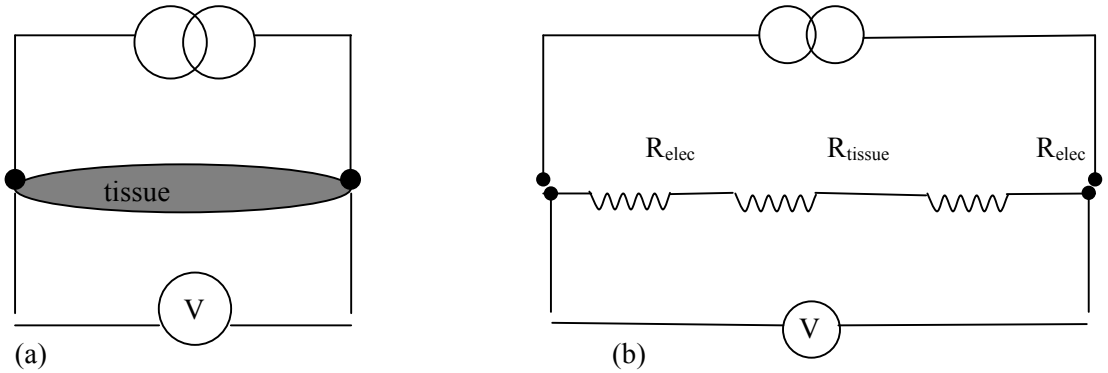

Figure 1-5: Two electrode measurement
The two-electrode measurement as (a) block diagram and (b) modeled as a simple electrical circuit.

For a four polar measurement, two voltage measuring electrodes are placed between the two current injection electrodes at a known distance. The voltage is then measured across these electrodes. In this method, only the current carrying electrodes have impedance. As the measuring electrodes are between the current injection electrodes, the impedance measured is that if the tissue without the resistance of the electrodes. Therefore no corrections need to be made for electrode impedance (Figure 1-6).

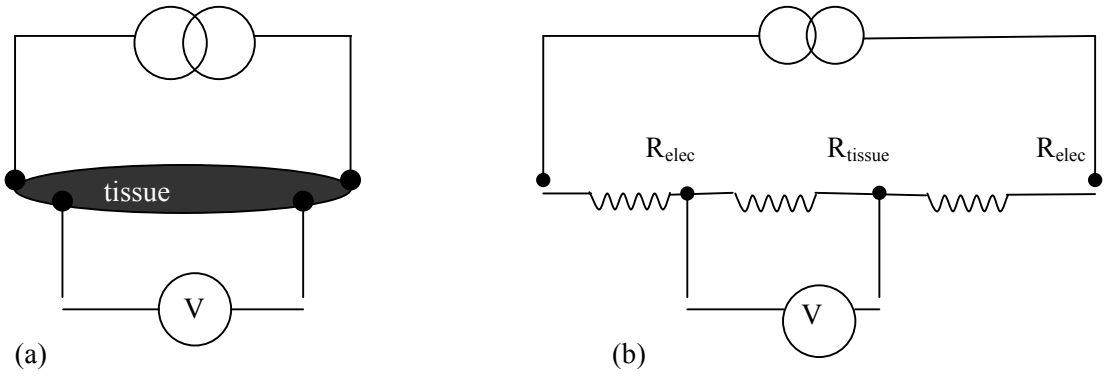

Figure 1-6: The four-electrode measurement
The four-electrode measurement as (a) block diagram and (b) modeled as a simple electrical circuit.

1.3.1.4 Factors affecting tissue impedance

There are several factors that influence measurements of tissue impedance, which include frequency of the injected current, temperature, directional placement of the measured tissue and the behavior if ion channels within a tissue. The behavior of ion channels is of particular importance during impedance measurement on neuronal tissue and shall be discussed later.

Temerature-dependance: Biological impedance decreases by approximately 1% for each increase of one-degree centigrade (1°C) in temperature. It is because the mobility of ions increases with increasing temperature (Pethig 1984).

Anisotropy-dependance: The impedance value of an anisotropic depends on the direction of measurement. For example, the impedance of bone and muscle measured transversely is ten times as long as that measured longitudinally (Hart et al. 1999). This is because, when current travels longitudinally, it travels across a larger area of cell membrane, which has lower impedance.

1.3.1 Impedance and physiology of cerebral tissue

1.3.2.1 Overview

The brain consists of neurons, surrounded by a framework of supporting cells. A typical neurone has a cell body, a number of dendrites (small processes) and a single log process, called the axon. The axon is also called the nerve fibre and transmits information, in the form of action potentials, from the neurone to others. The cell bodies make up the outer grey matter of the brain, whereas the fibres make up the inner white matter. Beneath the skull lies three membranes which envelope the brain. The outer membrane is called the dura mater. This is tough connective tissue, partly fused to the skull. The subdural space separates this layer from the deeper membranes. The next membrane is the arachnoid mater, which is a delicate continuous membrane. Beneath this is the subarachnoid space, which is contains cerebral spinal fluid (CSF). There are also blood vessels in this space. The next membrane is the pia mater, which directly covers the surface of the brain. Most of the resting brain cells have a resting potential across their cell membranes, the inside of the cell being just under 0.1V negative to the outside.

Physiologically**,** neuronal activity is based on action potentials, which are generated in a nerve either by sensory receptors or by activation from other neurons. Brain activity can be classified as spontaneous or evoked. Spontaneous activity is the result of rhythms generated by neural networks. This spontaneous activity of the brain is divided into four frequency bands, which are: delta (up to 4 Hz), theta (4-8 Hz), alpha (8-14 Hz) and beta (above 14 Hz). Evoked brain activity or response is the activity evoked by peripheral sensory stimulation projecting to the cortex along neuronal pathways.

These responses are commonly classified as visual, auditory and somatosensory evoked potentials, according to the type of sensors being stimulated. Compared with spontaneous brain activity, evoked potentials have clearly defined location and are usually smaller in amplitude. They may be monitored by recording the evoked potentials using an "averaging technique", as they are time-locked to the specific stimuli. Furthermore, spontaneous and evoked brain activity could be recorded using both depth and surface electrodes (Binnie et al. 1995).

1.3.2.2 Graded potentials and action potentials

All cells possess a membrane potential related to the non-uniform distribution of and permeability to sodium and potassium ions and large intracellular anions. Nerve cells however are specialized in that they can undergo transient rapid changes in their membrane potentials, forming electrical signals: graded potentials and action potentials. When a neurone is not being excited its membrane potential is known as its resting membrane potential, which is approximately -70mV. Graded potentials are local changes in membrane potential of varying grades or degrees, which only travel a short distance. As these changes travel along the membrane the amplitude decreases the further it gets along the membrane until it disappears. This occurs because current leaks into the surrounding extracellular fluid around unmyelinated nerves. This is similar to current leaking from an uninsulated wire. Action potentials are brief reversals of membrane potential brought about by rapid changes in membrane permeability. These reversals are able to spread throughout the membrane in a non-decremental fashion, hence the signal can be maintained over a long distance. A stimulus causes the membrane potential to decrease. If this reaches a critical level, known as the threshold potential, of -55mV an action potential will occur. At the threshold level the decrease in membrane potential becomes explosive so that the membrane potential reaches zero (depolarisation) then reaches +30-40mV as the potential reverses so that the inside of the cell is now positive relative to the outside. Just as rapidly the potential drops back towards the resting potential then exceeds it transiently (hyperpolarisation), to about -80mV, then returns to its resting potential (repolarisation). See figure 1- 7 below.

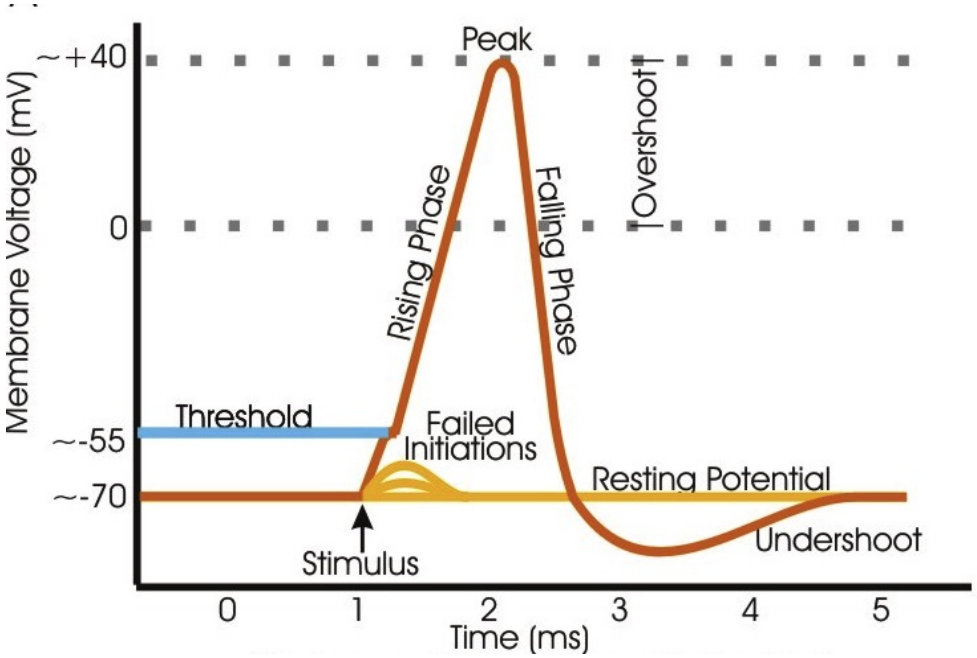

Figure 1-7: The compound action potential

This whole event only lasts several milliseconds. This occurs due to the movement of sodium and potassium ions through channels in the membrane, which are gated. A resting potential many potassium channels are open but most sodium channels are closed, hence the membrane is more permeable to potassium. A triggering event or stimulus causes the sodium channels to open and allow positively charged sodium ions to enter the cell thus depolarizing it. Once the threshold is reached, voltage gated sodium channels open causing a much faster influx of sodium leading to a positive membrane potential and the membrane is now more permeable to sodium. At the peak of the action potential +30-40mV all of the sodium channels rapidly shut and more potassium channels open so that now the membrane is only permeable to the outflowing potassium channels, thus returning the membrane potential to its resting state (figure 1-8).

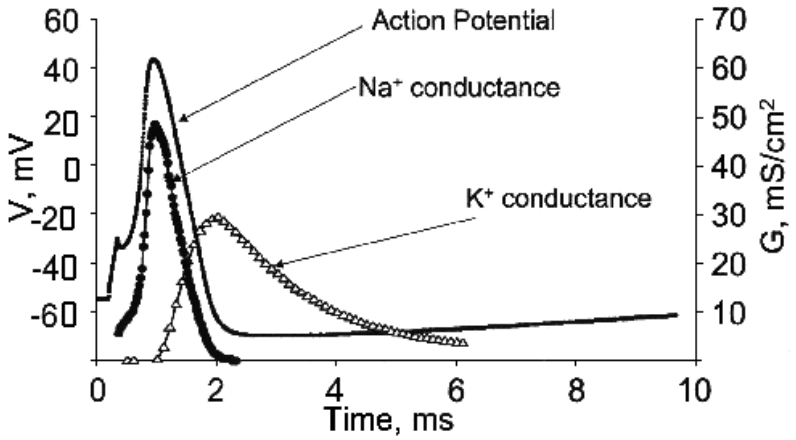

Figure 1-8: Ion fluxes during an action potential.

1.3.2.3 Measuring impedance during neuronal depolarization

As mentioned earlier**,** if low frequency current is passed through a tissue it will not cross the cellular membrane. However, during membrane depolarization, which occurs during an action potential as described above, ion channels in the membrane open, hence reducing the resistance to current. This decrease in resistance is only expected to occur over tens of milliseconds (Cole et al. 1939; Araki & Terzuolo 1962). EIT is capable of making measurements within this time resolution (Boone and Holder 1995). Boone predicted a resistance decrease of about 0.01% during neuronal depolarization when measured on the surface of the scalp.

1.3.2.4 Previous experiments on impedance measurements during neuronal depolarization.

The model of impedance in unmyelinated nervous tissue described by Boone (1995) suggests that when a nerve depolarises it exhibits a change in impedance. This change is greatest at DC and decreases with increasing frequency as more current crosses the cell membrane. Also unmyelinated neurons have less conductive tissue around them to shunt current away. Hence it is more practicable to measure neuronal resistance changes at DC in unmyelinated nervous tissue.

He first used a crab nerve (Cancer Pagurus) as it is unmyelinated, hence exhibiting a large enough resistance change to be measured. The nerve can be isolated, thus excluding other variables which may interfere such as blood pressure, level of anaesthesia and no surrounding tissue.

The current can be applied longitudinally with suitable electrode positioning ensuring depolarization of much of the tissue with reduced effect of measurement artifact.

The isolated nerves were approximately 10cm long. A constant voltage stimulus was applied via 2 electrodes close together at one end of the nerve to initiate a compound action potential. Further along the nerve, another two electrodes close together were used to inject a current of less than 5μA from a current source. Either side of these two electrodes were another two electrodes used to measure the voltage along the nerve. See figure 1-9 below.

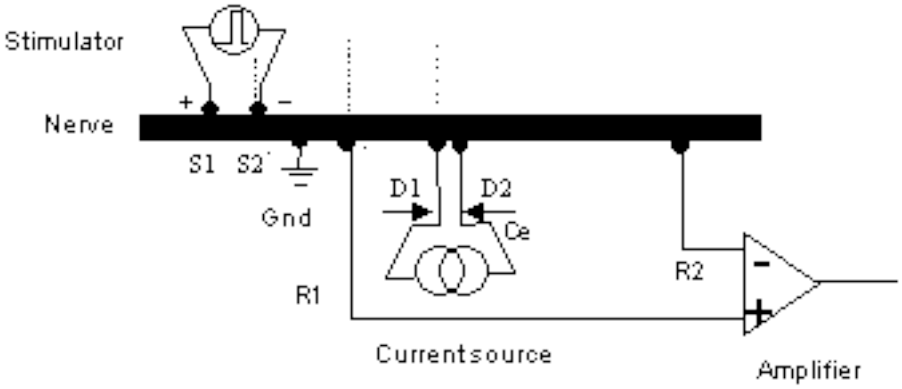

Figure 1-9: Arrangement for recording impedance on the crab nerve

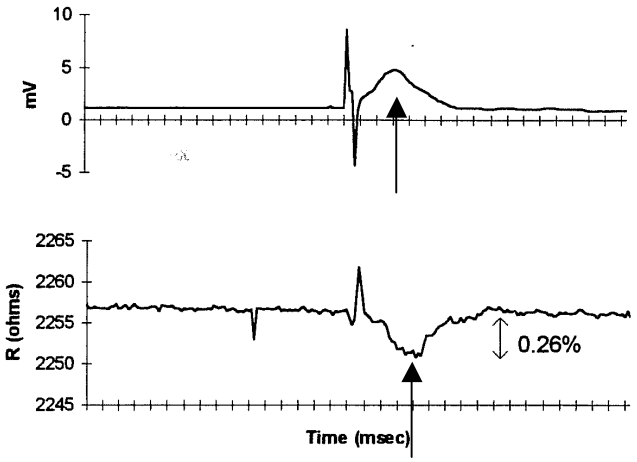

Figure 1-10: Crab nerve impedance measurements
Impedance change (lower graph) during compound action potential (above graph) in crab nerve.

This showed an action potential with a peak of 5mV (higher trace) and at the same time a drop in impedance ranging between 0.17% and 2.5%, depending on the condition of the nerve, temperature of the solution it was immersed in.

Boone et al then attempted to record impedance changes during neuronal depolarisation in the cerebral cortex of 2 anaesthetised rabbits New Zealand White rabbits. The animals mechanically ventilated whilst under neuromuscular blockade with pancuronium bromide. An array of electrodes were placed directly on the cerebral cortex. Two injected current whilst the remaining recorded voltages between themselves and a common reference electrode on the animals neck. This was done whilst the contralateral median nerve was being stimulated to provoke an evoked potential.

7 out of 20 satisfactory recordings were made.

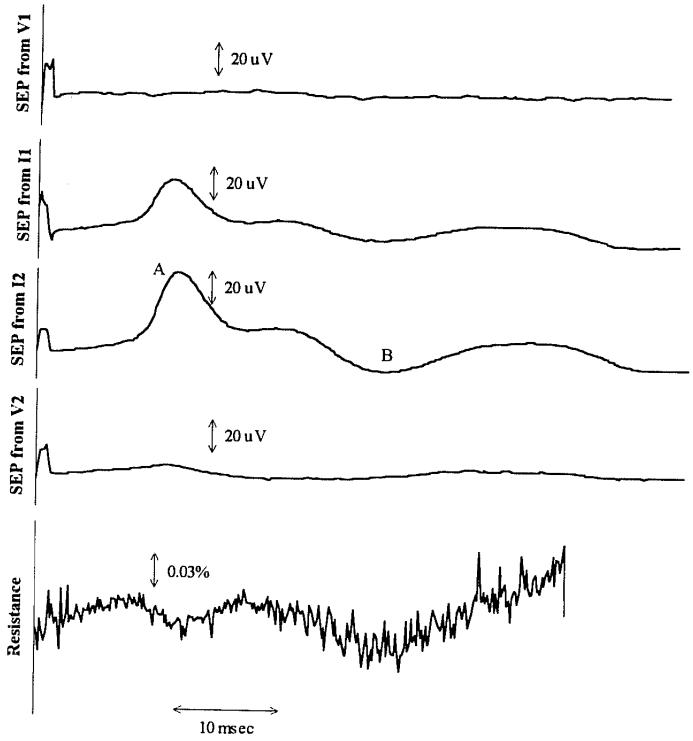

Figure 1-11: Rabbit brain impedance measurements
Impedance measurement (lower graph) during evoked responses (above graphs) in brains of anaesthetized rabbits.

The evoked potentials were 20uA in magnitude over the area of cortex representing the forepaw. A downward drift in the baseline of approximately 0.03% was noted, which coincided with the evoked potential (point A in figure 1-11 above). There was also a second drift further along which coincided with the EEG response at point B.

Liston's modeling attempted to show what order of magnitude of impedance changes might be expected during neuronal depolarisation (Liston et al. 2012). First, the changes of a peripheral nerve, being a simpler model, were predicted, then cortical nerves and bulk cortical tissue and finally the changes that might be measured on the scalp were modelled. Liston's predictions for peripheral nerves for direct current injection, once the effect of capacitance and incomplete depolarisation was taken into account, was 2.8%, which is somewhat larger than those found in Boone's recordings. Liston suggested that this disparity in results may have been due to experimental problems causing the peripheral nerve impedance changes to be underestimated. Liston et al. predicted a cortical decrease, with the same considerations as above, of 0.6 to 1.7 %, which with the attenuation of a highly resistive skull, would be between 0.006 to 0.17 % with an attenuation between 10 and 100 times. Liston noted that, with the impedance decreases recorded by Boone (1995), with the noise levels

reported and their smallest predictions for scalp changes, the SNR would be two and hence at the limit of detection. He also suggested the use of a better anatomical model might improve the localisation of such changes, as electrode mislocalisation is an important source of error as also noted by Gilad (2009).

Gilad et al (2007) examined a range of means of optimisation, an exceptionally important topic if such small changes are to be accurately reconstructed, and the calculation and limits of current density in the head (Gilad 2007). He commented on the importance of accurate meshes for reconstruction, and describe the use of a finite element method (FEM) mesh with 53 336 tetrahedra and realistic layering far more realistic than the homogeneous sphere often used in other reconstructions. Using a similar FEM mesh produced from high resolution MRI scans, modelling was undertaken by Gilad et al (2009) to predict the impedance changes that might occur as a result of visual evoked responses. Peak changes of 0.004% with an SNR of about 4 were predicted with the conclusion that *in vivo* recordings would find reproducible changes, but that the low SNR would be prohibitive to image reconstruction.

Earlier work had been undertaken to attempt to produce similar recordings that might later allow for recording in humans that might be reconstructed, but as with similar work since, these attempts were unsuccessful. The peak impedance changes were only about 0.001%, and these were not consistent and none of the short latency changes were significantly different to baseline (Holder 1987).

A more successful set of fast neural activity recordings were more recently undertaken by Gilad and Holder (2009). Although again single channel recordings, they produced more promising results regarding the feasibility of recording fast impedance changes. Using scalp electrodes and a visual stimulus of a checkerboard pattern changing twice a second, visual evoked responses were recorded with a current injection of a 1 Hz square wave of 0.1 to 1 mA at one of two injection sites over 10 min (O Gilad & Holder 2009). These recordings were performed 16 times in six subjects and an average impedance decrease of 0.0010 ± 0.0005 % (mean ± SEM) was recorded. This was in broad agreement with the suggested size of such changes from prior modelling studies, but, as suggested in Gilad's prior modelling study (2009), the SNR was too low, at 2:1, for imaging to have been possible if multiple injection had been undertaken. Again the concern of artefactual impedance changes due to the injected current affecting neuronal activity was addressed, but Gilad and Holder claimed that this could largely be dismissed due to the amplitude of the injected current being insufficient to alter neuronal activity and also citing the similarity with modelling changes. This study, although only a single channel recording, showed, for the first time, that such impedance changes could be measured in humans and also highlighted that if the ultimate aim of image reconstruction was to be met then further work would be required to improve the SNR, such as technical improvement, multiple injection sites, lengthened averaging times and the implementation of other means of noise reduction.

1.3.3 The role of EIT

Electrical Impedance Tomography (EIT) is a developing medical imaging modality that provides information regarding the internal electrical properties inside a body based on non- invasive voltage measurements on its boundary. Data acquisition is performed through an array of electrodes which are attached to the boundary of the imaged object. Sequences of small insensible currents, typically in the order of 1 mA, are injected into the object through these electrodes and the corresponding boundary electric potentials are measured over a predefined set of electrodes. The process is repeated for numerous different configurations of applied current (Figure 1-12). The internal admittivity (or impedivity) distribution can be inferred using this boundary data.

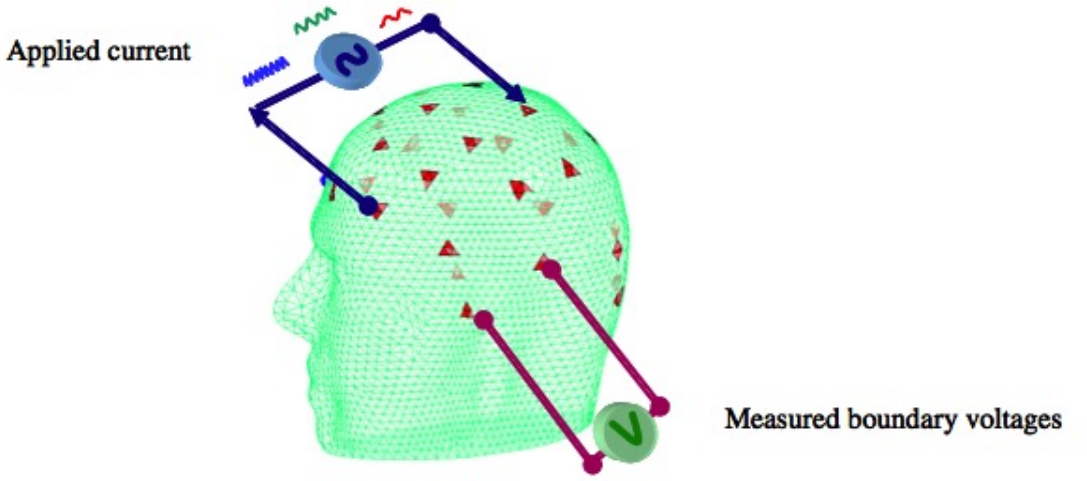

Figure 1-12: EIT data aquisition principle
Single or multi-frequency current waveform are injected through set of electrodes, while boundary voltages are recorded through a predefined set of electrodes (Horesh, 2006a)

EIT was first proposed as a medical imaging method in 1978 by Henderson and Webster (Henderson & Webster 1978), and in 1980 uniqueness was proven for the linearised inverse problem by Calder´on (Calder´on 1980). The realisation and popularisation of the method can be attributed mainly to Barber and Brown (Brown, 1985; Brown, 1987). The first three-dimensional EIT images were for the chest and were reported in Nature by Metherall and colleagues in 1996 (Metherall et al. 1996).

The potential medical applications of EIT are vast, including detection and classification of tumours from breast tissue (Mueller et al. 1999; Mueller et al. 2001; Soni et al. 2004) detection of pulmonary emboli and oedema (Newell et al. 1996; Cheney et al. 1999), monitoring of pulmonary and cardiac functions (Eyuboglu et al. 1988; Brown et al. 1994; Frerichs 2000; Frerichs et al. 2002; Isaacson et al. 2006), gastric imaging (Smallwood et al. 1994; Soulsby et al. 2006), imaging the eye (Jurgens et al.

1996), detection and monitoring of cerebral ischemia and haemorrhage (McArdle et al. 1988; Holder 1992; Gibson et al. 2000; McEwan et al. 2006; Romsauerova, McEwan & Holder 2006), localisation of epileptic foci (Bagshaw et al. 2003; Fabrizi et al. 2006), normal haemodynamic brain function (Tidswell, 2001) and neuronal activity (Holder, 1987; Boone, 1995b).

In the 1930's, a similar technique was suggested for geophysics applications, namely Electrical Resistivity Tomography (ERT). This method is used to locate resistivity anomalies using electrodes on the surface of the earth or in bore holes. In the field of industrial process tomography, this method is used to monitor mixtures of conductive fluids in vessels or pipes (Williams & Beck 1995) and for non-destructive testing and evaluation of materials and machine parts (Kaup et al. 1996; Bryan et al. 2006).

In the past two decades, there have been major advances in medical imaging, with the development of hard-field imaging methods, such as Magnetic Resonance Imaging (MRI), X- ray Computer Tomography (CT) and Positron Emission Tomography (PET). In spite of their immense benefits, these methods are all immobile, expensive, and image either anatomy or slow metabolic changes over time. Conversely, EIT is non-invasive, portable, inexpensive, and can potentially provide a high temporal resolution of the order of tens of milliseconds.

1.3.4 Imaging haemodynamic brain function with EIT (slow changes)

The main two mechanisms for haemodynamic impedance changes in the brain are: *Impedance decrease due to increased blood volume:* during physiological activity, a signal is sent to the blood vessels which increases blood flow and blood volume to that cortical area (Malonek et al. 1997). As blood has a lower resistivity than the surrounding brain (150 Ωcm and 350 Ωcm, respectively), the increase in the lower resistivity volume of blood will allow more current to flow through that area of tissue and decrease the bulk impedance of that volume of cortex (Figure 1-13 left).

Impedance increase due to cell swelling: during normal function, the size of the conductive extra-cellular space (ECS) is 20% of the brain volume. During epilepsy, moderate cell swelling occurs as water and ions enter the glial cells and the neurones (Lux et al. 1986), and the volume of the low resistivity ECS is reduced. This will increases the bulk impedance of that area of cortex. Larger changes of cell swelling are seen during ischemia and spreading depression, which cause much larger increases in brain impedance (Holder 1992; Boone et al. 1994) (Figure 1-13 right).

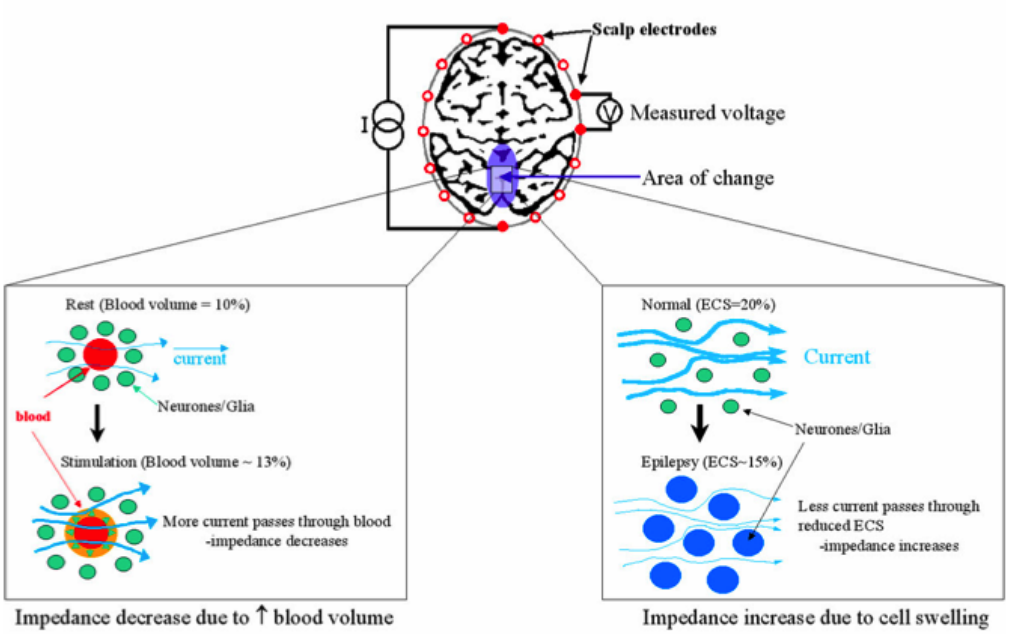

Figure 1-13: Mechanisms of haemodynamic impedance change within the brain:
Left: due to blood volume change (neuronal cells in green, blood vessel in the centre of the cells).
Right: due to cell swelling (Tidswell, 2006).

EIT has demonstrated preliminary images for the normal haemodynamic brain function (Tidswell, 2001) (Figure 1-14) and for localisation of epileptic foci (Bagshaw et al. 2003; Fabrizi et al. 2006) (Figure 1-15).

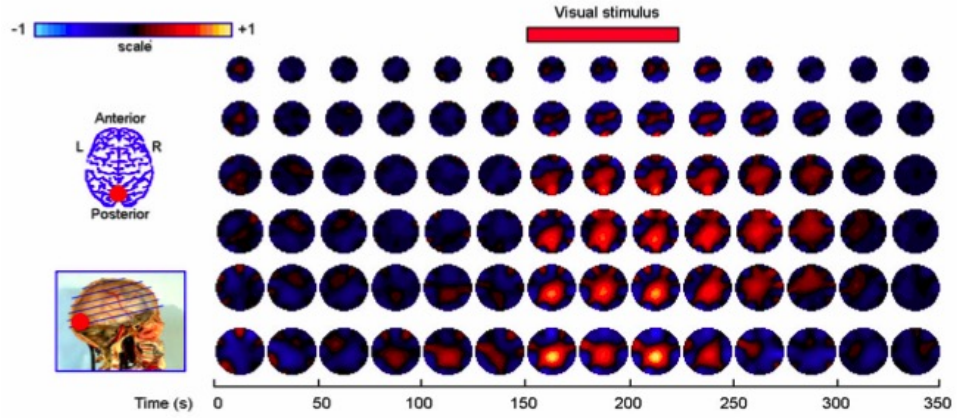

Figure 1-14: Examples of EIT images with scalp electrodes during visual evoked responses **(Tidswell, 2001).**

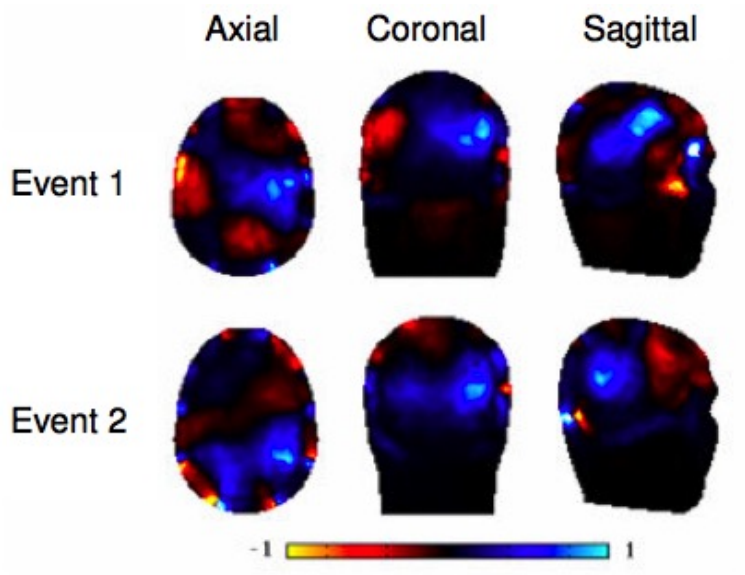

Figure 1-15: EIT in epilepsy
Reconstructions of data collected approximately 6s prior to the electrographic onset of two right temporal complex partial epileptic seizures (Bagshaw, 2003).

1.3.5 Instrumentation

Three main EIT systems have been recently used in the UCL group for studies on impedance changes in the human brain related to stroke and epilepsy (Fabrizi et al. 2007)(Figure 1-16):

UCH Mark1b: this utilizes a single four electrode impedance-measuring circuit with an analogue demodulator which is multiplexed to up to 32 electrodes (Yerworth et al. 2002). It serially addresses software selectable electrode combinations. The current source and cross point switches are included in a small head box separated from the main base box by a ribbon cable of 5 m, which was intended to enable continuous monitoring over days in ambulatory epilepsy subjects. The in-phase component of the impedance is measured with an analogue phase sensitive-demodulation voltage sensing circuit. A programmable gain amplifier is used to minimize the digitization noise for each electrode combination. It operates at a single selectable frequency between 225 Hz and 65.5 kHz and can apply a current of up to 5 mA peak-to-peak at 50 kHz. Leads to the patient are unscreened and so kept as short as possible, typically about 30 cm.

UCH Mark2.5: this utilizes one module of the Sheffield Mark3.5 multifrequency EIT system (Wilson et al. 2001), which comprises a four electrode impedance measuring circuit, multiplexed up to 32 electrodes (McEwan et al. 2006). The in-phase voltage is calculated with synchronized digital demodulation and has a single gain which was optimized for the range of the transfer impedance of the head of up to 70Ω (McEwan, 2006). It can operate at frequencies between 20 Hz and 1.6 MHz. It employs a multifrequency composite waveform and records a total of 30 frequencies, divided into

three sequential packets of ten frequencies (Romsauerova, McEwan, Horesh, et al. 2006). The current is fixed at 0.28 mA peak-to-peak for each frequency. Leads to the patient are unscreened.

KHU Mark1 16 Channel: this comprises a single current source which may address any electrode pair using a multiplexer and 16 parallel voltmeters in a novel radially symmetric architecture (Oh et al. 2007). It employs a digital phase-sensitive demodulator and current waveform generator. In principle, multiple frequencies may be synthesized and injected from the available range, 39 Hz to 500 kHz. The system employs general impedance converters which are individually calibrated for each electrode recording pair to optimize the output impedance at each frequency and the electrode leads are with an outer shield and inner driven screen.

For the application of measuring impedance changes related to neuronal activity which is the theme of this thesis, these systems were not suitable since they were not designed to operate near DC as would be required for neuronal activity. A dedicated prototype hardware was developed for this application and is later described.

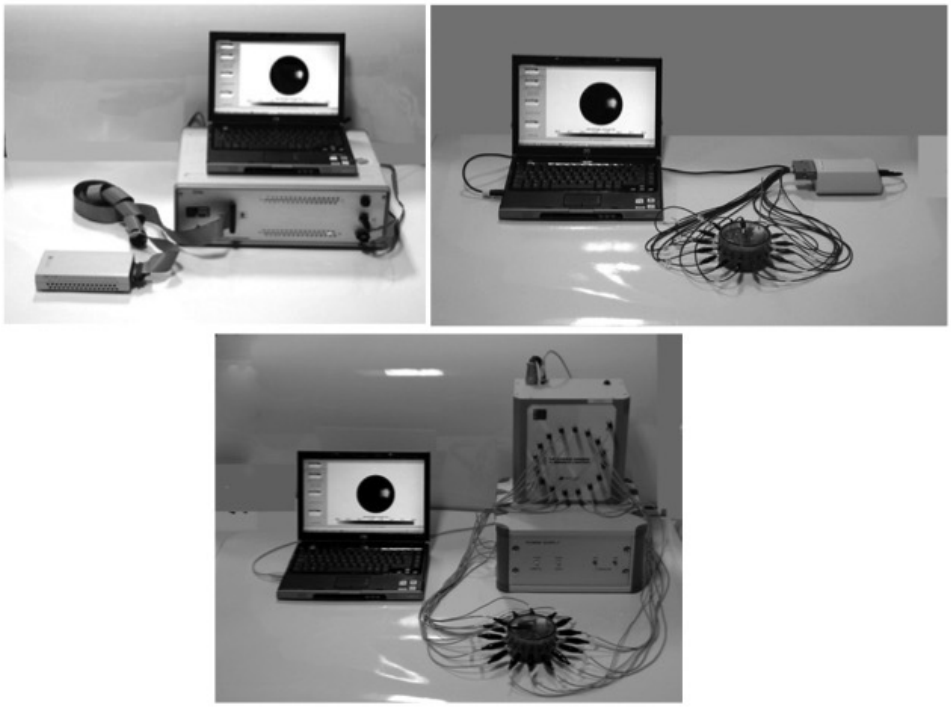

Figure 1-16: EIT systems used:
Top left—UCH Mk1b; top right—UCH Mk2.5; lower—KHU Mark1 16 channel. The two latter are shown connected to the cylindrical tank (Fabrizi, 2007).

1.3.6 The limitations of EIT

As opposed to hard-field imaging modalities which rely on collimated radiation beams which follow a well-defined straight-line trajectory such as in CT or PET, in EIT the electric current paths are less

definite. Electric current propagates in body tissue through ionic interaction, which is intrinsically diffusive. From a mathematical perspective, the problem of recovering inner admittivity distribution from boundary information is a nonlinear *inverse problem*. Moreover, the problem is also severely ill-posed in the sense that even small errors in the measured data may cause arbitrarily large errors in the estimate of the internal admittivity. In the presence of measurement noise, the solution can become unstable. Due to these inherited limitations, the spatial resolution of EIT reconstructed images is generally relatively poor.

1.3.7 Magnetic methods in EIT

The overall sensitivity of a single EIT measurement to local impedance changes during four terminal measurements (2 drive and 2 measure electrodes) is governed by two physical processes: 1. *Current injection:* only a small proportion of the current injected through the drive
electrodes reaches the Region of Interest (ROI) in the brain as a result of a current shunt path over the scalp, the highly resistive skull barrier, an additional shunt path through the CSF and the partial volume of brain ROI in relation to the entire brain volume. In a magnetic equivalent, the current would be induced, for instance by using coils. Due to the transparency of the skull to magnetic field, the induced current could be more focused since there are no shunt paths, the current density at the ROI could be higher and hence the measurement SNR (Freeston & Tozer 1995).
2. *Voltage measurement:* in EEG, the electrical potentials measured on the scalp due to endogenous neuronal currents are often strongly influenced by various inhomogeneities in the head, mainly the skull, making accurate determination of the activated area difficult. However, MEG could localize the activity more accurately since the skull is transparent to magnetic field (Hamalainen et al. 1993). A similar advantage might be beneficial in EIT if magnetic field produced by the injected (or induced) current is measured (Ahlfors & Ilmoniemi 1992).

Several magnetic variants of EIT have been previously proposed which utilize either MRI, superconducting quantum interface devices (SQUID) used in MEG technology or coils to detect the magnetic field resulting from an injected or induced current. These variants differ by the activation and sensing methods. In Induced Current EIT(IC-EIT) (Freeston & Tozer 1995; Zlochiver et al. 2004) coils are used to induce currents while electrodes are used to measure voltages. In Magnetic Induction Tomography (MIT) coils are used to induce eddy currents and to measure the external magnetic field (Gencer & Tek 1999; Karbeyaz & Gencer n.d.; Merwa et al. 2004; Rosell-Ferrer et al. 2006). The recently proposed Electromagnetic Impedance Tomography (EMIT) technique (Levy et al. 2002) uses EIT electrodes for injecting current and measuring voltages, but the boundary voltages are augmented by small number of exterior magnetic field measurements recorded using coils for improving the conditioning of the EIT problem. Another type of magnetic method known as MR-EIT (Ider et al.

2003), which was derived from Current Density Imaging (CDI) (Joy et al. 1999), uses magnetic resonance methods to measure the internal magnetic field induced by a current injected from surface electrodes. This method was also combined with conventional surface potential measurements (Voltage Scaled MR-EIT) (Birgul et al. 2003) or with coils to induce current instead of surface electrodes (Induced Current MR-EIT) (Ozparlak & Ider 2005). The advantages and limitations of the different approaches are discussed elsewhere (Ireland et al. 2004)and are beyond the scope of this study.

1.3.8 Magnetic Detection EIT

Another approach known as Magnetic Detection EIT (MD-EIT) or magnetic impedance tomography was proposed for biomedical applications by Ahlfors and Ilmoniemi. This method uses a pair of electrodes to inject current to an object, and an array of SQUIDs to measure the induced magnetic field. They used a single pair of electrodes to inject current at 16 Hz through a saline filled tank containing insulating cylinder, measured the external magnetic field 30-50 mm above the tank by a 24 SQUID system and reconstructed images of current density using minimum-norm estimates (Ahlfors & Ilmoniemi 1992). The use of MD-EIT for biomedical applications was preceded by geophysics applications with technique termed magnetometeric resistivity (MMR) (Edwards 1974).
Although SQUIDs have superior sensitivity over coils, they are suitable only for low frequencies below 1 kHz. Therefore, as the typical band of interest for EIT so far was between 1 kHz and 2 MHz (Brown 2003), most effort was made using the application of sensing coils (Tozer et al. 1999; Ireland et al. 2004) to image lung ventilation.

1.4 Purpose and design

The purpose of this thesis was to determine if EIT could be used to produce tomographic images of impedance changes related to neuronal depolarization during evoked responses, with electrodes on the surface of the brain of the anaesthetized rat.

In order to achieve this, the ideal hardware set-up, in terms of current source, current level, frequency and electrode design, for making the recordings had to be determined. This was validated with Crab nerve experiments described in chapters 2 and 3 as impedance changes have previously been measured this way.

Then using the same hardware setup, attempts were made to determine if reproducible impedance measurements on the cerebral cortex of the anaesthetised rat during somatosensory evoked responses

(SSEP) could be made. For this, optimal anaesthetic conditions were required with an adequate array of electrodes offering optimal contact impedance without causing damage to the cerebral cortex (Chapter 4).

Once this was achieved, further experiments were required to determine if the neuronal depolarisation secondary to SSEP's could be imaged with EIT. To do this, the impedance changes related to somatosensory and visual evoked responses were recorded to help prove the images were reproducible and physiologically plausible.

1.5 Statement of originality

The work presented in this thesis required a team. I personally undertook all physiological studies. Electronic instrumentation was undertaken by Dong-In Oh and biophysical modelling by Ori Gilad. I undertook data analysis in collaboration with team members. I have personally prepared all the data in this thesis. All the work presented in this thesis is my own work. The contributions from the other team members is presented below. Publications and conference presentations arising from the thesis are listed above. All the other work presented has not been published. All the work is original.

In chapters 2 and 3 the hardware arrangement and modifications and validation were carried out by Dong-In Oh, however the Perspex with platinum electrode array was made by myself.

The animal preparation including the crab nerve preparation (Chapters 2 and 3) and rat anaesthesia and surgery (chapters 4 and 5) were carried out by myself. The recordings in all the experiments were also carried out by myself. The data analysis was carried out jointly.

The silicone based electrode array in chapters 4 and 5 were made by Martin Schuettler (Department of Microsystems Engineering, IMTEK University of Freiburg, Freiburg, Germany).

The code for extracting the averaged action potentials, evoked responses and calculating the impedance changes in all chapters were written in Matlab by Ori Gilad.

In chapter 5, the algorithm written by previous member of the UCL EIT group was used for the image reconstructions with modifications to the script and the rat's mesh construction carried out by Ori Gilad. The statistical analysis in chapter 5 was carried out by Brett Packham in the UCL EIT group.

2. Measurement of impedance decreases in unmyelinated crab peripheral nerve during the compound action potential with a 1Hz square wave carrier.

2.1 Introduction

2.1.1 Orientating paragraph

In this chapter, a model of impedance change during the compound action potential (CAP) in an unmyelinated nerve has been described. Previous experiments, which study the impedance change on a crab nerve during a CAP are summarised here. The experiments were repeated in appendix 1 to confirm previous findings however there were certain technical issues with the nerve longevity and acquisition. Thus the experiments were repeated in this chapter to confirm previous findings with newer hardware, with the overall goal of using this method on the rat cerebral cortex. The crab nerve was placed on a series of electrodes, the nerve was stimulated whilst a low frequency square wave current was injected and the impedance changes were measured. Variations were made between the distances of the current injection electrodes and the amount of injected current to see if this had an effect on the overall impedance change. Impedance changes were seen at all current levels and spacings described. These changes were similar between 1 and 10μA and the change decreased with an increasing distance between current injection electrodes.

2.1.2. Background.

Cable theory (Taylor 1963) describes a mathematical model that can calculate the flow of current and voltage along neuronal fibres. The model regards the axons and dendrites as uniform cylinders composed of segments of capacitances and resistances combined in parallel (Figure 2-1). This theory was originally used to explain the decay of current traveling along telegram cables over a long distance. The cell membrane behaves as a capacitor and a resistor. At low frequency or DC current, the membrane completely restricts the flow of current. At higher frequencies the current will flow across the membrane. At DC, the current will only flow across the membrane when ion channels open during an action potential, therefore there will be a drop in resistance. Biophysiological modeling has shown that recording should be with carriers below 100Hz or the measured change in impedance will be significantly reduced (Boone and Holder, 1995; Liston, 2004).

Boone's biophysical model predicted a resistance change of 3.7%. In later experiments, a crab nerve was suspended on a series of electrode hooks. The nerve was stimulated at one end, a square wave current was injected via two electrodes and the impedance measured by another two. The impedance change measured was 0.5-1%, which validated the biophysical model (Boone 1995; Holder 1992, Liston 2004).

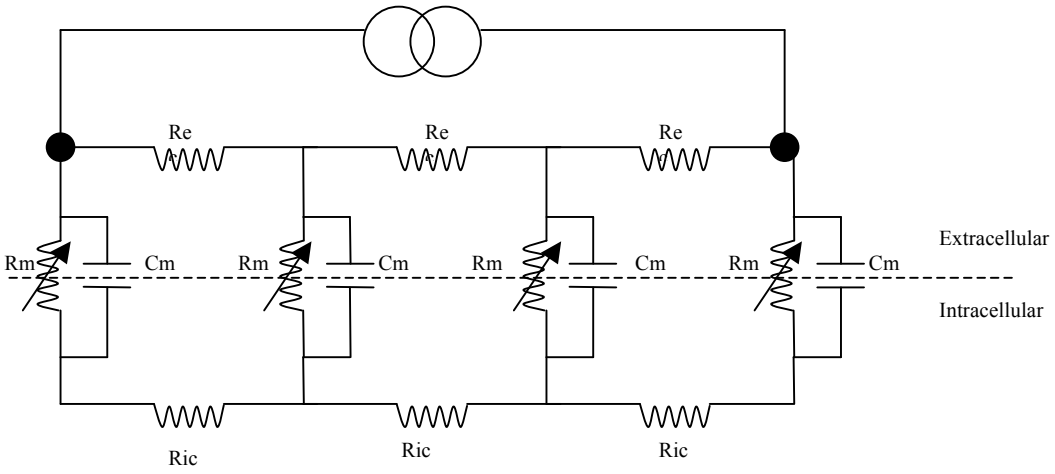

Figure 2-1: Electrical model of impedance along axon

A similar electrode design was used in this thesis (appendix 1) however significant deterioration in the health of the nerve during recordings led to artefactual changes and the blotting technique could not be as consistent as described in this chapter. Therefore a newer electrode design was required.

2.1.3 Purpose

This study was very similar to that already undertaken by Boone in our group (Boone, 1995), and that described in appendix 1. The overall purpose was to verify that similar physiologically plausible changes could be reproduced with improved instrumentation, using bi-polar square wave with paired control recording and linear model formulation for calculating the resistance changes detailed below.

The aims of this study were to examine the following:

1. If an impedance change using a square wave current source could be measured during the CAP to confirm Boone's findings.

2. To see the effect of different current levels on the impedance change. According to cable theory this should not affect the amplitude of the impedance change. The experiments in appendix 1 have shown that currents of around 20μA can be excitatory and therefore lower current levels needed to be used in this study.

3. To see the effect of different distances between the two current injection electrodes on the impedance change. As this distance increases, the overall resistance between the electrodes should increase, so we expect the overall impedance change to decrease (2.4.4). Previous experiments (appendix 1) showed that spacing as little as 1mm led to significant inconsistencies in the amount of fluid blotted between each recording. Therefore this chapter assessed spacings of 2mm and above.

2.1.3. Experimental design.

Impedance was recorded using a crab nerve placed on an array of electrodes housed in perspex, where the nerve was stimulated to induce action potentials. At the same time, a square wave current was injected into the nerve using two of the electrodes and impedance was measured via another two electrodes (figure 2-3). The impedance was measured whilst injecting various current levels and varying the spacing of the current injection electrodes It was important that the applied current did not change the characteristics of the measured compound action potential. This could be ensured if both measuring electrodes (R1 and R2) were a significant distance from the excitation. Electrode R2 was so distant (12cm) from the stimulus that measurement from this electrode, although affected by the excitation, could not contribute significantly to the overall action potential. Also R1 was proximal to the current injection electrodes. However, the distance of electrode R1 from the excitation current was limited by the need for the excitation electrodes to be as close to the stimulus as possible in order to reduce the effect of dispersion of the compound action potential, which would make the resistance change small at distances more than about 16 mm from the stimulus. The radius of each nerve was about 0.5 mm, and the predicted length constant in previous modelling was about 0.6 mm (Boone, 1995). Thus the closest voltage electrode to the excitation was around 5 length constants from its nearest current electrode and current densities at these distances were proven to be insignificant by Boone.

2.2. Methods

2.2.1. Crab nerve prep

As soon as the crabs were killed, ten walking legs were excised between the ischium and the basis (figure 2-2). The ligaments supporting the joints between the merus and carpus and between the manus and dactyl were divided respectively. By traction on the dactyl, the nerve was pulled free from the leg. A short length of 5/0 surgical silk was then tied to each end of the nerve, the dactyl was removed and the nerve was immersed in crab ringers solution (table 2.1) at approximately 4°C.

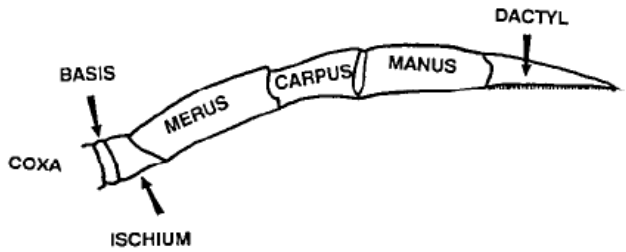

Figure 2-2: Anatomy of crab walking leg

Table 2-1: Composition of crab's Ringers solution.

Electrolyte	***Concentration***
NaCl	460 $mmol.1^{-1}$
$MgCl_2$	27.6 $mmol.1^{-1}$
$CaCl_2$	5.5 $mmol.1^{-1}$
KCl	10.4 $mmol.1^{-1}$

During recordings, the nerve was placed in a square groove 1.5 mm wide by 1.5 mm deep in a block of Perspex (20 cm × 4 cm) (figure 2-3). Electrodes comprised platinum or chloride silver foil, (1.5 mm wide), placed in perpendicular grooves, 1.5 mm wide by 3 mm deep, except for the ground electrode which was 2 mm wide. Since silver is toxic to nerves, all electrodes were made of platinum apart from the measurement electrodes R1 and R2 which were silver/silver chloride in order to yield low noise from the electrode–electrolyte interface. The central 1 cm or so of the electrode grooves near the nerve were filled with Agar equilibrated with Crab Ringer's solution, in order to avoid direct contact of the electrode metal with the nerve. The remaining part of the groove was filled with silicone rubber glue to cover the remaining electrode wire and copper wires soldered to them, which led away to the recording apparatus. The entire array was kept at a temperature of 4 ° C by bathing in ice water. Nine electrodes were used and comprised two for stimulation of the action potential (S1, S2), ground electrode (G), four for injection of the square wave current for resistance measurements (D1–D4 – two were selected at a defined spacing for any one recording) and two for recording the resulting potentials (R1, R2). The spacing between electrode pairs S1–S2, S2–G, G–R1, and D1–D2 was 2 mm; R1–D1 was 3 mm; D1–D3 was 4 mm; D1–D4 was 8 mm and D4–R2 was 100 mm (figure 2-3). These spacing values are between the outer edges of the electrodes.

Once placed within the longitudinal groove, the nerve was immersed in crab Ringer's solution. The nerve was blotted using filter paper at the start of each 1 min recording and then irrigated again as

soon as it was completed.

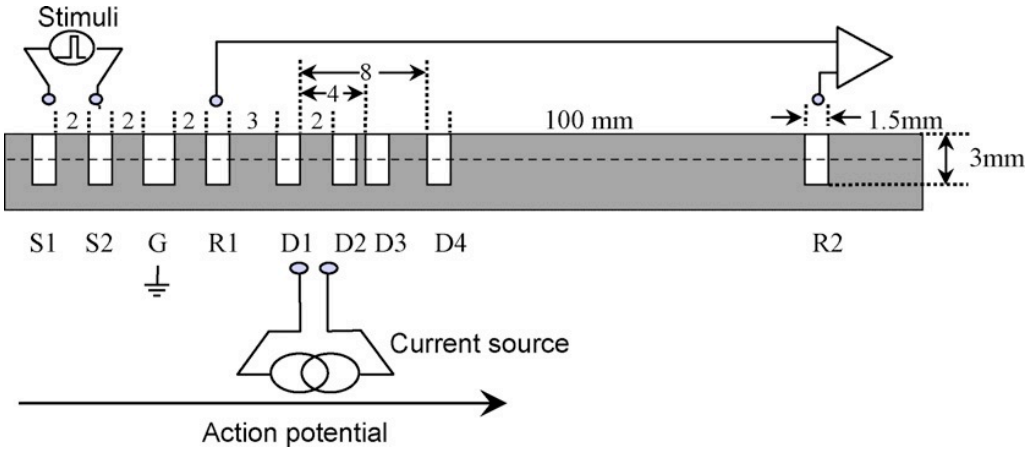

Figure 2-3: Electrode array for crab nerve

2.2.2. Instrumentation

The acquisition system comprised a Neurolog NL900D case (Digitimer, Welwyn Garden City, UK), DC coupled pre-amplifier (NL106, common mode rejection ratio >68 dB @ 50 Hz and input impedance >1 MΩ) set to a gain of 50, low pass filter of 1kHz (NL125/6) and National Instruments (Austin, Texas, USA) analog to digital converter (NI USB 6259) set to ±1 V dynamic range (covering ±20 mV after the pre-amp), 10 kHz sampling rate and with 16 bits resolution enhanced to 18 bits (76 nV) using 16× oversampling (figure 2-5). A custom made communication box and control units controlled the timings of the square wave current source, pulse buffer (NL510A) and stimulus isolator (NL800A, Digitimer) so that each stimulus occurred 150ms after the beginning of each square wave (figure 2-4).

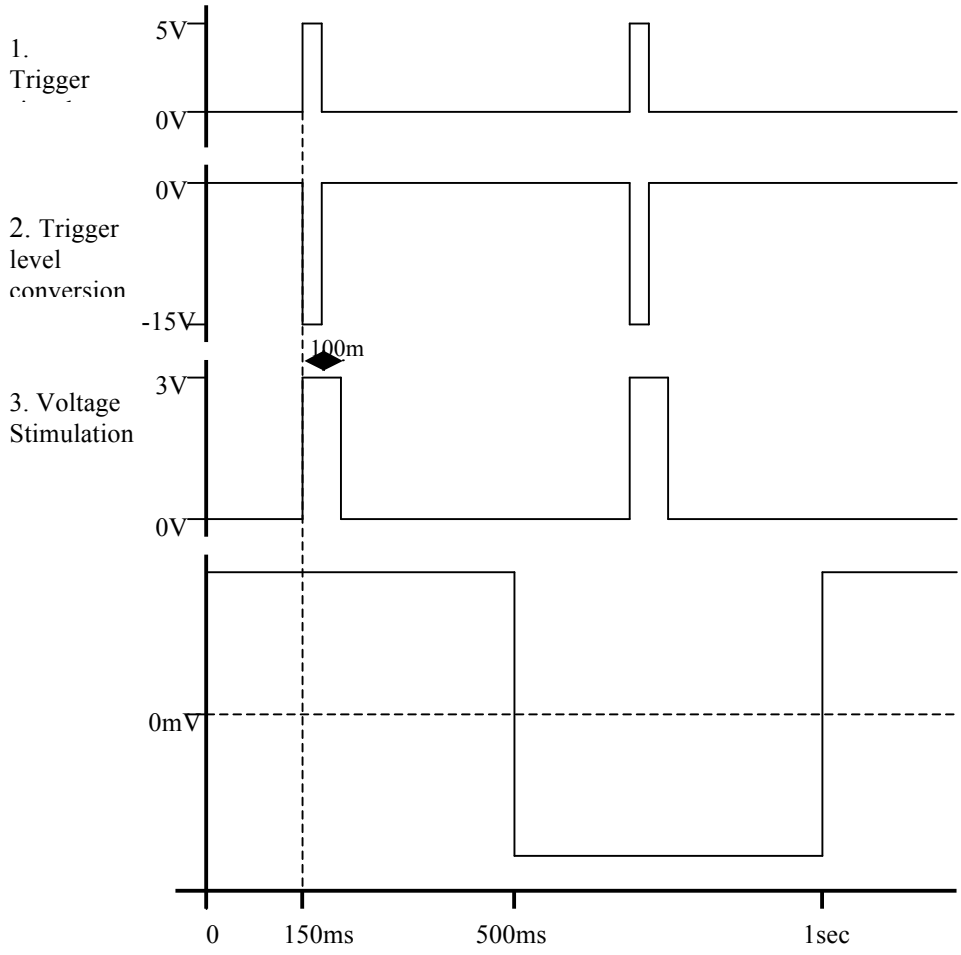

Figure 2-4: Synchronisation of stimulus trigger with carrier

The current source was a custom made isolated bipolar square wave current source with maximal current of 100 µA (Boone, 1995) with a negligible bias of 10^{-5} under typical load of 1 kΩ. Prior to each recording, the current source was calibrated so that the DC offset was <1%. A 0.1 µF capacitor was connected to the output of the current source so that with a typical load of 1 kΩ the bandwidth of the square wave applied to the nerve was limited to approximately 1.5 kHz. Since the power spectrum of a square wave decays with frequency as 1/*f*, 70% of the power was applied below 100 Hz and the remaining 30% were applied up to 1.5 kHz. This square wave resistance measuring current did not produce neural stimulation as the current levels used were less than 25% of the threshold for stimulating neuronal activity.

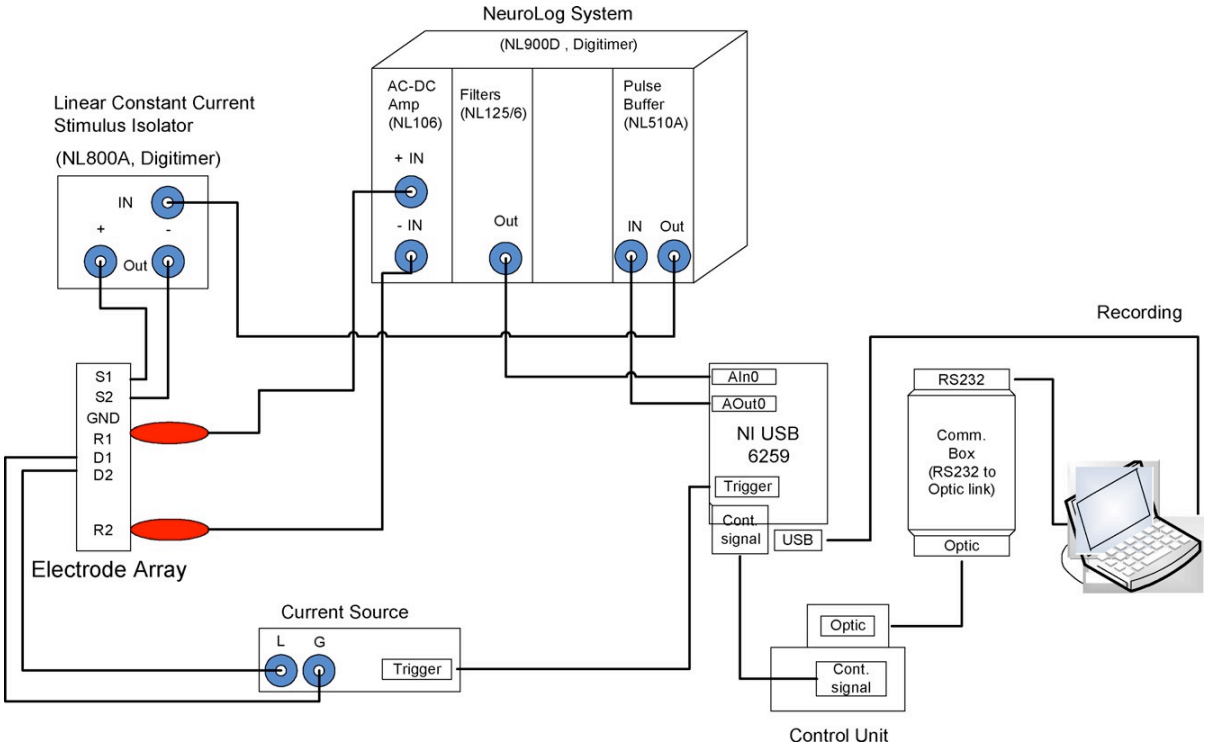

Figure 2-5: Instrumentation setup

2.2.3 Recording

The CAP was initiated using 2 stimuli/s of 3–10 mA and 0.5 ms duration through electrodes S1–S2; the current was adjusted to provide supramaximal stimulation, defined as 50% above the lowest level which produced a maximal largest compound action potential. For studying the effect of current level, the D1–D2 spacing of 2 mm was fixed and 8 recordings with currents of 1, 2, 5, 10, 10, 5, 2 and 1 μA were recorded from 4 nerves. For studying the effect of current drive spacing, the current level was fixed to 2 μA and 6 recordings with spacing of 2, 4, 8, 8, 4 and 2 mm were recorded from 4 nerves. The signals were always recorded through electrodes R1 and R2 and the spacing of 2, 4 and 8 mm was obtained using drive electrodes D1–D2, D1–D3 and D1–D4, respectively.

2.2.4. Extracting the compound action potential and impedance change

Firstly averaging of a minute was necessary to improve the signal to noise ratio (SnR) so the signal is time locked to the evoked CAP. The resulting voltage therefore contained three elements: 1) the square wave carrier, 2) the evoked compound action potential and 3) the change in the square wave due to the transient resistance change. By using a bipolar square wave, addition of the two phases yields the compound action potential and subtraction of the two phases should yield the square wave with the resistance change. However during recordings the amplitude of the CAP decayed and varied unpredictably. Therefore recordings were paired by making a control recording for a minute, which

involved injecting the square wave carrier but not evoking a CAP. Hence by subtraction the CAP and impedance change could be extracted (figure 2-6).

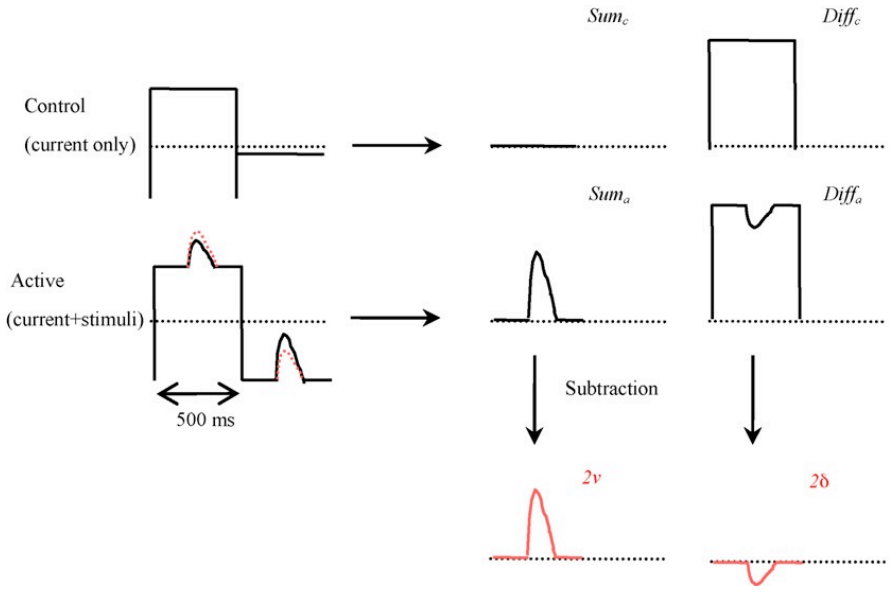

Figure 2-6: Extraction of the impedance change:
Where v is the CAP and b is the resulting voltage produced by the square wave current.

The principle of removing the evoked neurophysiological activity by subtraction rests on the assumption that it remains constant and is unaffected by the current used to record the impedance change. Therefore recordings to find the current level which gave as high a SnR as possible but did not affect the evoked activity were made by injecting different amounts of current and trying to measure any CAP's. Once this threshold current was established, the current used for recordings was set at about 10% of this threshold.

2.2.5 Data analysis

Following averaging and extraction of the impedance changes as described above the maximal impedance changes for each recording was determined. The delay from the stimulus of these peak changes was also measured. The SnR for each recording was estimated as the ratio between the absolute maximal impedance change and the root mean square (rms) of the noise during the pre-stimulus time.

Recordings were further analysed and excluded if there was evidence of external interference causing artifact or if there was an inconsistency of greater than 50% in the magnitude of the resistance changes in recordings from the same nerve in close proximity. These were mainly inconsistencies in the amount of ringers solution blotted from the nerve between recordings.

The remaining valid recordings were then analysed with Student's *t*-test for a negative mean with a critical value of $p<0.05$. One way analysis of variance (ANOVA) was used to test wether the means and delays for different current levels or electrode spacing were different. Data was presented as mean ± 1SD unless stated otherwise.

2.3 Results

A total 57 recordings were made using a total of eight nerves. Four of these recordings were excluded due to external interference and a further five were excluded due to inconsistencies mentioned above. Thus there were 43 technically valid recordings. The SnR of individual recordings was 80±50 which ranged between 5.8-16.1mV.

2.3.1 Compound action potential's (CAP's)

The peak amplitude of the CAP's was 10±2.4mV, which ranged ranged between 5.8-16.1mV (figure 2.7). The delay in the stimulus to the peak of the CAP was 3.3±0.2ms which ranged between 3-3.7ms. This was constant when varying both current levels (p = 0.37; F = 1.07; d.f. = 28) and current drive spacing (p = 0.68; F = 0.4; d.f. = 25). Assuming that the CAP originated from S2, the conduction velocity was 2.6 ± 0.2 m/s.

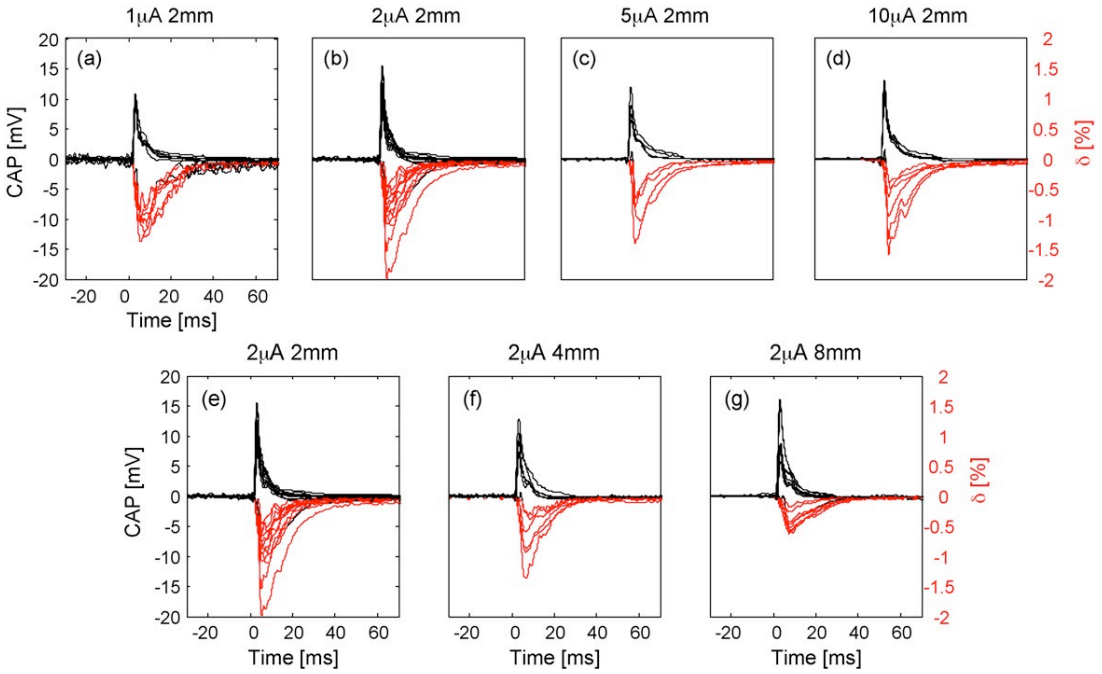

Figure 2-7: CAP's and impedance changes:
Group display showing CAP's (black waveforms and leftmost axes) and the impedance changes (red waveforms and rightmost axes) with varying current (above group) and drive electrode spacing (below group).

2.3.2 The impedance changes

Across all the 43 valid recordings, significant impedance changes of −0.85 ± 0.4% were observed ranging between -0.2 to -2.0%. When using different applied currents no significant change in impedance was observed (p = 0.67; F = 0.53; d.f. = 28; figure 2.8a). When increasing the distance between the current drive electrodes (D1-D2), the measured impedance change decreased significantly from -0.97±0.43% at 2mm spacing to -0.46%±0.16% at 8mm spacing (p = 0.02; F = 4.73; d.f. = 25; figure 2.8b).

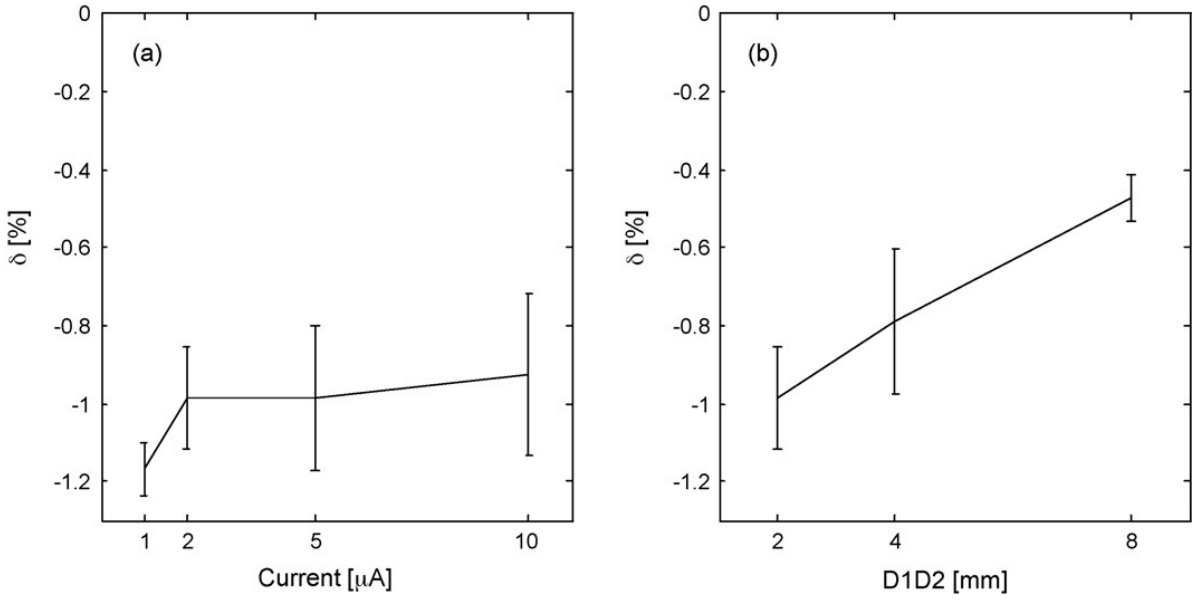

Figure 2-8: Peak impedance changes
Peak changes in impedance with (a) different current levels and (b) different current drive spacing.

The delay in the peak impedance change was 5.7±0.4ms (range 5-6.5ms) and was constant with varying current (p = 0.86; F = 0.25; d.f. = 28; figure 2.9a). However, when increasing the current drive spacing from 2 to 8mm the delay in the peak impedance change increased from 5.7±0.3ms to 7.0±0.4ms (p=7e−9; F=47; d.f. = 25; figure 2.9b).

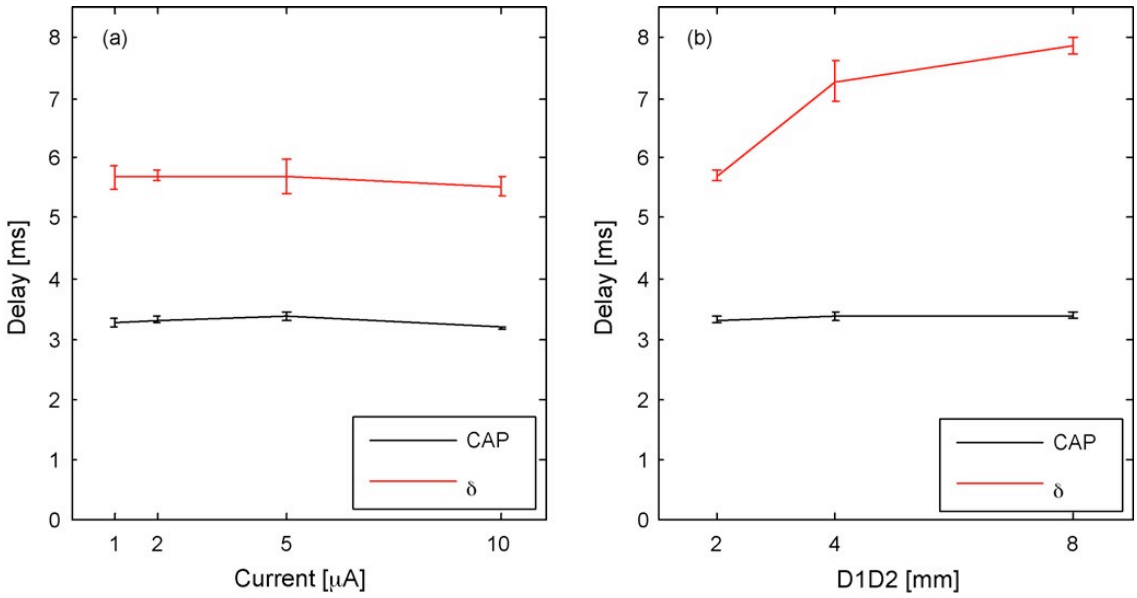

Figure 2-9: Delay of CAP and impedance change.
Delay from stimulus of Peak CAP (black) and peak impedance change (red-δ) with varying current (a) and current drive electrode spacing (b).

The propagation speed of the impedance change therefore was 2.6 ± 0.1 m/s, assuming that the resistance change occurred between the two drive electrodes, 14.75 mm from the mid-point between S2

2.4 Discussion

2.4.1 Summary of method and results.

Modelling studies and consideration of the underlying physiology unfortunately suggested that recording needed to be below 100 Hz (Boone and Holder, 1995; Liston, 2004).

For use on the rat's cerebral cortex this requires recording in the band of the endogenous cortical EEG or evoked potentials. In principle, the endogenous activity therefore would have to be subtracted instead of removing it with filters directly as it is within in the same frequency band. In principle, this could be efficiently achieved using a scheme of summation and subtraction of two phases of a bi-polar square wave carrier (Boone, 1995). The original method of Boone was extended in this chapter by introducing an additional control recording to compensate for variable baseline decay. In addition, a linear model was introduced for deriving the model parameter, their standard error and testing for significant changes.

The method was validated in this study and reproducible peak impedance changes of −0.85 ± 0.4% (n = 43) during CAP of 10 ± 2.4 mV were measured with high SNR (80 ± 50) were recorded. These

were of similar magnitude as those previously measured (Holder 1992b; Boone 1995; Liston, 2004).

2.4.2 Technical issues

Impedance changes were variable under the same conditions on the same nerve. This was mainly due to the inconsistency in the amount of solution blotted between recordings. By leaving different amounts of solution behind following blotting, different amounts of current were shunted through the solution instead of the nerve fibres. Another variable difficult to control was the deterioration in an individual nerve's heath during a recording, thus the recorded amplitude of the CAP would decrease after multiple recordings as more nerve fibres die. The use of a reversed protocol within each nerve (e.g. 2, 4, 8, 8, 4, 4, 2mm spacing) and excluding pairs of identical recordings which had differences of greater than 50% in peak changes helped overcome this problem to some degree. The use of humidified chambers (Shanes 1949) and liquid paraffin (Chapman 1966) have been described as environments for recording on nerves, the method described in this study of irrigation with Ringer's solution appeared better for overall nerve survival and indeed greater overall nerve health was achieved in this chapter than that described in appendix 1.

2.4.3 Effect of varying current on impedance change.

Varying the amount of current did not change the overall recorded peak impedance change (p=0.67). This is in keeping with previous modeling and the current amplitudes in this study did not stimulate the nerve in order to interfere with the compound action potential.

2.4.4 Effect of varying current drive electrode spacing on impedance change.

Peak impedance changes decreased with increasing drive electrode spacing (p=0.02). cable theory also predicts that as the distance between current injection (D1-D2) increases, the percentage impedance change should decrease. This is beacause as D1-D2 increases, the resistance will also increase as the current travels further (figure 2-12). Therefore from the equation V =IR, the amplitude of the square wave will increase as D1-D2 increases. Therefore the change in impedance will be a smaller percentage of the amplitude of the square wave.

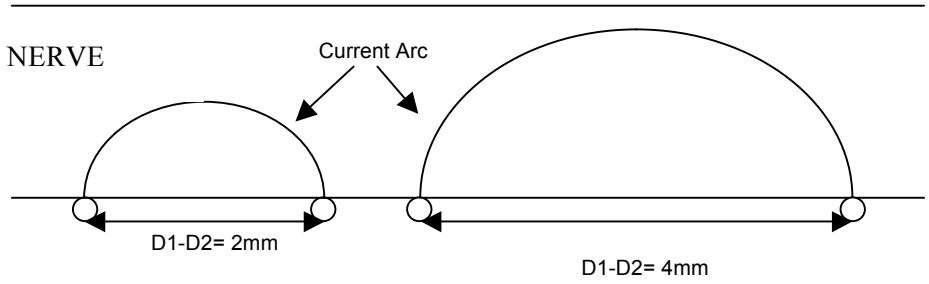

Figure 2-10: Effect of increasing D1-D2 on current path

2.4.5 Implications and further experiments

This study has shown that with this new hardware configuration and described method, reproducible impedance changes can be recorded during evoked neuronal activity, which are in keeping with previous work. Previous experiments were carried out on the cerebral cortex of anaethetised rats to record impedance changes during evoked responses using the same square wave carrier (Boone 1995). However, using this carrier, were of similar size to the background ECoG activity. Therefore experiments with a low frequency sine wave carrier and the above validated hardware setup used on crab nerves were carried out (chapter 3) with a view to using the same carrier and hardware setup on the rat cerebral cortex.

3. Measuring electrical impedance changes in unmyelinated crab nerve using a low frequency carrier

3.1 Introduction

3.1.1 Orientating Paragraph

In the previous chapter, studies indicated that impedance changes of near 1% occurred during the compound action potential in crab nerve. In a separate human study, (O Gilad & Holder 2009) it was found that it was not possible to image impedance changes in human subjects with scalp electrodes with this square wave current because the signal was obscured by the uncorrelated EEG. Biophysical analysis indicated that a greater signal to noise ratio could be achieved by recording with a sine wave a higher frequencies. This study was therefore undertaken to determine the size of the impedance changes and validate the instrumentation, using crab nerves again as a test arrangement.

Crab nerves were placed in a newly designed casing of electrodes, and stimulated to generate compond action potentials (CAP). Using a low frequency carrier (125-825Hz), impedance recordings were made whist varying current, frequency, phase and current drive electrode spacing. Impedance changes (δz) were successfully recorded at all settings with no change in δz when varying the current as predicted. The impedance change however decreased with increasing frequency and increasing current drive electrode spacing.

3.1.2 Background

Using a 1 Hz square wave carrier, impedance changes in the crab nerve have been recorded (chapter 2); (Gilad et al. 2009). However the instrumentation was suboptimal as frequent blotting of the nerve was required which led to inconsistencies between recordings (appendix 1). When using this carrier on the human scalp during visual evoked potentials, impedance changes of 0.0010 ± 0.0005% were recorded in 16 recordings over 6 subjects (O. Gilad & Holder 2009). However a signal to noise ratio of 2:1 was not sufficient enough for imaging without impractically long recording times.

Recording lies within the bandwidth of endogenous nervous activity: Electro- encephalogram (EEG), electrocorticogram (ECoG), EP or compound action potential, so that the voltages recorded from the injected square wave for impedance recording are mixed with the endogenous potentials. Uncorrelated signals, such as the EEG, may be reduced by averaging, whereas correlated ones, such as the evoked potentials, may be removed by subtraction.

The original modelling indicated that recording should be as near to DC as possible (Boone & Holder 1995a), so that the current remains in the extracellular space under resting conditions as it cannot

cross the capacitive cell membrane until ion channels open during an action potential (figure 3-1). Therefore a higher signal can be achieved. But consideration of the above main noise source (ECoG) led to the unexpected conclusion that recording at a higher frequency of a few hundred Hz may produce a higher signal-to-noise ratio (SNR), as the power of the ECoG or EEG falls off more rapidly with frequency than the resistance change. With recordings made at 225Hz compared to dear DC, for example, the resistance change during depolarisation fell by 10 X to 0.1% but the background ECoG fell by 1000 X to 1μV, thus the SNR is greater.

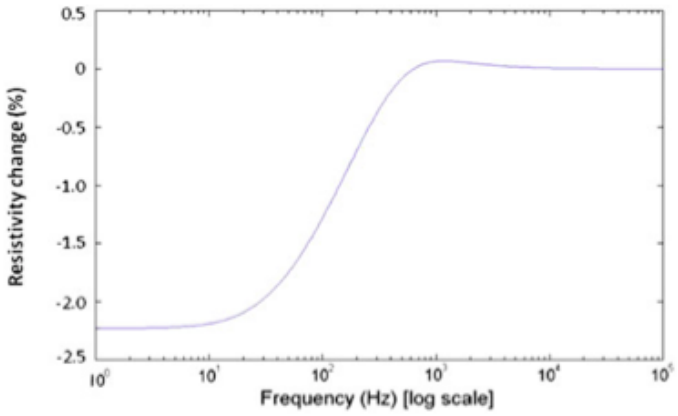

Figure 3-1: Predicted resistivity change versus frequency (Boone 1995, Liston 2004).

3.1.3 Purpose

The purpose of this study was to develop and refine this method of impedance measurement (with a low frequency sine wave carrier) using the compound action potential in crab peripheral nerve, in which the resistance change occurs contemporaneously with the compound action potential.

The specific aims of this study were to examine the following:

1. The effect of varying current levels on the impedance change. As explained from cable theory in chapter 1 and demonstrated in chapter 2 this should not effect the size of the impedance change however higher currents of around 20μA can be excitatory (appendix 1). Higher currents are expected to yield a better SNR and so the optimum current could be determined.
2. The effect of varying frequency on the size of the impedance change and overall SNR. As mentioned above, currents of higher frequencies are expected to cross the capacitive cell membrane at rest thus reducing the size of the overall impedance change however the overall

background noise will also be reduced. Thus the optimum frequency for the best possible SNR could be determined.

3. The effect of current phase on the impedance change. This is not expected to alter the size of the impedance change. However higher current levels may distort the waveform due to stimulating neural activity and as the phase varied by 180° and so in theory the evoked activity could have been distorted differently.
4. The effect of current drive electrode spacing. As demonstrated in chapter 2 by increasing current drive electrode spacing the overall resistance between electrodes should increase and so the overall change in impedance should decrease.

3.1.4 Experimental Design

Nerves from the walking leg of the edible crab (Cancer Pegurus) were placed on a newly designed electrode array described in chapter 2. They were stimulated to generate a compound action potential. Carriers ranging from 125-825Hz were used whilst also varying the amount of current injected, the phase and the distance between the current injection electrodes.

3.2 Method

3.2.1 Nerve preparation

The nerves from the walking legs of the crab (Cancer Pegurus) were dissected free and stored as described in chapter 2.

The nerve was placed in a square groove 1.5 mm wide by 1.5 mm deep in a blockof Perspex (20 cm × 4 cm). Electrodes comprised platinum or chloride silver foil, (1.5 mm wide), placed in perpendicular grooves, 1.5 mm wide by 3 mm deep, except for the ground electrode which was 2 mm wide (Figure 3-2). Since silver is toxic to nerves, all electrodes were made of platinum apart from the measurement electrodes R1 and R2 which were silver/silver chloride in order to yield low noise from the electrode–electrolyte interface. The central 1 cm or so of the electrode grooves near the nerve was filled with Agar equilibrated with Crab Ringer's solution, in order to avoid direct contact of the electrode metal with the nerve. The remaining part of the groove was filled with silicone rubber glue to cover the remaining electrode wire and copper wires soldered to them, which led away to the recording apparatus. The entire array was kept at a temperature of 4 ◦ C by bathing it in ice water.

Nine electrodes were used and comprised two for stimulation of the action potential (S1, S2), a ground electrode (G), four for injection of the sine wave current (D1–D4 – two were selected at a defined spacing for any one recording) and two for recording the resulting potentials (R1, R2). The spacing between electrode pairs S1–S2, S2–G, G–R1, and D1–D2 was 2 mm; R1–D1 was 3 mm; D1–D3 was 4 mm; D1–D4 was 8 mm and D4–R2 was 100mm. These spacing values are between the

outer edges of the electrodes.

Once placed within the longitudinal groove, the nerve was immersed in crab Ringer's solution, the composition of which is described in chapter 2.

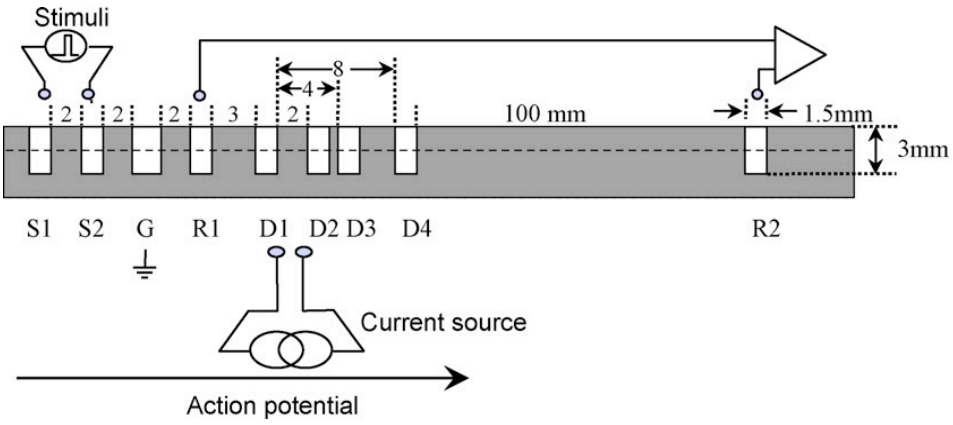

Figure 3-2: Electrode arrangement in perspex container

3.2.2 Instrumentation

Electronic instrumentation comprised an ultra low noise programmable constant current source which could produce a sinusoidal waveform from 1 Hz to 1 kHz with an amplitude of 0.1–100 μA, the 'UCL-CS1'. This was constructed from a FPGA (EP1K50, Altera, USA), programmed as a main controller and digital waveform generator. It received commands from a PC and produced timing and control signals to the acquisition system. The sine waveform was digitally generated in a ROM which contained 2,000 samples of sine waveform data which were read by the FPGA and able to generate frequencies from 125 to 825 Hz. The DC component and high frequency clock noise were rejected by a band pass filter (10 Hz– 10 kHz). There were two independent current sources to supply 0.1–10 μA or 10–100 μA. These comprised a floating Howland current source, which contained digitally controlled potentiometers (DS1267-010 and DS1267-050, Dallas, USA) to equal provide equal resistance ratios. Power was supplied from batteries. The output impedance was over 1 MΩ. Voltages were recorded with a 1 channel Neurolog pre-amplifier (NL106, Digitimer, UK), filter unit (NL125, Digitimer, UK), with a gain of 50 and bandpass of DC to 10 kHz. Data were sampled at 160 kHz by a National instruments 16 bit data acquisition system set to oversample and so provide 18 bit resolution (NI USB 6259, National Instruments, USA). The system was optically isolated and controlled by a Windows PC. The current source and voltage measurement unit operated synchronously. A control signal generated from UCL-CS1 was passed to the NI data acquisition system which in turn produced a timing control signal for nerve stimulation using a driven buffer (NL510) and isolated stimulator (NL800A, Digitimer, UK) which was a battery powered and opto-coupled. All systems operated with the same clock (figure 3-3).

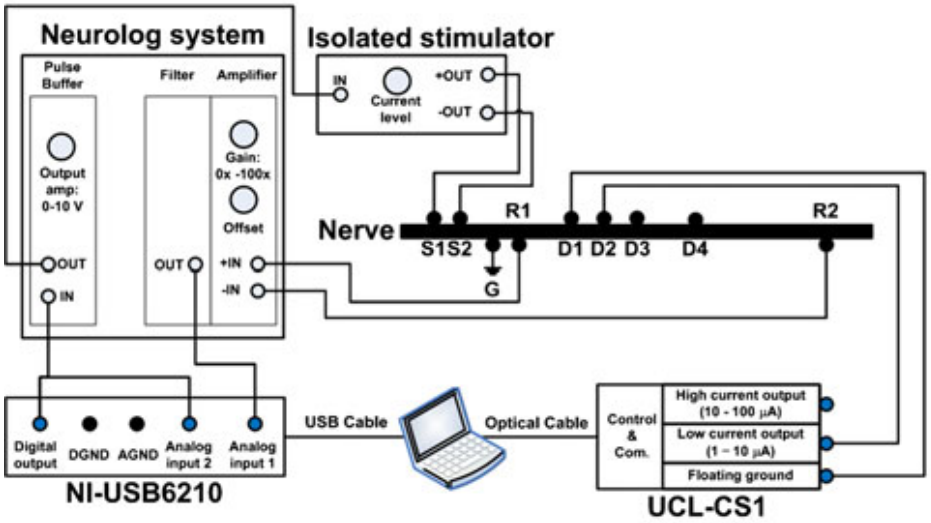

Figure 3-3: Instrumentation for data acquisition

Compound action potentials were produced at 2 stimuli/ s by uni-polar pulses of approximately 3 mA and 500μs duration through electrodes S1–S2 to produce supramaximal stimulation. 225 recordings were made in 15 different nerves at frequencies of 125,175, 475 and 825 Hz and currents of 0.5, 1, 2, 5 and 10 μA for drive electrode spacing of 2 mm, and with spacing of 2, 4 and 8 mm with applied current of 5μA and all frequencies. In three nerves, recordings were also made with a current phase shift of 90° at all frequencies, at 175 Hz for drive electrode spacing of 2 mm and current of 5 and 10μA. The frequencies were chosen as multiples of 25 Hz to be far from any harmonics of 50 Hz mains noise which were filtered out during the analysis.

3.2.3 Resistor and agar phantom validation

The UCL-CS1 was tested by recording from a 1.5 kΩ resistor to which the drive and record circuits were connected in a four terminal mode with a parallel 430Ω and 22 nF and series 200Ω resistor to simulate electrode impedance. A reed relay was used to switch in a resistor of 330 kΩ in parallel with the 1.5 kΩ for periods of 20 ms to produce a transient resistance decrease of 0.38%. Noise was examined with the groove of the crab nerve array filled with agar equilibrated with crab Ringer's solution. Recording in both cases was with a current of 1 μA at 125 Hz with averaging over 1 min.

3.2.4 Method for calculating the impedance change

Compound action potentials were produced every 0.5 s. A constant current sine wave was applied which was in phase for the first 500 ms segment and antiphase for the next. 60 or 300 such paired epochs comprised one recording and were averaged. The two 500 ms phases were summed to produce

the compound action potentials. The impedance modulus was produced by subtracting the first and second segment. The modulated carrier was then demodulated by: (1) the signal from the subtracted segments was band pass filtered with a bandwidth of 250 Hz to eliminate most of the residual noise at the EEG band (<100 Hz) left after the averaging as well as high frequency instrumentation noise. (2) Then, demodulation was performed by calculating the absolute values and phases on an analytic version of the signal, created using the Hilbert transform. The modulus of the resulting change was taken to be the real component.

3.2.5 Data analysis

The entire dataset of 225 recordings was inserted into a four way analysis of variance to evaluate the effect of frequency, current, spacing and phase of applied current. Analysis indicated an effect of the highest current applied, 10 μA. Results are presented as mean ± 1SE.

3.3 Results

3.3.1 Validation of experimental setup

With the switched resistor network, a resistance change of -0.38% was recorded as 0.36% in peak amplitude. The effects of filters in the recording circuit were examined with computer simulation. A square wave voltage change of -0.12% lasting 20 ms was recorded with a peak change of -0.10% after filtering. With the crab nerve recording block filled with agar, the noise was less than 0.95 μV. With injection of 125 Hz, 1 μA current into the agar, with R1–R2 spacing of 2 mm, the noise was 0.4 μV, equivalent to 0.05%.

3.3.2 Impedance recordings.

There were consistent significant decreases in impedance in all nerves tested with a similar time course to the compound action potential (225 recordings in 15 nerves) (Figure 3-4).

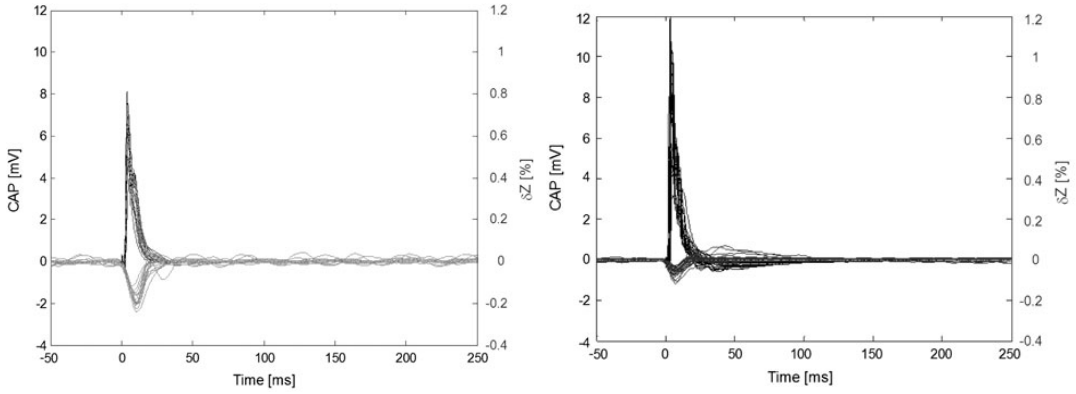

Figure 3-4: Action potentials and impedance change
Examples of compound action potential (positive, black) and associated resistance change (δZ, negative, grey). ***Left:*** *125 Hz, n = 16 in 1 nerve. Peak δZ was -0.18 ± 0.002%, δΦ 0.10 ± 0.002° and CAP 6.2 ± 0.07 mV.* ***Right:*** *825 Hz, n = 30 in 1 nerve. Peak δZ was -0.06 ± 0.0007%, δΦ 0.18 ± 0.0007° and CAP 8.4 ± 0.08 mV (2 mm R1-R2 spacing, 2 μA, zero phase in both cases)*

δZ did not vary significantly with applied current of 0.5–5 μA (P = 0.25) but decreased at all frequencies with 10 μA (Figure 3-5, P <0.001).

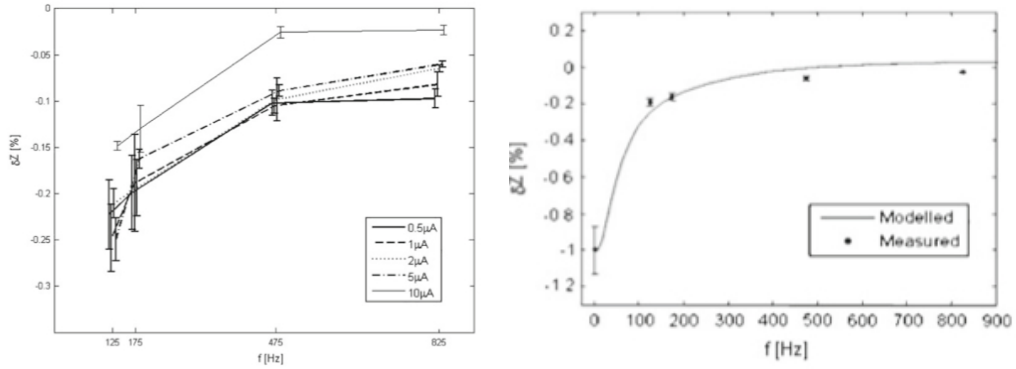

a) *(b)*

I [μA]	0.5	1	2	5	10
Hz					
125	-0.22±0.04/4(2)	-0.25±0.04/4(2)	-0.21±0.02/20(3)	-0.25±0.02/16(6)	-0.148±0.005/4(1)
175	-0.20±0.04/4(2)	-0.19±0.05/4(2)	-0.19±0.03/4(2)	-0.16±0.01/16(6)	-0.13±0.03/4(1)
475	-0.10±0.01/4(2)	-0.11±0.01/4(2)	-0.10±0.02/4(2)	-0.09±0.01/17(6)	-0.03±0.01/4(1)
825	-0.10±0.01/4(2)	-0.08±0.01/4(2)	-0.064±0.004/34(3)	-0.060±0.003/18(6)	-0.023±0.005/4(1)

(c)

Figure 3-5: Impedance results:
Impedance changes (δZ) in crab nerve during the compound action potential. (a): Changes with frequency for different applied currents (mean ± 1 SE, recordings (nerves)). (b): Comparison of experimentally recorded δZ over frequency (5 μA, D1– D2 2 mm) measured in this study and at 1 Hz with predictions from biophysical modelling normalised to the measured change at 1 Hz. (c): table summarizing impedance changes at the above mentioned frequencies and current levels.

For example, with applied current of 5 μA and R1–R2 spacing of 2 mm, δZ was -0.25 ± 0.02, -0.16 ± 0.01, -0.09 ± 0.01 and -0.06 ± 0.003% for applied frequencies of 125, 175, 475 and 825 Hz,

respectively. δZ also decreased with increasing spacing of the drive electrodes for all four applied frequencies and applied current of 5 μA (Figure 3-6, P = 0.18). There was no significant change in δZ with applied phase of 0 or 90° (P = 0.97). Both the decrease in δZ with frequency and recording electrode spacing were in concert with biophysical modelling previously described (Liston 2004).

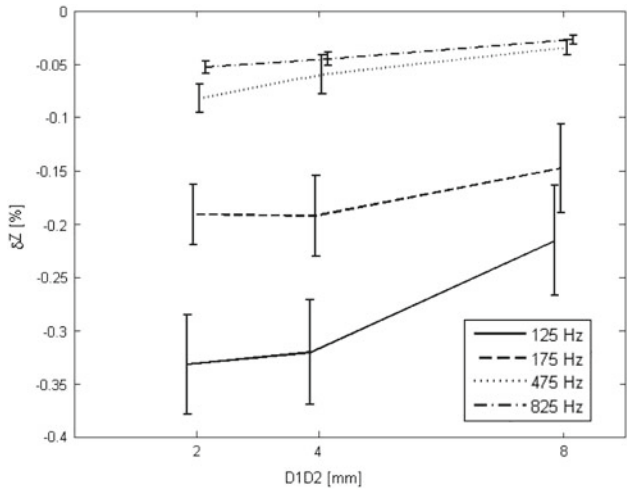

Spacing [mm]	2	4	8
Frequency [Hz]			
125	-0.33±0.05	-0.32±0.05	-0.22±0.05
175	-0.19±0.03	-0.19±0.04	-0.15±0.04
475	-0.08±0.01	-0.06±0.02	-0.03±0.01
825	-0.05±0.01	-0.05±0.01	-0.027±0.004

Figure 3-6: Effect off electrode spacing with each frequency:
Figure 3-6: Impedance changes (δZ) in crab nerve during the compound action potential. Effect of electrode spacing between drive electrodes, D1 and D2 on δZ [%] for each frequency (mean ± 1 SE, recordings (nerves); all n = 4 in 2 nerves except 2 mm/475&875 Hz, n = 5)

3.4 Discussion

3.4.1 Summary of results

A method was described above for measuring impedance changes in the walking leg nerve of a crab (Cancer pagurus) during a compound action potential using a sinusoidal carrier. Reproducible changes of 0.25% at 125 Hz and 5 μA were observed which decreased to 0.06% at 825 Hz. They were constant with applied current up to 5 μA and with phase and their frequency response and variation with recording electrode spacing were as anticipated from modeling (Liston 2004). As expected these changes were similar to that with a 2Hz square wave carrier (Chapter 2).

3.4.2 Technical Issues

The new electrode design allowed better consistency between recordings than that described in chapter 2, as frequent blotting of the nerve was not required. This design allowed the nerve to be kept at 4° Celcius throughout the recordings, and its length to have enough ringers solution around it to last the duration of the experiments.

3.4.3 The effect of current

A better signal to noise ratio (SNR) is expected at higher current levels provided that the applied current does not effect the neuronal activity. At each frequency, the impedance change when using 0.5-5μA were not significantly different. When injecting 10μA, there was a decrease in the impedance change. This was noted at all carrier frequencies. It is therefore likely that at above 5μA, graded potentials (chapter 1) are being triggered within axons immediately adjacent to the electrodes and hence affecting the recorded action potential hence altering the recorded impedance change. This will need to be considered and investigated when experimenting on rat's cerebral cortex in order to identify the optimal current level for impedance recordings and indeed for imaging. Due to current dispersion from the electrodes this effect may wear off several mm away from the electrodes and hence it may be possible to inject a higher current on the cerebral cortex of the rat before the evoked response in effected.

3.4.4 The effect of Phase

There was no change in δZ with different phases of the sinusoidal wave (0-90°). Hence the phase of the applied current has no effect on the impedance change as it did expected. There was no recorded distortion in the waveform as proposed above.

3.4.5 The effect of Frequency

Higher frequency carriers should yield a better SNR. However, there is an expected decrease in δZ with increasing frequency as some current will cross the membrane at rest with higher frequencies. The results did indeed show a decrease with increasing frequency, in keeping with biophysiological modelling (Liston, 2004). With the rat cortex this will be a more significant problem to tackle due to the background ECoG activity, when selecting the optimal frequency.

3.4.6 The effect of applied current electrode spacing

Also as described in the biophysiological modelling, δZ decreased as D1-D2 increased. This is expected as with increasing length of nerve that current must travel through, there is an overall increase in resistance. 2mm is hence the optimum distance.

3.4.7 Future work.

Impedance changes in the crab nerve during a compound action potential can be recorded with a sinusoidal carrier. The same method described above has thus been used on the cerebral cortex of the anaesthetised rat (chapter 4) with an appropriate electrode array to measure the impedance change during a sommatosensory evoked potentials. The optimum current and frequency was then determined to optimise the chance of imaging neuronal depolarisation in the brain.

4. Measuring electrical impedance changes on the cerebral cortex of anaesthetised rats using a low frequency carrier

4.1 Introduction

4.1.1 Orientating paragraph

In this chapter the experiments for recording impedance changes on the cerebral cortex of the anaesthetised rat by using a low frequency (125-1225Hz) carrier are described. The rats underwent forepaw stimulation in order to generate somatosensory evoked potentials (SSEP's). These were recorded with a newly designed array of electrodes placed directly on the cerebral cortex. Via the array of electrodes, different current levels at different frequencies were injected into the rat cortex and the resulting voltages were measured, thus allowing calculation of the resulting impedance change (δZ) during the SSEP's. Reproducible impedance changes were recorded at all the currents and frequencies investigated, with the optimum SNR (>50) with 50μA at 225Hz.

4.1.2 Background

In this thesis the method for recording impedance changes during compound action potentials on the unmyelinated nerve of the walking leg of the edible crab with a 2Hz square wave carrier was first attempted in appendix 1 unsuccessfully then successfully in Chapter 2; (Gilad et al. 2009). On previous human scalp and rat cerebral cortex experiments however, the SNR was sub optimal and as a result reproducible impedance changes were not recorded (Boone & Holder 1995b; O. Gilad & Holder 2009).

Part of the SNR dilemma was because of background ECoG activity of the rat recorded by the electrodes when recording using a near DC square wave carrier. If this were to be reduced by long averaging, the time required would be impractical for imaging, which is the end goal of this thesis. The applied current also had to be low enough as to not interfere or alter the SSEP, also attributing to a poor SNR.

The original modelling indicated that recording should be as near to DC as possible (Boone, 1995), in order to deliver the largest possible signal, but as explained in chapter 3, consideration of the above main noise recording at a higher frequency (125-825Hz) may produce a higher signal-to-noise ratio (SNR), as the power of the ECoG or EEG falls off more rapidly with frequency than the resistance change.

In order to tackle the SNR problem, a new method of recording the impedance change during neuronal depolarisation using a low frequency sinusoidal wave carrier had to be validated on the unmyelinated crab nerve (chapter 3); (Oh et al. 2011). Here reproducible changes were seen when recorded at 125-825Hz. At each frequency, varying currents up to 5μA did not affect the size of the change, which is in keeping with biphysiological modelling (Liston, 2004), but when recording at 10μA, the size decreased. This could be attributed to the applied current causing excitation of the axons immediately adjacent neurones to the electrodes, thus interfering with the recorded action potential and impedance change.

This factor will need consideration when applying this method to the rat cerebral cortex.

4.1.3 Purpose of this study

The purpose of this study was to assess whether reproducible impedance changes during neuronal depolarisation on the cerebral cortex of the anaesthetised rat could be measured whilst using a low frequency carrier (125-1225Hz).

This study also aimed to assess the effect of the following variations on the measured impedance change:

1. Frequency
2. Applied Current

Then the study aimed to identify the frequency and current level that yields the optimum signal-to-noise ratio (SNR).

4.1.4 Experimental Design

The rats were anaesthetised, a craniotomy was performed and a new array of 29 electrodes was placed directly onto the cerebral cortex. This was custom made and described below. The forepaw was stimulated electrically to generate SSEPs. Recordings were then made with carriers of varying currents and frequency were applied in order to measure raw impedance change during the SSEP.

4.2 Method

4.2.1 Animal preparation

Anaesthesia was induced in an induction chamber ventilated with 4% halothane, and a 70:30 mix of oxygen and nitrous oxide. Subsequently, a tracheostomy was performed to introduce an endotracheal

tube and the halothane reduced to a maintenance concentration between 0.5 to 1.5%. Electrocardiography (ECG) leads were attached to the paws, and the femoral artery and vein were cannulated. The arterial cannula was used to monitor the arterial blood pressure and measurement of arterial blood gases (ABGs). Additionally, the rat's core body temperature was maintained at 37 $^{\circ}$C with the use of a heat mat and rectal thermometer. To minimise movement artefact related to ventilation, mechanical ventilation and bilateral pneumothoraces were performed, and so paralysis, via the administration of pancuronium bromide, was induced. Following these preparatory procedures, the rat was placed in a stereotactic frame and a craniotomy of approximately 8 mm × 8 mm was performed.

A new array of electrodes was placed on the cortex (figure 4-1). A layer of cling film was then placed over the array, thus trapping moisture over the cerebral cortex and therefore frequent irrigation with artificial CSF was not necessary.

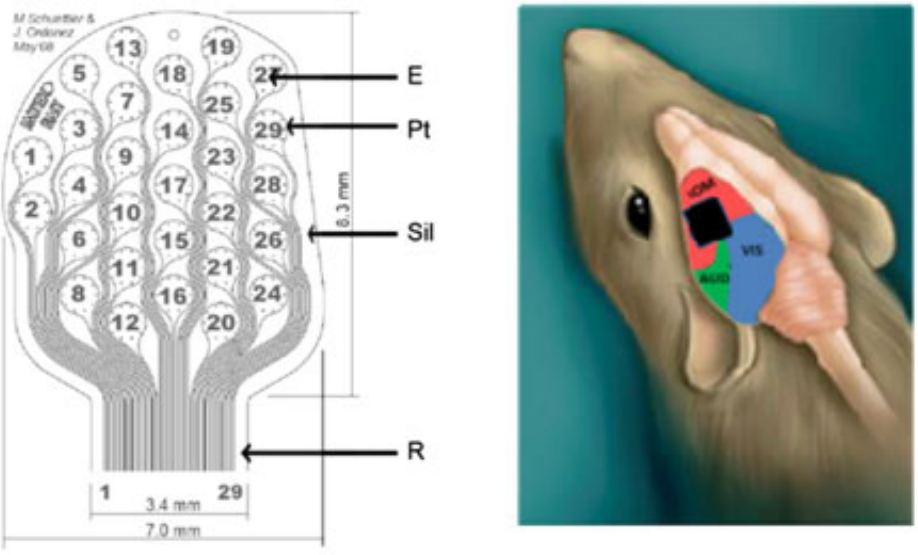

Figure 4-1: Design of electrode array:
E electrode site, Pt platinum, Sil silicone rubber substrate, R ribbon cable and diagrammatic illustration of its position on exposed rat cerebral cortex.

4.2.2 Instrumentation

The hardware including the current source was identical to that described in chapter 3, but a 32 × 8 analogue switch array was added to the front stage to permit addressing of any pair of 29 electrodes in the electrode array. The output impedance of current source was over 1 MΩ. The same isolated stimulator (NL800A, Digitimer, UK) was employed to produce somatosensory stimulation. Recording was performed with a 32 channel EEG acquisition system (SD32R, Micromed, Italy) which was

modified to provide a dynamic range of 102.4 mV. However when assessing the effect of varying frequencies, described below, the Neurolog aquisition system (NL106, Digitimer, UK) described in chapter 3 was used as it allowed for recording at higher frequencies but with a single channel. Sampling was with 22 bit A/D at 2 kHz per channel and hardware filters of 0.15–570 Hz (Figure 4-2).

A new custom designed electrode array, 8 × 8 mm was placed on exposed cortex. This was constructed of platinum foil on a silicone rubber backing which had been laser cut to provide 29 circular electrodes, 0.6 mm in diameter, hexagonally arranged with a centre-to-centre distance of 1.2 mm (Schuettler et al. 2008). The electrodes were platinized to reduce contact impedance and noise from the electrode– electrolyte interface (Figure 4-1).

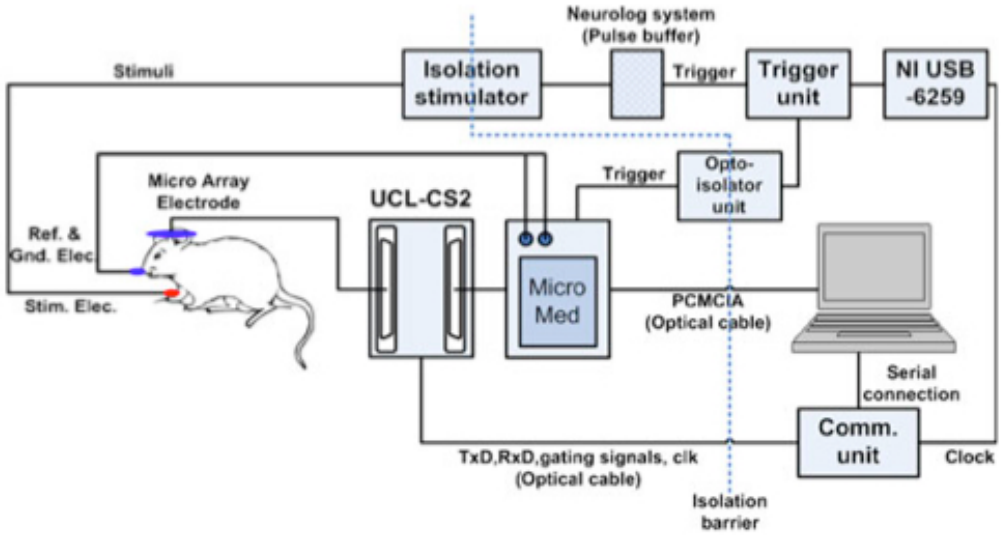

Figure 4-2: Instrumentation for recording on rat cerebral cortex

A Faraday cage was then placed around the rat to help reduce noise from the surrounding mains.

4.2.3 Recordings

Somatosensory evoked responses were produced by stimulation of the contralateral forepaw with pulses 100 μs in duration and 5–10 mA at 2 Hz. Cortical evoked potentials were first recorded by averaging 128 responses. The electrode array was repositioned if needed so that the maximum response was near the centre of the array. Impedance was then recorded by averaging for 5 minutes with evoked response stimulation at 2 Hz. Current was injected from adjacent electrodes located where the SSEP was maximal in the preliminary SSEP recordings and voltages were recorded from the remaining 27 channels. For the effect of frequency, 51 recordings were taken from six rats, all

with current of 5 μA. Frequencies tested were 125, 225, 325, 625 and 1225 Hz with single channel recordings using the Neurolog pre-amlifier (NL106, Digitimer, UK). For the effect of current, 64 recordings were taken from 11 rats, all with a frequency of 225 Hz. Currents tested were 2, 5, 10, 20, 50 and 100 μA.

The impedance change was calculated as described in chapter 3.

4.2.4 Data Analysis

For rat cortical recordings, the effect of current and frequency were analysed with one way Anova with repeated measures. Results are presented as mean ± 1SE.

4.3 Results

4.3.1 Validation of experimental setup

As described in chapter 4, with the switched resistor network, a resistance change of -0.38% was recorded as 0.36% in peak amplitude. The effects of filters in the recording circuit were examined with computer simulation. A square wave voltage change of -0.12% lasting 20 ms was recorded with a peak change of -0.10% after filtering.

4.3.2 Evoked potentials.

Evoked potentials of 150–800 μV were recorded which lasted for up to 200 ms with an N12 peak (figure 4-3). These had the highest amplitude over the appropriate aspect of the cortex.

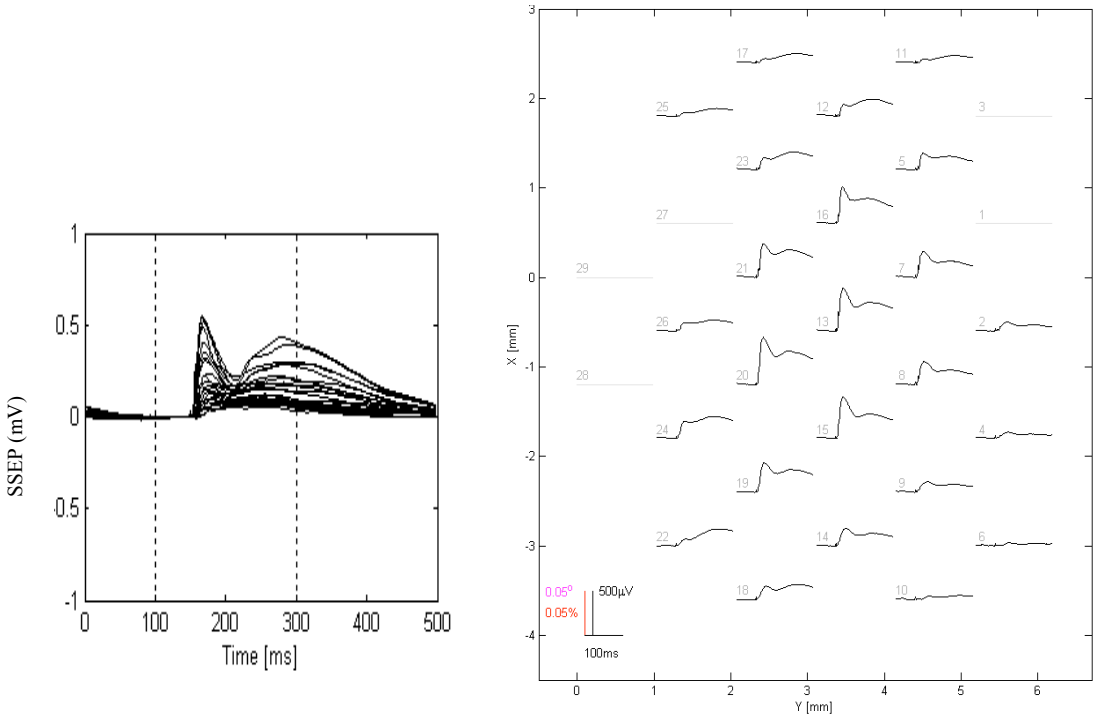

Figure 4-3: A typical SSEP recording
Left recording from each channel overlapped showing a channel of greatest amplitude of 0.5mV for this recording. Right each individual SSEP's displayed over its associated channel the electrode array over the cortex.

4.3.3 Impedance recordings

Reproducible resistance and phase changes could be observed with a distribution around the electrodes used for current injection, with an appropriate pattern for the greatest current density. These could be observed reliably in approximately one third of electrodes and had a time course which corresponded to the evoked potential, peaking at about 12 ms (figure 4-4).

The signal to noise increased with applied current. With an applied current of 50 μA, the SNR was approximately 50 in most channels (figure 4-4).

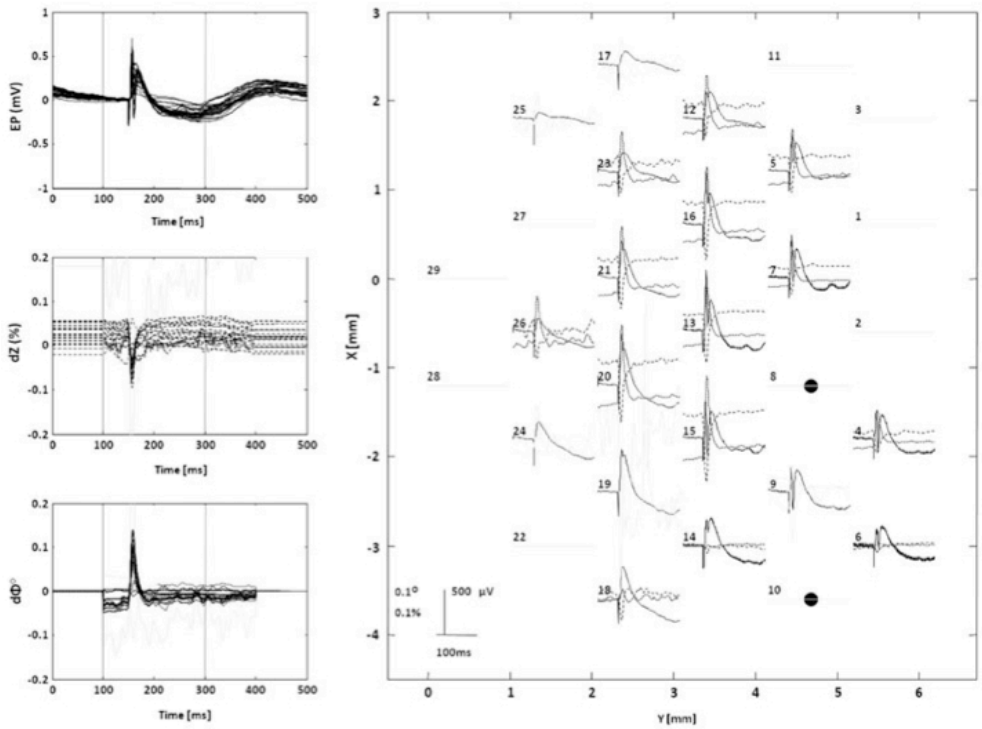

Figure 4-4: SSEP, impedance and phase displayed topographically
Left: Superimposed from all channels: evoked potentials (EP, solid), impedance change (δZ, dashed), phase change (δΦ, dotted). Right: EP, δZ and δΦ displayed topographically over the cortex. Current, 225 Hz, 50 µA, was applied through electrodes 8 and 10 (filled circles). Peak evoked activity (EP, solid line) may be seen from electrode 13 (centre of display). Electrodes with >0.05% noise are greyed out. Resistance changes of up to 0.2%, SNR ~50, may be seen with a similar distribution of amplitude to the evoked potentials

4.3.4 Effect of Frequency

The peak changes were -0.074 ± 0.01, -0.070 ± 0.006, -0.027 ± 0.005, -0.022 ± 0.003 and -0.01 ± 0.01% for current applied at 125, 225, 325, 625 and 1225 Hz (n = 51 in six rats), respectively, (figure 4-5). The size of the changes significantly decreased with increased frequency (P = 0.00001). The SNR was best at 225Hz (with 50µA) (figure 4-4).

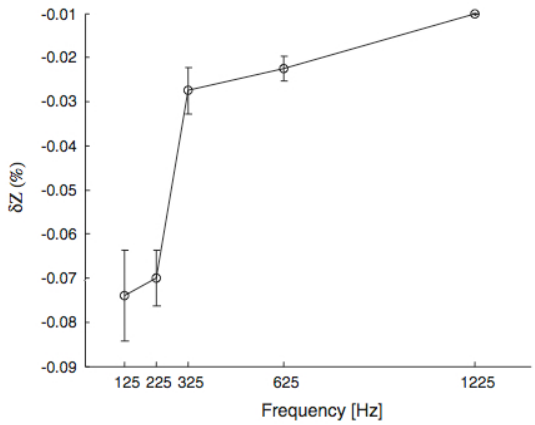

Figure 4-5: Change in δZ during evoked responses in rat cortex with varying frequency.

4.3.5 Effect of Current

The changes were constant with applied current up to 50 μA (n = 64, 11 rats, 225 Hz, P = 0.68) but decreased, although not significantly, with current injected at 100 μA (P = 0.14) (figure 4-6).

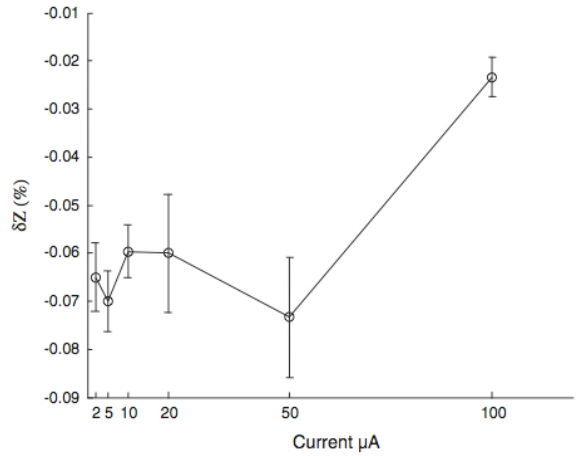

Figure 4-6: Change in δZ during evoked responses in rat cortex with varying current.

4.4 Discussion

4.4.1 Summary of results

Reproducible impedance changes were seen at all the above currents and frequencies. Varying the current did not alter the impedance change except at 100μA, however this was not significant. The size of the impedance change decreased with increasing frequency. Overall the optimum settings were applied current of 225 Hz and 50 μA which yielded peak changes with an SNR of 50.

The criteria for believing that the changes observed in this study were physiological and genuine were that they agreed with the modelling and also were independent of the applied current. These appear to have been met.

4.4.2 Selecting the carrier frequency.

As expected, the impedance change decreased with increasing frequency. In selecting carrier frequencies for recording the impedance signal, the main consideration was to maximise the SNR. This was achieved by a balance between maximising the magnitude of the impedance change ('the signal') at low frequencies and minimising the background EEG signal ('the noise') at high frequencies as well as selecting a pass band which excluded most of the ECoG band. A secondary technical consideration was to use a carrier frequency in between any pair of mains 50 Hz harmonics to best enable their cancellation. Several frequencies in the range 125–1225 Hz were assessed. In the event, the optimal frequency was 225 Hz. An optimal bandwidth was selected as ±125 Hz, as this

enabled satisfactory capture of the EP related impedance change while excluding most of the ECoG noise. Unfortunately, this combination of carrier frequency and bandwidth introduced a possible artefact due to aliasing. In principle, a carrier frequency must exceed half the bandwidth of the modulated signal to avoid aliasing (Fc >BW/2) as any modulated frequency components above the carrier frequency will reach the negative frequencies domain and will fold back into the positive frequency domain. As the actual impedance change might have frequency components above 225 Hz, this could in theory have introduced an artefact during any demodulation procedure. To address this potential problem, a fast impedance change with frequency content similar to the compound action potential of the crab was modelled. This indicated that any such aliasing artefact altered the resulting demodulated impedance changes by <10% of their original vales. Therefore, this indicated that this source of artefact was negligible. This artefact is lower for recordings on the rat's cerebral cortex as the highest frequency components of ECoG and SSEP's were lower than those for compound action potentials. A commercial EEG amplifier was used, with which the maximum sampling rate was 2 kHz per channel and a hardware anti-aliasing filter of 570 Hz limited the recording bandwidth. As it was desirable to restrict the bandwidth to avoid the EEG in the band of 1–100 Hz, we set the bandwidth to ±125 Hz in order to enable recording at 225 Hz.

4.4.3 Selecting the current

An important consideration was the choice of applied current. In order to improve SNR, it was desirable to inject as much as possible, but the integrity of the method depended on subtraction of the evoked neural response, so it was essential that the applied measuring current did not alter the response and produce artefactual apparent impedance changes. For the crab nerve (chapter 3), the maximal current that could be applied was 5 μA. On the rat's cortex however, the SNR of recordings with 5 μA current injection was only about 5. Although it appeared to exceed the above limit, we assessed higher applied currents. In the event, both the evoked potentials and impedance responses appeared to be unaffected up to 50 μA, which was unexpected. The explanation is not entirely clear. It seems probable that the current limit depends critically on current dispersion from the electrode. Whereas it may be possible that neurones very close to the injecting electrodes are indeed affected, this rapidly falls off, so that neural activity in the region of interest, several mm away, is not.

4.4.4 Future Work

The optimum current and frequency has been identified to yield an SNR of 50. With the instrumentation settings described above. The next set of experiments were focused at measuring

impedance changes during SSEP's of different modalities (forepaw, hindpaw, visual evoked responses) with the same hardware, then using the above frequency and current to reconstruct images of neuronal depolarization within rat brain.

5. Imaging neuronal activity in the rat cortex using electrical impedance tomography during evoked responses

5.1 Introduction

5.1.1 Orientating paragraph

In this chapter the experiments for reconstructing images of neuronal depolarization of different modalities of evoked responses (EP's) (forepaw, hindpaw, vibrissae and visual) on the cortex of the anaesthetized rat using Electical Impedance Tomography (EIT) are described. The different modalities were triggered whilst injecting a sinusoidal wave current through various combinations of pairs of electrodes that were placed on the rat's cerebral cortex. The recorded impedance changes were then calculated and the data was processed by the algorithm to reconstruct the images. The image reconstructions demonstrated that the changes were seen over the appropriate part of the rat's cerebral cortex corresponding to the modality being imaged. These are the first ever images of fast neural activity recorded within the cerebral cortex.

5.1.2 Background

In order to image neuronal depolarisation using EIT, reproducible impedance changes during neuronal depolarisation need to be recorded with a satisfactory signal to noise ratio, such that the applied current does not interfere or cause neuronal excitation that could distort the data.

The previous chapters of this thesis aimed to address the above. Biophysical modeling (Liston 2004) suggested that the impedance change would be greatest at near DC. At near DC all the current would pass through the extracellular space and only cross the cell membrane during neuronal depolarisation (when ion channels are open). As current frequency is increased, the cell membrane becomes more permeable to current hence the overall change in impedance to current during neuronal depolarisation will be smaller.

Chapter 2 demonstrates that impedance changes during compound action potentials (CAP's) in the unmyelinated crab nerve could be recorded with a near DC carrier, however if this were applied to the rat cerebral cortex or human scalp, this would be within the bandwidth of the background EEG activity and long recording times for averaging would be required which would be impractical.

Therefore a balance is required in using a carrier of high enough frequency to reduce noise to an acceptable level, but a low enough frequency to be able to allow a measureable reduction in impedance during the EP. Chapters 3 and 4 addressed this. The method of using a low frequency sinusoidal carrier was first validated on the crab nerve (chapter 3), then on the cerebral cortex of the

rat reproducible impedance changes were seen at all current levels, and reduced with increasing frequency (chapter 4); (Oh et al. 2011). With applied current of 225Hz and 50μA the SNR was 50:1. Simulation studies have shown that an SNR of 4:1 or above should be suffice for imaging such changes (Fabrizi et al. 2008). Although a summation and subtraction method for extracting the signal was used, the paired data used were segments within the same recording thus keeping the recording times more practical.

Imaging modalities described in chapter 1 such as EEG/ ECoG, MEG, Direct MRI mapping and DOI (table 1-2) are either invasive or limited to activity close to the surface with results in the early research stages (Michel et al. 2004; Lin et al. 2006; Franceschini & Boas 2004) . The reconstruction of moving images of neuronal activity at depth within the brain with the aim of eventually recording non-invasively is indeed a significant breakthrough.

5.1.3 Purpose

The purpose of the experiments in this chapter was to image neuronal activity in the cerebral cortex of the anaesthetized rat during evoked responses and to answer the following questions:

1. Are the images reproducible across modalities (Vibrasse, forepaw, hindpaw, visual)?
2. Are the images physiologically plausible?
    a. Are the changes seen in the controls (in the dead animal or ipsilateral to the side of stimulation)?
    b. Does the size match the modeling?
    c. Is the time course sensible? *(These are moving images)*
    d. Are the changes imaged constant with phase and current?
    e. Is the distribution of the images over the brain physiologically plausible?

5.1.4 Experimental Design

An array of electrodes was placed on the cerebral cortex of the anaesthetised rat. Four evoked response modalities were triggered (whiskers, forepaw, hindpaw and visual evoked potentials). Recordings were made with a 225Hz carrier. The EP and the impedance changes were extracted. The electrode positions on the cortex were mapped with a robot arm then EIT moving images were reconstructed.

5.2 Method

5.2.1 Animal preparation

The rats were anaesthetised as described in chapter 4. The craniotomy was fashioned the same way and the electrode array described in chapter 4 was placed such that it anatomically covered the sensory areas of the cerebral cortex that correspond with the whiskers, forepaw, hind- paw and the primary visual cortex (Figure 5-1). Pairs of stimulation electrodes were placed in the contralateral forepaw, whiskers and hindpaw to the side of the craniotomy. In addition LED's were placed over the rat's eyes, with covers to disallow external light entering the rats eyes. The remaining ground electrode was placed in the contralateral cheek to the side of the craniotomy as previously described. The common electrode was placed in the snout. For the control recordings, the stimulation electrodes were placed in the ipsilateral whiskers, forepaw and hindpaw to the craniotomy with the ground electrode in the opposite cheek.

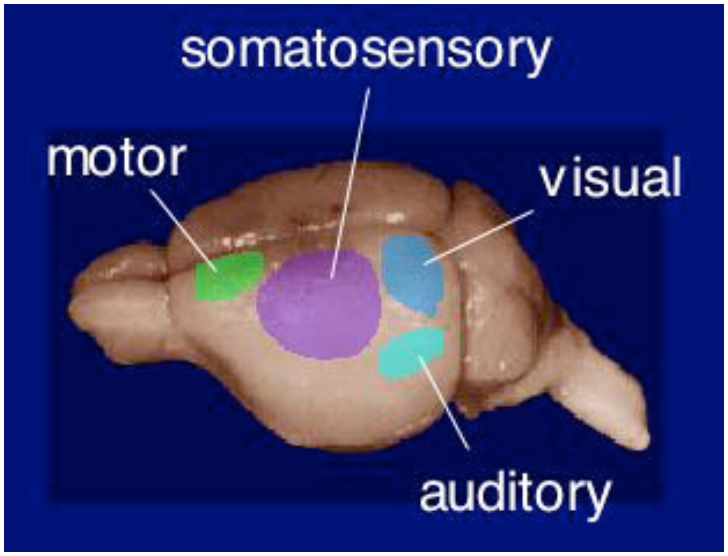

Figure 5-1: Rat cerebral cortex displaying motor, somatosensory, visual and autitory cortex

5.2.2 Instrumentation

The same current source, acquisition system and their arrangement as described and illustrated in chapter 4 was used (figure 4-2). A multiplexer (MUX) was also employed into the arrangement to allow current injection serially, in a predetermined order, through various pairs of electrodes within the array.

The same 29 electrode array described in chapter 4 was used (figure 4-1).

In addition to the stimulation electrodes, LED's were connected and set by the same trigger to stimulate at 2Hz.

5.2.3 Protocol and recordings

Current was injected serially (using MUX) from 30-40 adjacent current pairs while recording through the remaining 27 electrodes which yielded a total of about 900 four terminal traces. For each current pair, 70 seconds were recorded while the first 10 seconds were discarded due to stabilization time of the EEG amplifiers following MUX switching. The total recording protocol lasted just under an hour for each modality.

The stimulation rate was 2Hz so there were 120 valid stimulations in each 60 second segment. The injected current was phase locked to the stimulus.

For control, recordings were made whilst stimulating the ipsilateral whiskers, forepaw and hindpaw. Recordings were also made in the same manner with the animal dead as a control as well. In addition recordings were made using different frequencies, currents and phase to the active recordings (Table 5-1).

For active recordings a carrier of 50μA at 225Hz at zero phase was used, as this was the optimum carrier demonstrated in chapter 4 (Table 5-1).

Invalid recordings were discarded, thus the valid recordings were with the rat being in a stable physiological condition with EP's of above 200μA (unless it was a control recording).

	Forepaw Recordings /Rats	**Whiskers** Recordings /Rats	**Hindpaw** Recordings /Rats	**Visual** Recordings /Rats
Active (Recordings/ rats)	22 /8	6 /3	5 /2	5 /3
Controls				
Ipsilateral stimulation		1	1	1
No stimulation	1	1	1	1
Dead	1	2 /2	1	1
Effect of Current : 20μA	3 /3			
10μA	3 /3			
Effect of Phase : 45º	3 /3			
90º	2 /2			
135º	1			

Table 5-1: Summary of recorded data:
Displaying numbers of recordings in total number of rats per data set. Unless defined otherwise in a table cell, the current in all recordings was 50 μA, the frequency was 225 Hz and the phase between the stimulation and EIT current was 0 º.

5.2.4 Data analysis

In each 1hour recording, the raw data consisted of 900 traces (30-40 current pairs X 26 voltage pairs) of 60 seconds sampled at 2048 Hz. Each of these traces contained 120 evoked potentials (EP's), a 225Hz carrier sine wave with modulated impedance changes (δZ) during each EP and background EEG noise. These traces underwent the following analytical steps:

1. Segmenting into 60 segments of 1 second long, each segment containing 2 stimuli, and starting 150ms before a stimulating trigger.
2. Rejecting segments with high EEG or glitches above 1mV.
3. Averaging the remaining segments (about 95% of segments).
4. Summation of two 500 ms parts to yield the EP's.
5. Subtraction of two 500 ms parts to yield the sine wave with the modulated δZ.
6. Using a band pass filter (BW 250Hz), amplitude and phase demodulation were applied to the subtracted waveform to yield δZ actually calculated as a change in conductivity (δσ).
7. The first and last 100ms in the δZ waveform were truncated to remove "ripples" caused by applying a demodulation filter over a short signal (500ms long). The final wavefom consisted of 50ms during the pre-stimulus time and 250ms post stimulus.

The 900 δσ traces were reduced to 400 (384 ± 140 mean ± SD; range 137-691; n=57 recordings) by rejecting traces with the following criteria:

- High noise over the pre-stimulus time (>0.3 μV),
- Low boundary voltage (noise over the pre-stimulus time > 0.01 % of the boundary voltage)

This resulted in average noise level of 0.004±0.001% (SD), range 0.001-0.007% (0.18±0.04 μV, range 0.10-0.24 μV).

The δσ data was taken at 21 time points for image reconstruction from 0 to 40ms every 2ms for SEP's and 0 to 300ms at 15ms intervals for VEPs (see red markers in figure 5-2).

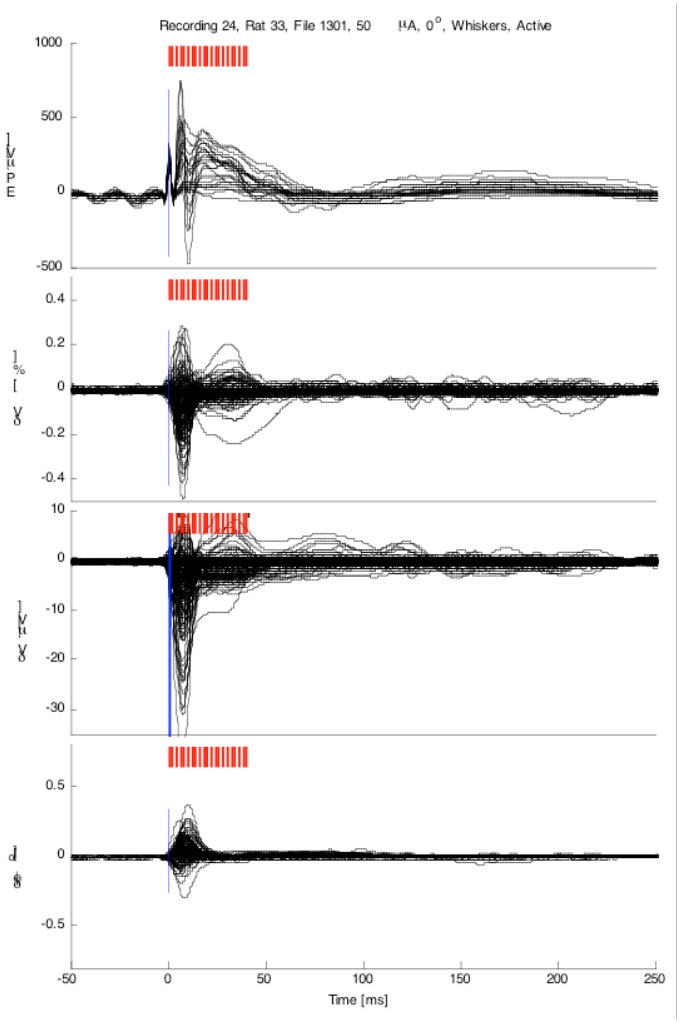

Figure 5-2: Segments (in red) of δZ trace used for image reconstruction.

5.2.5 Image reconstruction

5.2.5.1 Mesh and electrode localization

A computerized mesh of the rat's brain was constructed using a CT scan of the rats brain. The mesh consisted of 1,072,558 tetrahedral elements. All elements passed stretch analysis criterion (S>0.05). Using a MicroScribe robotic arm in a fixed position relative to the rat's brain (also in a fixed position with ear-bars), each electrode was localised within a Cartesian co-ordinate system along with fixed skull landmarks so that the array in its position for different modalities could be accurately placed on the mesh (figure 5-3).

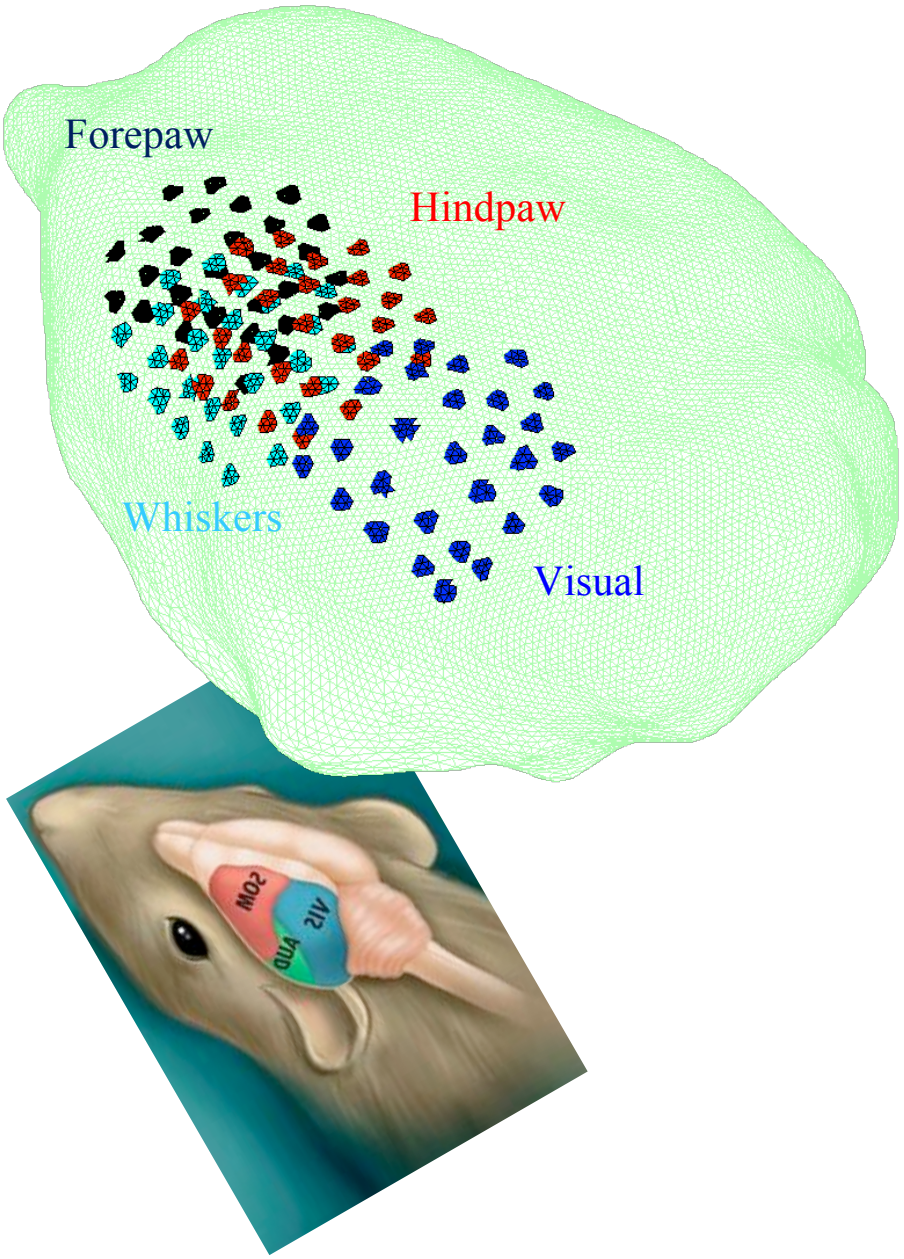

Figure 5-3: Mesh showing location of electrode array for different modalities.

5.2.5.2 The forward equation

Boundary voltages were calculated for multiple current injection and voltage measurement electrode pairs using the UCL SuperSolver package developed in the EIT group (Horesh et al. 2006). This is based on EIDORS 3D (Polydorides & Lionheart 2002), and the generalized Laplace equation was solved using the Neumann to Dirichlet map to obtain the electric potentials at each element. The numerical solution was performed with a preconditioned conjugate gradient linear solver. The relative residual tolerance was set and monitored to be below 10−12. An incomplete Cholesky factorization was used as a preconditioner, with a drop tolerance threshold of 10−5 (Horesh et al 2006, Gilad 2009).

5.2.5.3 Inverse Problem

Truncated Singular Value Decomposition (tSVD) with row normalisation only, and singular value thresholds of 25, 50, 75, 100, 125 and 150 were used.

5.2.5.4 Slicing

Tomographical slices were made of 11 depths from 0.2 to 2.2mm beneath the electrode array, 0.2mm apart.

This was repeated for 21 time points from 0 to 40ms every 2ms for SEP's and 0 to 300ms at 15ms intervals for VEP's.

For each time and depth, the image over the entire mesh was 3D interpolated over a Cartesian 0.01mm grid at the region of interest of the electrode array size followed by a spatial smoothing filter of size 0.5mm to give a clearer image due to the resolution of the mesh.

5.2.5.5 Calibration

For each recording, an additional image reconstruction was obtained for simulated perturbation of 1% at 1.4mm depth using the specific protocol for that recording. This image was used to calculate a recording specific scaling factor for obtaining 1% changes in the simulated image. This factor was then used to scale the changes in the rat image.

5.2.6 Statistical analysis

A singlular value (SV) threshold of 50 was set for the statistical analysis as it was the highest number of SV's which yielded an interpretable image for all the recordings including those with a lower SNR (both visual stimulation and low current forepaw stimulation recordings at 10 and 20 μA).

Images of the conductivity change ($\delta\sigma$) in the recordings with the highest $\delta\sigma$ for each modality were reconstructed along with images of the mean $\delta\sigma$ of all the recordings were reconstructed for each modality using tSVD.

Images are also reconstructed of the t values which were calculated using an unpaired, one-sided Student's t-test, which is calculated as $t = (x-u0)/(SE)$, where t is the t value, x is the data point, u0 is the null hypothesis value, and SE is the standard error, which is the standard deviation divided by the square root of the number of the sample. The null hypothesis value was zero as changes significantly different from zero, were sought. Therefore as u0 is zero, the calculation is the mean over the standard error. So for a given pixel the ratio of its mean value compared to its variability across recordings can be determined. If the value is far from zero and the SE is small its significance could be determined. A one-sided test was used as changes significantly greater than zero were sought as negative conductivity changes are not expected.

By using a t distribution look-up table, for a given number of degrees of freedom and confidence interval there is a t-value which is the minimum value required to be significant.
A one way analysis of variants (ANOVA) was used for the effect of current and phase. All numeric values are given with ±1SD.

5.3 Results

5.3.1 Recordings and conditions

Overall, there were 56 technically valid recordings with the rat in a physiologically stable condition and the EP above 200µA (except for control recordings) (table 5-1).

5.3.2 Raw data - Impedance changes.

Reproducible evoked potentials between 390 ± 130µV and 650 ± 140µV (n= 38 in 16 rats) and impedance changes (represented as conductivity changes) at the surface between 0.07 ± 0.03% and 0.4 ± 0.1% were recoded with all modalities (table 5-2). Local impedance changes were also reproducible at their respective depth (table 5-2 and figure 5-4).

	EP [µV]	Peak surface δσ [%]	SNR	Peak local δσ [%]	Depth [mm]	t-value (n)	Time [ms]	N rec. (rats)
Forepaw	650±140	0.2±0.1	30±20	0.7±0.3	0.66±0.14	1.7214 (22)	11±2	22 (8)
Whiskers	630±200	0.4±0.1	80±40	0.9±0.2	1.2± 0.5	2.015 (6)	7±1	6 (3)
Hindpaw	640±190	0.15±0.03	16±5	0.7±0.3	0.4± 0.3	2.132 (5)	14±1	5 (2)
Visual	390±130	0.07±0.03	8±3	0.11±0.03	0.8±0.3	2.132 (5)	143±8	5 (3)

Table 5-2: Maximal conductivity change at surface and at depth.
With t-values and its time from stimulation of each modality.

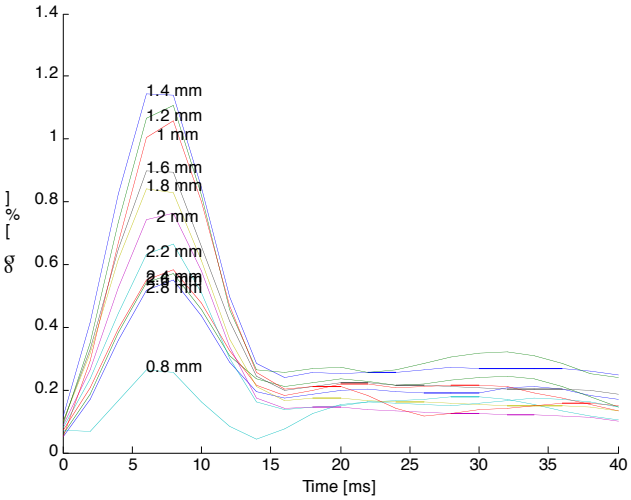

Figure 5-4: Peak conductivity change for whisker stimulation measured at various depths.

With ipsilateral stimulation much smaller EP's and impedance changes were recorded. With no stimulation or whilst stimulating a dead rat no significant EP's or impedance changes were seen (table 5-3)

	EP [µV]			Peak surface δσ [%]			Peak local δσ [%]		
	Ipsilateral	No stim.	Dead	Ipsilateral	No stim.	Dead	Ipsilateral	No stim.	Dead
Forepaw	-	3	9	-	0.05	0.06	-	0.05	0.02
Whiskers	500	7	63	0.22	0.06	0.05	0.15	0.03	0.02
Hindpaw	270	18	11	0.19	0.13	0.05	0.17	0.13	0.06
Visual	150	7	25	0.06	0.05	0.10	0.04	0.05	0.04

Table 5-3: Control recordings
Showing very small changes when stimulating ipsilaterally and no significant changes when stimulating a dead rat or no stimulation at all.

5.3.3 Image reconstructions

Images of the highest conductivity change of all the recordings for each modality and images of the mean conductivity change of all the recordings for each modality and the respective t values are displayed below with spatial resolution of 0.2-0.5mm (figures 5-5 to 5-16).

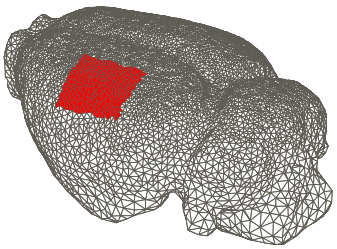

Whisker image area

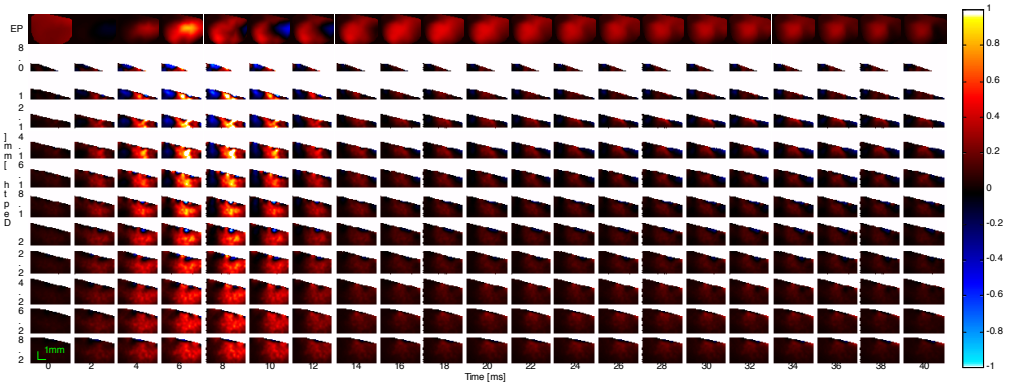

Figure 5-5: Example image reconstruction of δσ:
During whisker stimulation displayed in slices at a given depth (y axis), at a given time (x axis). The top row displays the EP (surface) over time.

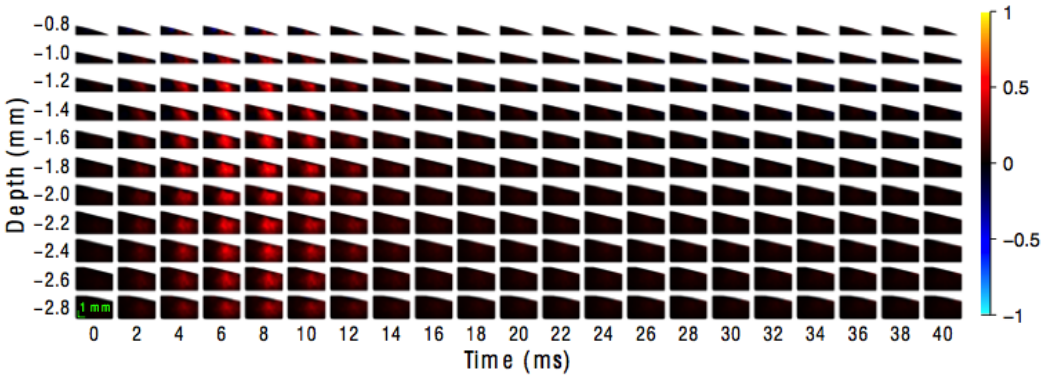

Figure 5-6: Images of mean δσ of all recordings over time when stimulating whiskers.

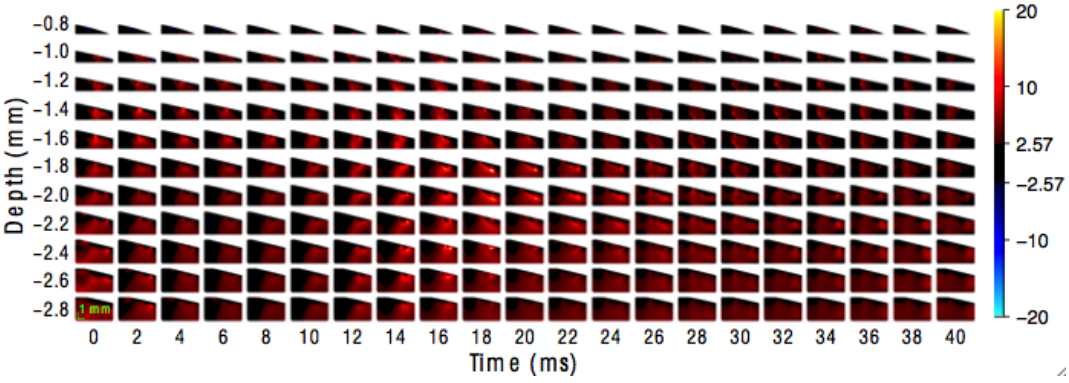

Figure 5-7: Images of t value over time with whisker stimulation.

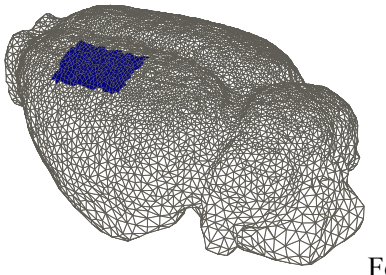

Forepaw image area

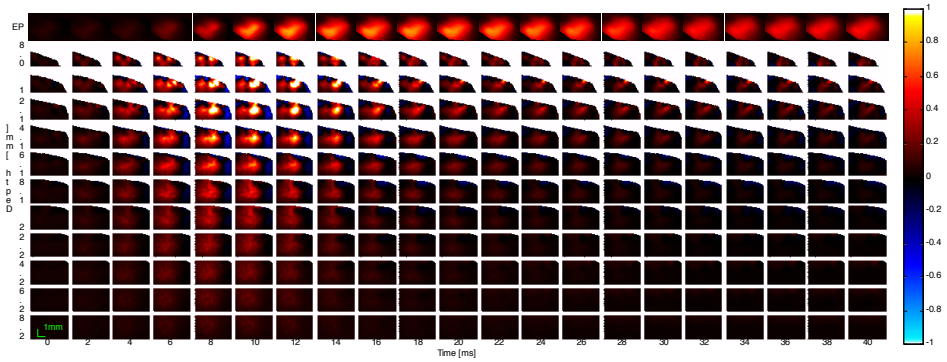

Figure 5-8: Images of δσ over time with EP over time for forepaw stimulation.

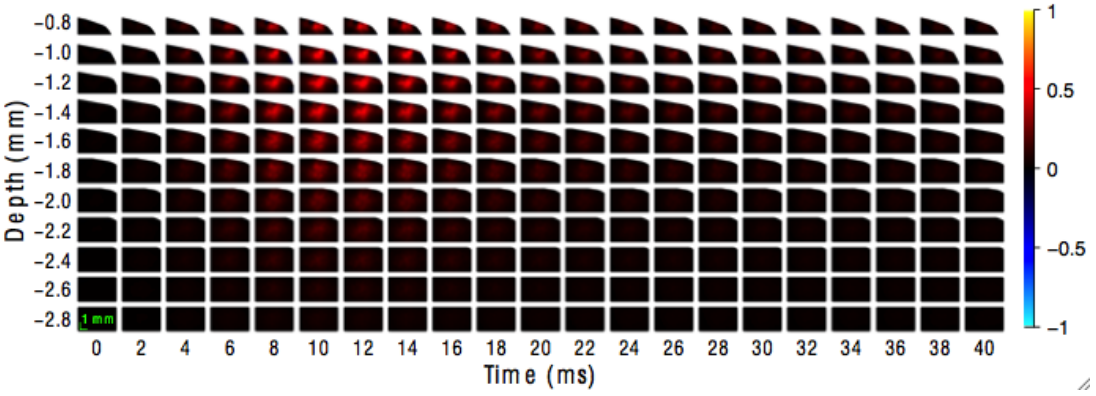

Figure 5-9: Images of mean δσ of all recordings over time when stimulating the forepaw.

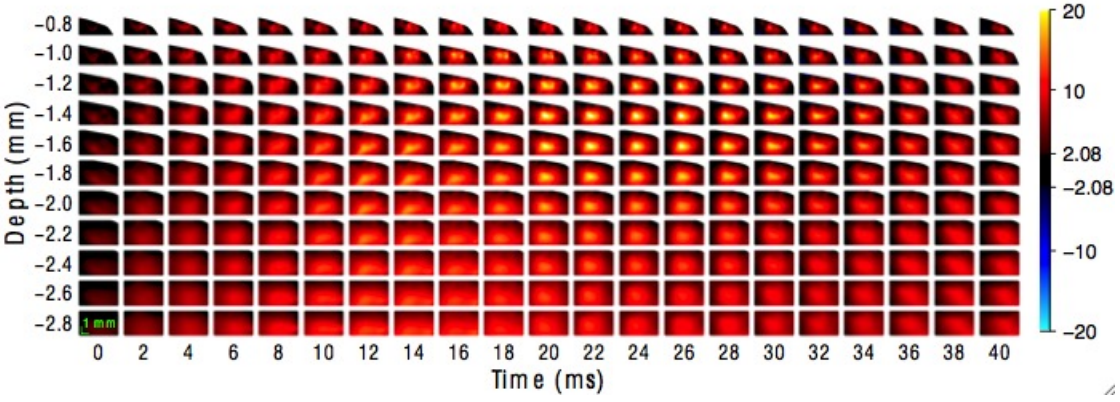

Figure 5-10: Images of t value over time with forepaw stimulation.

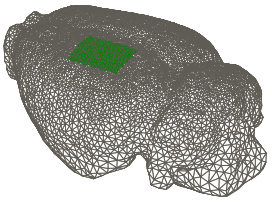

Hindpaw image area

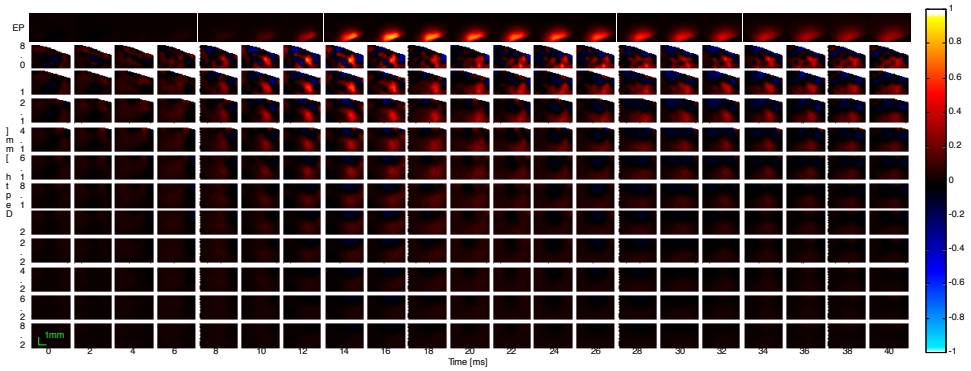

Figure 5-11: Images of δσ over time with EP over time for hindpaw stimulation.

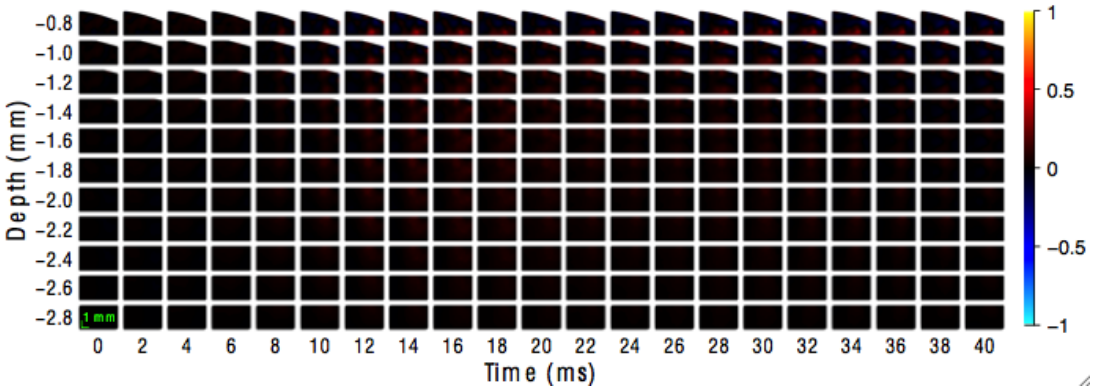

Figure 5-12: Images of mean δσ of all recordings over time when stimulating whiskers.

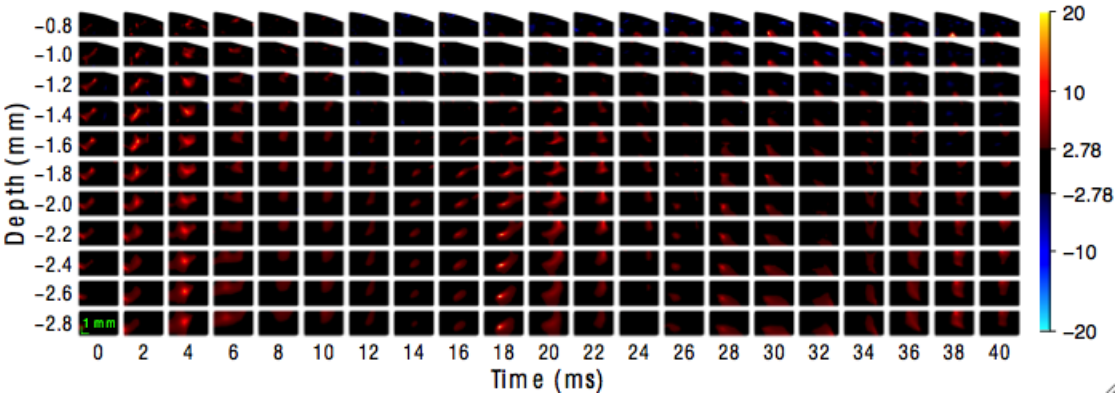

Figure 5-13: Images of t value over time with forepaw stimulation.

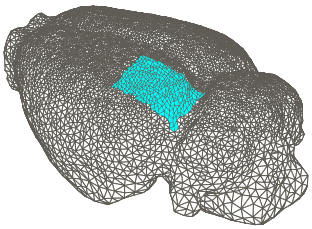

Visual image area

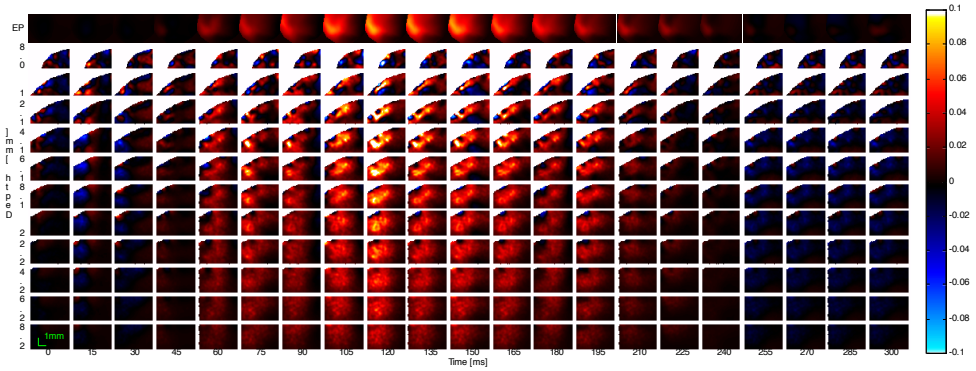

Figure 5-14: Images of δσ over time with EP over time for visual stimulation.

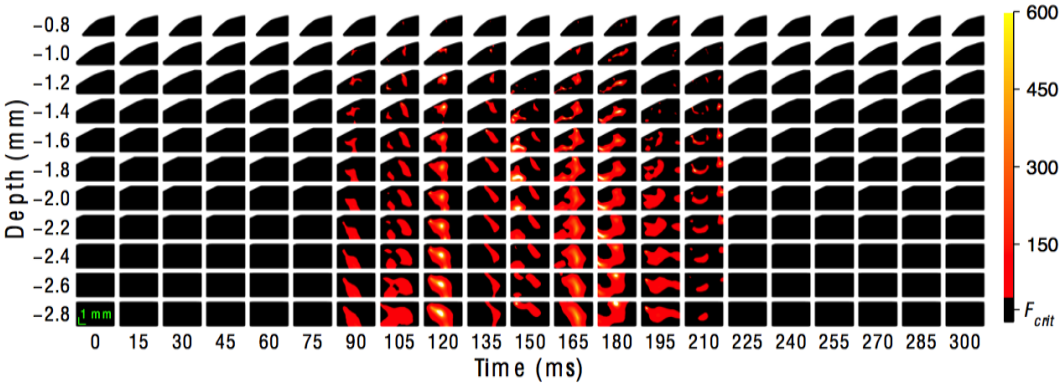

Figure 5-15: Images of mean δσ of all recordings over time with visual stimulation.

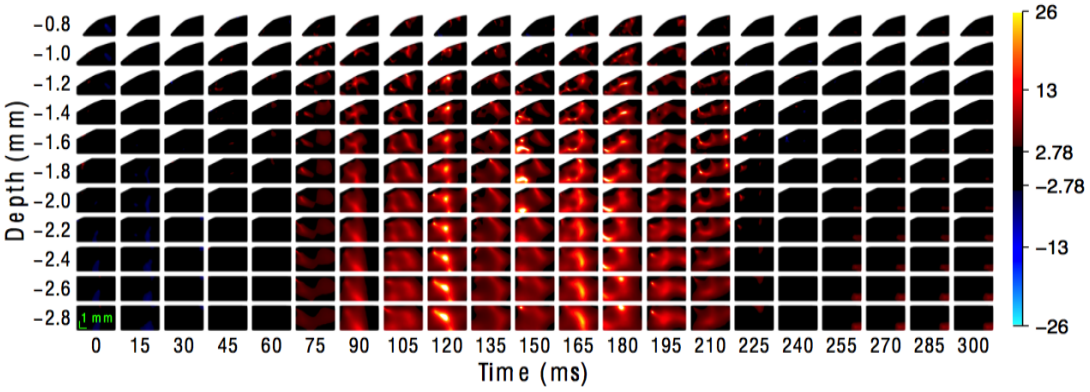

Figure 5-16: Images of t value over time with visual evoked responses.

5.3.4 Signal to noise ratio (SNR)

The lowest SNR in the peak pre-imaging surface changes were 9:1, 50:1, 10:1 and 5:1 for forepaw, whiskers, hindpaw and visual stimulation respectively, with sensible images obtained for all these recordings.

5.3.5 Effect of current and phase

Both surface and local changes were independent of applied current of 10, 20 and 50 μA ($p=0.69$, d.f.=2; $F=0.38$).

The surface and local changes were also independent of current phase of 0, 45, 90 and 135 º at 50μA ($p=0.79$, d.f.=3; $F=0.35$ and $p=0.70$, d.f.=3; $F=0.48$ respectively).

5.3.6 Time course

The time course of the conductivity change was consistent with the anticipated response at around 12ms (figure 5-17).

For forepaw stimulation, the time course was consistent across current levels suggesting that the current does not alter neuronal activity at the active region.

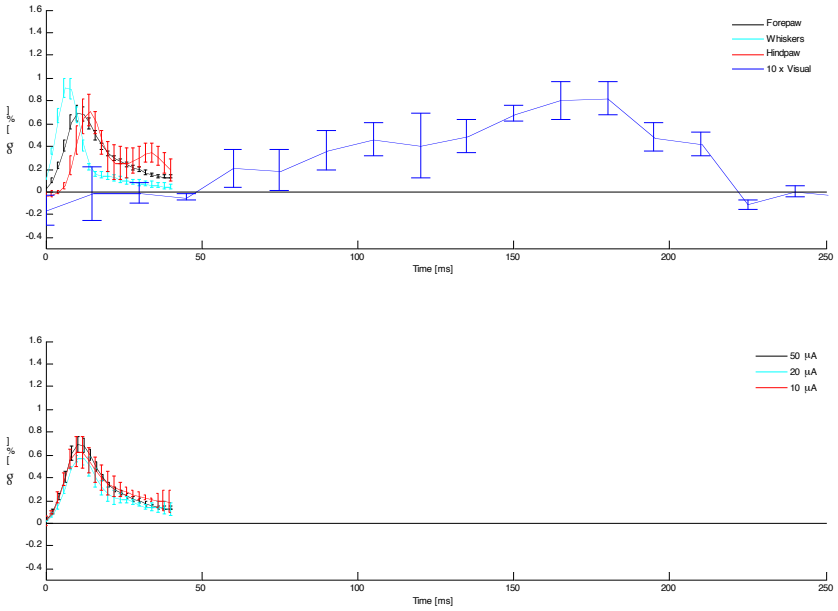

Figure 5-17: Time course of local changes.

Upper panel: time course of the local changes at the depth of maximal change across all modalities. The visual case is magnified by x10 (error bars are ±1SE)
Lower panel: Time course of the local changes at three different current levels for forepaw stimulation only showing a similar change at the 3 current levels.

5.3.7 Distribution in the brain across recordings

The different modalities and their respective distribution including depth within the brain mesh are displayed in figure 5-18 below.

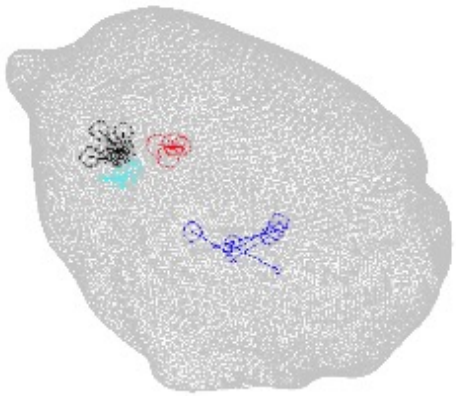

Figure 5-18: Distrubution of images of different modalities across the brain mesh.
Black= Forepaw, Red= Hindpaw, Cyan= Whiskers, Blue= visual. Various sized shapes refer to the depth of image.

5.4 Discussion

5.4.1 Summary of results

Reproducible impedance changes across all modalities (forepaw, hindpaw, whiskers and visual) were recorded and imaged at the surface and at their respective depths. Both current level and phase had no effect on the impedance changes measured. No impedance changes were recorded in the control measurements with no stimulation of the respective modality or with the rat dead. However in the control recordings using ipsilateral stimulation, very small changes were measured.

5.4.2 Technical issues

5.4.2.1 Spatial resolution

In these experiments with 30 electrodes on the surface of the rat brain spaced at 1.2mm, an effective spatial resolution of about 0.2-0.5mm was obtained across different experimental conditions. This was down to a depth of about just 1-2 mm. This resolution is in agreement with the 'rule of thumb' in EIT of obtaining spatial resolution of about 5-10% of the diameter of the imaged volume. In these experiments the diameter of the electrode array was about 5mm. Hence, if deeper activity is to be imaged in the future the special resolution will be less.

5.4.2.2 Time resolution

The effective time resolution of 8ms in this study was a complex tradeoff between the choice of carrier frequency and band width set in this study to maximize SNR, minimise the frequency folding problem due to the limited sampling rate of the data acquisition system used. With faster acquisition, it may be possible that a sensible balance between these factors could be obtained somewhere between 200 and 1000 Hz allowing effective time resolution of 1-2 ms.

5.4.3 Impedance changes and their images (answering the questions set in the purpose of this study)

1. The results have shown that reproducible impedance changes can be measured and imaged across different modalities (Vibrissae, forepaw, hindpaw, visual).

2. The images are physiologically plausible in that they are broadly in-keeping with the modeling (Liston 2004), with regard to the size and time course. The distribution of the images is also anatomically where expected. As expected the measurements are constant with different phases and current.

With respect to the control experiments, no changes were expected with no stimulation of a modality, with the animal dead or by stimulating the ipsilateral side. Although this was found for the former two controls, a change was noted when stimulating the ipsilateral side. This was a very small change when compared to the active measurements.

A possible explanation is that a small number of fibres of the spinothalamic tract within the spinal cord do not decussate and hence a smaller change may therefore be seen on the ipsilateral side.

Further experiments with ipsillateral stimulation will need to be done to examine this theory will be required in the future.

Overall this study has demonstrated that impedance changes of different modalities of evoked responses can be invasively measured in the rat's cerebral cortex and the respective neuronal activity can be imaged with EIT.

6. Discussion and future work

6.1 Summary of results.

In order to image neural activity within the brain using EIT, reproducible impedance changes during neural depolarisation with the best possible signal to noise ratio (SNR) need to be recorded.

The "holy grail" would be to achieve this non-invasively with a time and spatial resolution of 1 ms and 1mm respectively.

Biophysiological modeling suggests that recording at near DC would yield the best signal as all the current passes through the extracellular space and only crosses the cell membrane during neural depolarisation. Chapter 2 therefore demonstrated that reproducible impedance changes of -0.85 ± 0.4% (range -0.2 to -2%) with a 1Hz square wave carrier could be recorded with SNR of 80 ± 50 (range 17 -194) in unmyelinated crab nerve. So although the SNR was good there was significant variability in impedance changes with recordings under the same conditions. This is partly due to the condition of the nerve deteriorating during a single recording. Thus a method requiring a more practical recording time would be better and also more practical in human recordings at the scalp to reconstruct images.

Chapters 3 and 4 demonstrated that reproducible impedance changes during neural activity could be recorded with a sinusoidal wave carrier in the unmyelinated crab nerve and on the cerebral cortex of the anaesthetised rat respectively. On the rat more consistent changes of -0.07 ± 0.006% were recorded at 225Hz with the SNR always above 50. The optimum SNR was achieved with a carrier of 225Hz. Although more current can cross the capacitive cell membrane at rest the overall background noise (mostly from ECoG) is reduced by a greater factor. The time constant achieved was 8ms.

In chapter 5 reproducible images of different modalities of evoked activity (forepaw, hindpaw, vibrissae and visual) by using a 225Hz carrier on the cerebral cortex of the rat. Using a multiplexer the current was injected through different combinations of pairs of electrodes. The images yielded are the first ever images of neural activity within the rat cerebral hemisphere.

6.2 Comparison with other methods of functional neural imaging

This thesis has demonstrated that EIT can be used to image neural depolarisation (fast changes) within the rat brain with temporal resolution of 8 ms. The ultimate aim would be to eventually imaging the same changes non-invasively in the human brain.

Other modalities discussed in chapter 1 have been used in functional brain imaging, but none have been able to image fast changes non-invasively at different depths in the brain.

Slow changes can be imaged with advanced applications of CT and MRI. By using a contrast agent perfusion CT can image slow haemodynamic changes. This however involves ionizing radiation and the intravenously injected contrast can be nephrotoxic. Similarly fMRI can image slow neurovascular changes related to neural activity. Despite good spatial resolution of less than 1mm, the temporal resolution is more than one second. This is a costly investigation requiring the subject to be placed still within the scanner.

Positron emission tomography (PET) and single photon emission tomography (SPECT) allows radioactive isotopic labeling of a biologically active molecule thus allowing imaging of regions of the brain undergoing increased metabolic activity secondary to an increase in neural activity, similar to haemodynamic changes. The spacial and temporal resolution of 4 mm/ 30 s and 7mm/ 15 minutes respectively is quite poor.

Attempts have been made to image neural activity directly (as opposed to the sequelae described above). These include imaging from source with EEG activity (Baillet et al. 2001), and with its variant MEG described in chaper 1. The temporal and spacial resolutions of both are 1 ms and 10 mm respectively and results were poor. EEG is only sensitive to superficial gyral activity and although MEG is more sensitive to sulcal activity, inverse source modeling involved does not have a unique inverse solution and hence require simplifying assumptions, therefore accuracy is unknown.

Optical activity of the fast scattering signal is a recent modality for imaging neural activity within 1 ms or less however is limited to imaging superficially (Franceschini & Boas 2004) and the ability to replicate findings has been brought into question (Syre et al. 2003).

So far EIT has is the only modality that has reproduced images of neural activity in the brain with both high temporal and spacial resolution that allows for imaging deeper structures.

6.3 Work since this thesis

Since the work described above, more work has been undertaken to improve both the signal and the temporal resolution (Packham 2013). As previously mentioned the vibrissae have a greater area of representation on the rat cerebral cortex, in theory making them a better modality to image. However with electronic stimulation there was significant stimulus artifact due to the close proximity of the stimulation electrodes to the recording electrode array on the brain despite placement of a large ground electrode in between. By stimulating the vibrissae mechanically, thus generating a more

physiological evoked response, Packham was able to eliminate the stimulus artifact altogether. He was then able to make recordings at much higher frequencies of 1.7 kHz and although the signal was lower, he was able to filter out background ECoG activity to extract the signal instead of using summation and subtraction thus being able to significantly reduce the recording time required. At this frequency he was able to reduce temporal resolution to 2 ms.

6.4 Future possible applications.

In epilepsy surgery, arrays of intracranial electrodes are already in use using ECoG to map out epileptic foci within the brain, which can be resected to reduce seizures. EIT can potentially use the same electrodes to image both the slow changes during epileptic activity (e.g. cellular swelling) but also directly image the fast neuronal acivity during a seizure. If this could be achieved extracranially (i.e. non-invasively) epilepsy surgery can be revolutionised.

In cognitive neuroscience fMRI is in use to try and understand various pathways involved in many psychiatric disorders such as schizophrenia and depression. This however relies on slow changes. If neural activity was imaged directly one could map out and analyse neural pathways more accurately in such conditions.

There has been great interest in developing a brain machine interface (BMI) over the last decade to allow human-computer interaction for both communication and prosthetic devices. As EIT can image neural depolarisation, it can potentially be used to map and decode speech signals from the brains language centre. In doing so existing BMI's would be rendered obselete. This would be an invaluable tool in helping patients with specific neurological disabilities where verbal communication is difficult such as locked-in syndrome.

The achievement of imaging neural activity in the brain with EIT is indeed a huge breakthrough given the potential future applications.

Appendix 1

Initial experiments measuring impedance decreases in unmyelinated crab peripheral nerve during the compound action potential with a 1 Hz square wave carrier.

A1.1 Introduction

A1.1.1 Orienting paragraph

A model of impedance change during the compound action potential (CAP) in an unmyelinated nerve has been described here. Previous experiments, which study the impedance change on a crab nerve during a CAP are summarized in chapter 2. This appendix presents the experiments undertaken before those in chapter 2, using older hardware and an older array of electrodes, in an attempt to confirm previous findings. The crab nerve is placed on a series of electrodes, the nerve is stimulated whilst a low frequency square wave carrier was injected and the impedance changes are measured. Variations were made between the distances of the current injection electrodes and the current recording electrodes to see if this had an effect on the overall impedance change. Impedance changes were seen at all current levels and spacings described. These changes were similar between 5 and 10μA and the change decreased with an increasing distance between current injection electrodes.

A1.1.2 Purpose

This study was very similar to that already undertaken by Boone in our group (Boone, 1995). The overall purpose was to verify that similar physiologically plausible changes could be reproduced, using bi-polar square wave with paired control recording and linear model formulation for calculating the resistance changes detailed below.

The aims of this study were to examine the following:

1. If an impedance change using a square wave current source could be measured during the CAP to confirm Boone's findings.

2. To see the effect of different current levels on the impedance change. According to the cable theory this should not affect the amplitude of the impedance change.

3. To see the effect of different distances between the two current injection electrodes on the impedance change.

4. To see the effect of changing the distance between the 1st recording electrode and current injection electrodes on the impedance change. We do not expect this to alter the impedance change.

A1.1.3 Experimental design.

Impedance was recorded using a crab nerve suspended on an array of electrode hooks, where the nerve was stimulated to induce action potentials. At the same time, a square wave current was injected into the nerve using two of the electrode hooks and impedance was measured via another two electrodes (figure A1-3). The impedance was measured whilst injecting various current levels and varying the spacing of the current injection electrodes It was important that the applied current did not change the characteristics of the measured compound action potential. This could be ensured if both measuring electrodes (R1 and R2) were a significant distance from the excitation. Electrode R2 was so distant (7.5cm) from the stimulus that measurement from this electrode, although affected by the excitation, could not contribute significantly to the overall action potential. Also R1 was proximal to the current injection electrodes. However, the distance of electrode R1 from the excitation current was limited by the need for the excitation electrodes to be as close to the stimulus as possible in order to reduce the effect of dispersion of the compound action potential, which would make the resistance change small at distances more than about 16 mm from the stimulus. The radius of each nerve was about 0.5 mm, and the predicted length constant in previous modelling was about 0.6 mm (Boone, 1995). Thus the closest voltage electrode to the excitation was around 5 length constants from its nearest current electrode and current densities at these distances were proven to be insignificant by Boone.

A1.2 Methods

A1.2.1. Crab nerve preparation.

Crab nerves were prepared as described in chapter 2

A1.2.2. Instrumentation

The current source (made in UCL's EIT laboratory), delivered a bipolar square wave direct current at 1Hz. The current level was adjustable from 0-50uA. The recording, reference and ground electrodes were connected to an SD-32R EEG head box (Micromed, Italy) for recording. The headbox was

connected to a laptop (figure A1-1) which used System Plus software to record the data, and scripts in Matlab for analysis.

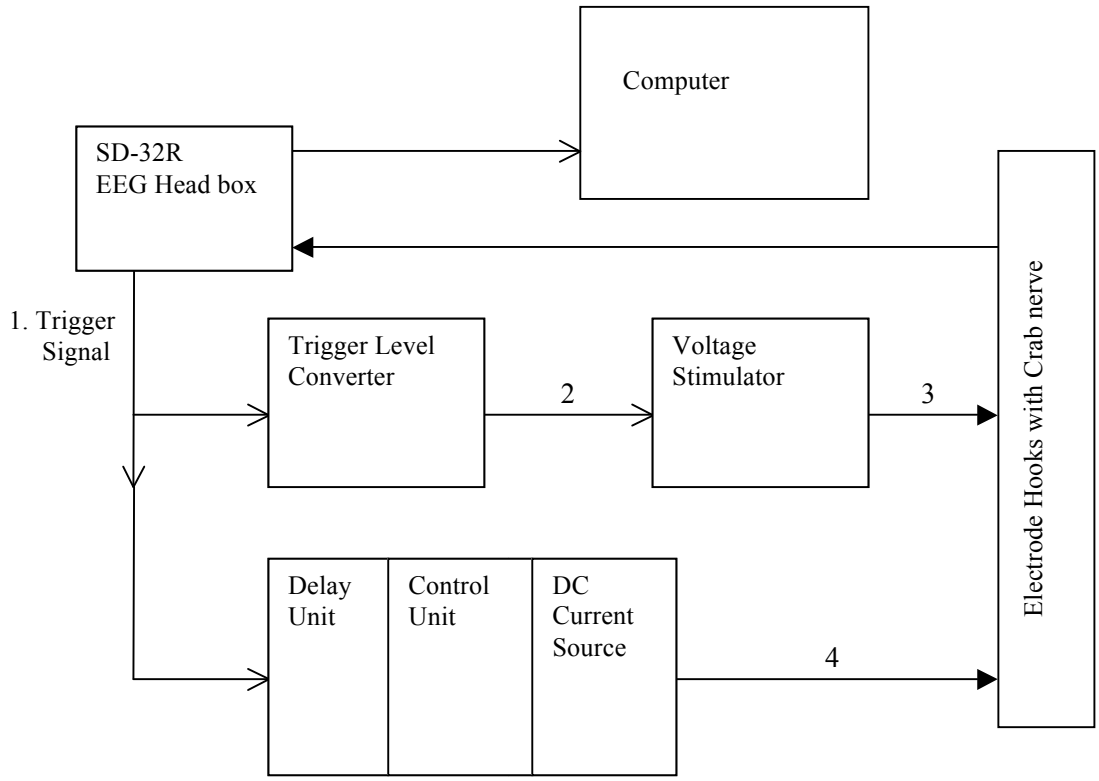

Figure A1-1: hardware arrangement for impedance recordings on the crab nerve.

The SD-32R head box triggered a signal of 5V at 2Hz. A trigger signal converter converted this signal to -15V. A Voltage stimulator (Digitimer UK) then converted this signal into a voltage stimulation pulse of 3V, each pulse lasting 100ms. The same trigger signal from the SD-32R head box was supplied to the current source, which produced a square wave current at 1Hz timed so that the stimulation pulse occurred at 150ms after the beginning of each square wave (figure A1-2).

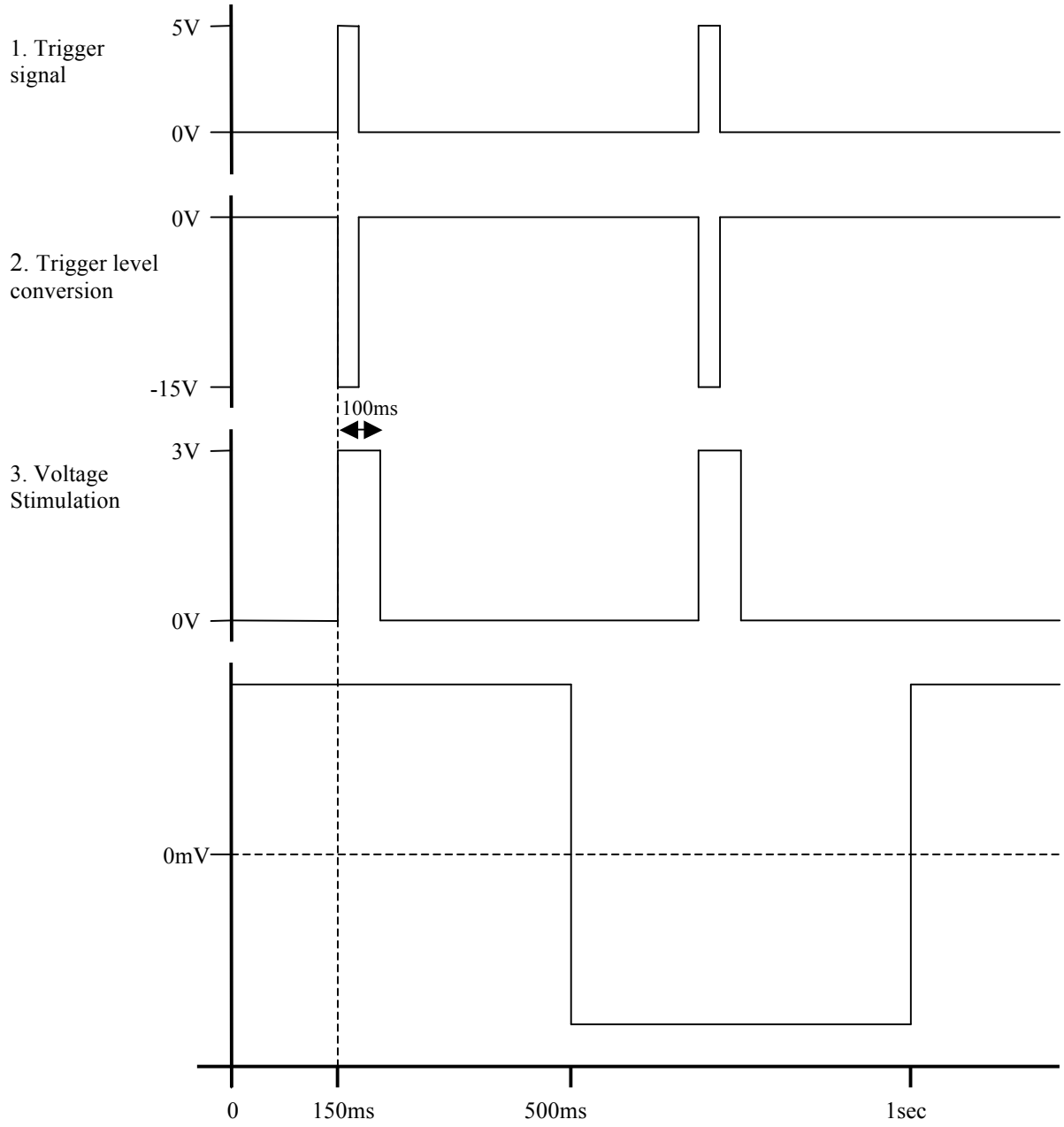

Figure A1-2: Illustration of synchronization of stimulus trigger with carrier source.

A1.2.3. Recording arrangement

A1.2.3.1 General

Each nerve was placed on 8 Ag/AgCl electrode hooks. (Figure A1-3)The stimulating electrodes (S1&S2) were 2mm apart. The ground electrode was a silver plate of 3mm by 8mm, which is 3mm from S2. The reference electrode (R2) was 7.5cm away from S2 and the recording electrode (R1) was

3mm away from the ground electrode. The recordings were hence made between R1 and the reference (R2). The current injection electrodes (D1 and D2) were between R1 and R2. For each recording the nerve was raised from the solution and dried with blotting paper. Each recording lasted one minute. Between recordings the nerve was immersed in the crab Ringer's solution.

A1.2.3.2 Variations

When testing the effect of current, D1 and D2 were always 2mm apart and D1 was 2mm from R1. 1uA, 5uA, 10uA and 20uA were injected with a 2Hz square wave through D1 and D2. For each current level, 6 alternating recordings were carried out. 3 of these were with stimulation (active) of 3volts 2Hz (supramaximal stimulation), and three without stimulation (control). Each comprised repeated averaging over one minute (n=60). This was then repeated on a second nerve. When testing the effect of changing the spacing between D1 and D2, D2 was moved so that recordings were made with D1 and D2 being 1mm, 2mm, 4mm and 8mm apart. A current of 5uA was used and R1 was again kept at 2mm from D1. The same number of recordings were made for each spacing and repeated on a second nerve. To study the effect of using different R1-D1 distances the current was kept constant (5uA) and D1-D2 was constant at 2mm. The R1-D1 distances were 2mm and 4mm. Again, for each distance, six 1 minute recordings were carried out (3 active and 3 control) and repeated on another nerve.

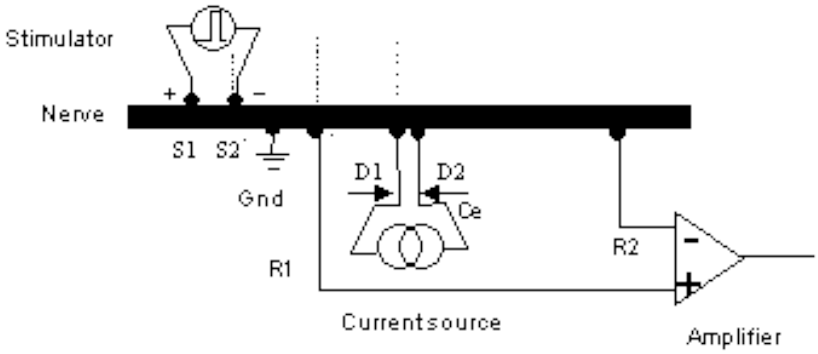

Figure A1-3: S1&S2 are the stimulating electrodes. D1&D2 are the electrodes injecting the square wave current. R1 is the recording electrode with R2 as a reference.

Whenever recordings were repeated on another nerve, the order in which these recordings were made was reversed. For example, on one nerve recordings were carried out with D1-D2 spaced at 1mm, 2mm, 4mm and 8mm in that order. Then on the second nerve the recording started with 8mm and finished with 1mm. The same was done for the effect of current and R1-D1 spacing (table A-1).

Current	D1-D2	R1-D1	Sets of Recordings
1uA	2mm	2mm	2
5uA	1mm	2mm	4
5uA	2mm	2mm	6
5uA	2mm	4mm	4
5uA	4mm	2mm	4
5uA	8mm	2mm	4
10uA	2mm	2mm	4
20uA	2mm	2mm	5

Table A1-1: Summary of experiments on Crab nerve.

A1.2.4. Analysis

For each experiment listed in table 1 above, the potential difference between R1 and R2 was measured. The following steps were then taken for the analysis.

1. The square waves were rectified and then the control wave was subtracted from the active waveform.

2. A 100ms section of each waveform, which included the trigger signal, was saved and the rest removed.

3. These sections were then averaged. The averaged waveform then analysed by eye to see if there was a drop in impedance.

There were some factors during the recording that were difficult to control or keep constant. When blotting the nerve it is difficult to remove the exact same amount of solution in each recording. This is particularly a problem with different D1-D2 distances, i.e. the narrower, the more difficult to use the blotting paper. Also the rate of nerve decay during recordings and between two different nerves is not constant. So pairs of recordings were rejected if there were inconsistencies in the resistance changes of greater than 50% when compared to recordings in close proximity on the same nerve.

4. The remaining recordings for each of the above settings (table A1-1) were averaged to produce a graph for each setting.

Unless stated anywhere results are presented as mean ± 1SD.

A1.3. Results

For each setting listed in table A1-1, there were between 2 to 6 sets of recordings, hence there were a total of 32 recordings carried out on 10 nerves.

A1.3.1 Compound action potentials (CAP)

The amplitude of the CAP ranged between 2.52 and 8.66mv (mean 5.02 ±1.49) in amplitude throughout the recordings:

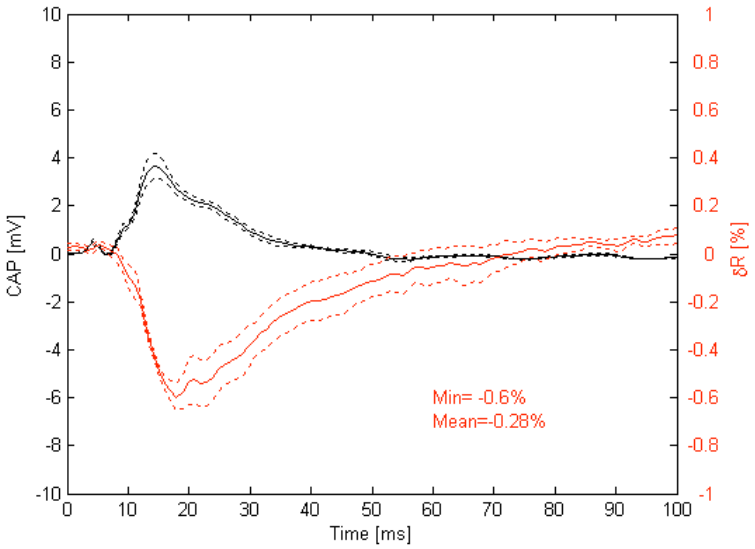

Figure A1-4: An example of a compound action potential (black) with impedance change beneath, with a current of 5uA, D1-D2 of 2mm and R1-D1 of 2mm. The dotted lines represent the maximum and minimum CAP and δZ respectively

An appropriate impedance decrease was taken to be a negative deflection in the impedance line directly beneath a compound action potential (figure A1-4).

A1.3.2. Effect of different current levels

There were impedance changes between 0.22-0.89% when using different current levels When using a current of 1uA, there was a positive deflection prior to the negative impedance change (figure A1-5), which was seen in all recordings at this level.

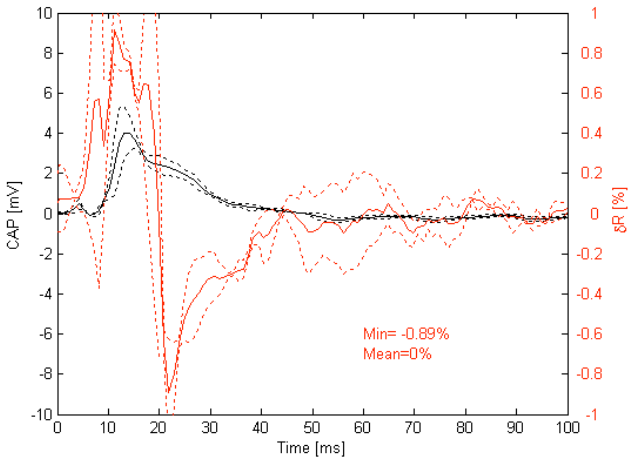

Figure A1-5: 1uA D1.D2=2mm, R1-D1=2mm.

This positive change was not present at all higher current levels. The impedance change when using 5, 10 and 20uA ranged between -0.22 and 0.6% (figure A-6). The mean impedance change was similar when using 5 and 10uA (ANOVA p=0.554), but different between 20uA, 10uA and 5uA (ANOVA p=0.001). The mean of 1uA data was excluded from the statistical analysis due to the positive change.

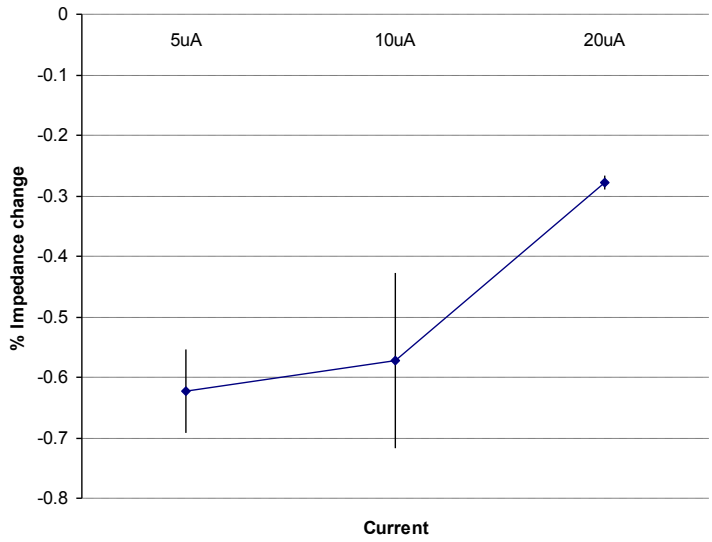

Figure A1-6: Impedance changes with 5uA, 10uA, 20uA, with SE bars.

A1.3.2. Effect of altering D1-D2 (current injection spacing)

The mean impedance change at 5uA decreased from -0.62% to -0.37% as the interval between D1 and D2 increased from 2 to 8 mm but was smaller at -0.48% at 1 mm (figure A1-7) (ANOVA p= 0.102).

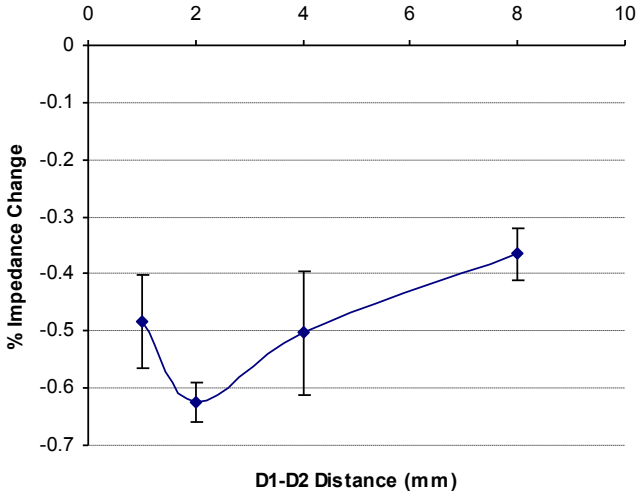

Figure:A1-7: Impedance change at different D1-D2 spacing with SE bars.

A1.3.3 Effect of Altering R1-D1

With R1-D1 at 2mm and 4mm the impedance changes were 0.62%±0.069 and 0.44% ±0.09) respectively. These differed significantly (p= 0.026, 2-tailed t-test).

A1.4. Discussion

A1.4.1. Summary of results.

Decreases in impedance were seen at all current levels, D1-D2 spacing and R1-R2 spacing, as predicted. The largest change seen was using 5uA with D1-D2 and D1-R1 both at 2mm (-0.62%). When using 1uA there was an unexpected positive apparent impedance change in the waveform. The impedance changes when using 5uA and 10uA are similar, as the cable theory predicts, but when using 20uA the change is smaller. The impedance changes are different when the spacing between the current injection electrodes were adjusted, showing a decrease in impedance change as the space was increased between 2mm and 8mm (in keeping with previous modeling), but at 1mm the impedance change was less than it was at 2mm (figure A1-7). There is a clear difference in the impedance changes with different distance of R1-D1, not in keeping with previous modeling.

A1.4.2. Technical issues.

A1.4.2.1 Blotting

Although best efforts were made to keep the conditions the same i.e, between two recordings (current, electrode distances, temperature), some factors are difficult to control. When blotting the nerve to remove solution prior to recording, the same amount of solution is not always removed. Hence, different amounts of current are shunted through the solution. The more current shunting through solution, the smaller the impedance. Therefore the impedance changes are not always consistent.

A1.4.2.2. Positive apparent impedance change with 1μA applied current

This appears to be artefactual and due to decreasing CAP over time.

With a small current of 1uA, there is a positive peak (figure A1-5) occurring before the impedance decrease. During a recording the amplitude of the CAP decreases gradually. During analysis the second wave (negative polarity) is subtracted from the first (positive polarity). Hence as the second CAP of each cycle will be smaller than the first, due to decay,

there will be an initial positive change in impedance. The lower the amplitude of the square wave, the greater this positive change is noticed. If for example there is a decrease from 6mV to 5mV (1mV) in one minute, this equates to 8uV per half second or per half square wave cycle. With 1uA the square wave amplitude will only be 2mV or 2000uV. Hence 8uV as a percentage of the square wave amplitude is:

$$8/2000 \text{ X } 100 = 0.4\%,$$

So in this case the positive change will be 0.4% which is quite comparable to the negative change.

A1.4.3. Effect of current

Cable theory predicts that the impedance change should be the same for each current level. However in this study there were differences which we shall examine. When using 5uA and 10ua the impedance changes are statistically similar as the cable theory predicts. But when using 20uA the impedance change is smaller. When injecting a current above the threshold for an action potential (i.e. when using 20uA), this will have some effect on the action potential generated by the stimulus electrodes. During the positive polarity of the square wave this current will increase the amplitude of the CAP, but in the negative polarity it will suppress it. After averaging the CAP will however appear normal (i.e. the same as before any square wave current injection). However the impedance during the negative polarity will be smaller and hence the overall impedance change after averaging and subtraction will appear smaller. This therefore suggests that with 20μA injected current, the CAP was significantly distorted.

A1.4.4. Effect of spacing

The cable theory also predicts that as the distance between current injection (D1-D2) increases, the percentage impedance change should decrease. This is because as D1-D2 increases, the resistance will also increase as the current travels further. Therefore from the equation V = IR, the amplitude of the square wave will increase as D1-D2 increases. Therefore the change in impedance will be a smaller percentage of the amplitude of the square wave.

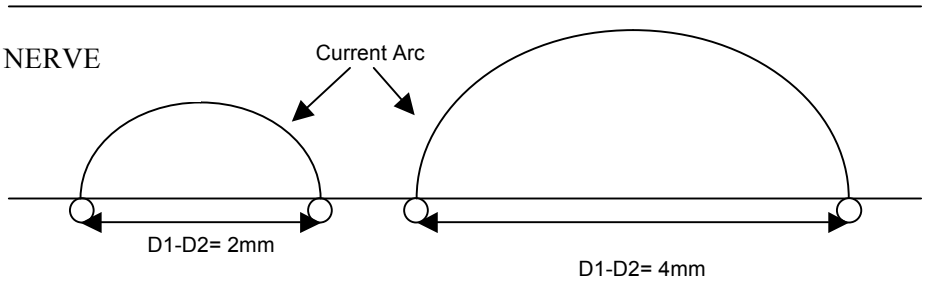

The results fitted with this prediction as the distance increased from 2mm to 8mm. However, at 1mm the impedance change was smaller than it was at 2mm. At a spacing of 1mm, blotting the nerve becomes difficult. It therefore seems probable that applied current was shunted by a film of saline so that the predicted larger impedance decrease was not observed.

Different R1-D1 spacing should not have altered the impedance change according to the cable theory because the crab nerve space constant is 0.6mm (Boone 1995). However this study revealed an average of -0.62% for R1-D1= 2mm and -0.44% for R1-D1= 4mm. This may have indicated that the space constant is longer than predicted and thus the current was altering the CAP with the lower spacing. A more plausable explanation may be due to current shunting through a saline film and difficulties in blotting.

A1.4.5. Future work.

This study has shown, that an impedance change during depolarization of an unmyelinated nerve can be measured when using a square wave current source and are broadly in-keeping with previous work. However prior to applying this method on the rat cerebral cortex further work was needed with a better acquisition system and electrode array to overcome the technical issues raised above.

References

Ahlfors, S. & Ilmoniemi, R., 1992. Magnetic Imaging of Conductivity. , 5, pp.1717–1718.

Araki, T. & Terzuolo, C.A., 1962. Membrane currents in spinal motoneurons associated with the action potential and synaptic activity. *J.Neurophysiol.*, 25, pp.772–789.

Bagshaw, A.P. et al., 2003. Electrical impedance tomography of human brain function using reconstruction algorithms based on the finite element method. *Neuroimage.*, 20(2), pp.752–764.

Baillet, S., Mosher, J.C. & Leahy, R.M., 2001. Electromagnetic brain mapping. *IEEE Signal Processing Magazine*, 18(6), pp.14–30.

Belliveau, J.W. et al., 1991. Functional mapping of the human visual cortex by magnetic resonance imaging. *Science*, 254(5032), pp.716–719.

Binnie, C.D. et al., 1995. Normal finding by modality O. JW, ed. , 1st(3.4), p.-.

Birgul, O., Eyuboglu, B.M. & Ider, Y.Z., 2003. Current constrained voltage scaled reconstruction (CCVSR) algorithm for MR-EIT and its performance with different probing current patterns. *Phys Med Biol*, 48(5), pp.653–671.

Boas, D.A., Dale, A.M. & Franceschini, M.A., 2004. Diffuse optical imaging of brain activation: approaches to optimizing image sensitivity, resolution, and accuracy. *Neuroimage.*, 23 Suppl 1, pp.S275–S288.

Bodurka, J. et al., 1999. Current-induced magnetic resonance phase imaging. *J.Magn Reson.*, 137(1), pp.265–271.

Bodurka, J. & Bandettini, P.A., 2002. Toward direct mapping of neuronal activity: MRI detection of ultraweak, transient magnetic field changes. *Magn Reson.Med.*, 47(6), pp.1052–1058.

Boone, K., Lewis, A.M. & Holder, D.S., 1994. Imaging of cortical spreading depression by EIT: implications for localization of epileptic foci. *Physiol Meas*, 15 Suppl 2, pp.A189–A198.

Boone, K.G., 1995. *The possible use of applied potential tomography for imaging action potentials in the brain*. University College London, London, UK.

Boone, K.G. & Holder, D.S., 1995a. A model of the effect of variations in contact and skin impedance on electrical impedane tomography measurement artefacts. *Innov.Tech.Biol.Med.*, 16(suppl. 2), pp.61–70.

Boone, K.G. & Holder, D.S., 1995b. Current approaches to analogue instrumentation design in electrical impedance tomography. *Physiol Meas.*, 17(4), pp.229–247.

Brown, B.H. et al., 1994. Cardiac and respiratory related electrical impedance changes in the human thorax. *IEEE Trans.Biomed.Eng*, 41(8), pp.729–734.

Brown, B.H., 2003. Electrical impedance tomography (EIT): a review. *J Med Eng Technol.*, 27(3), pp.97–108.

Brown, B.H. et al., 1999. Medical Physics and Biomedical Engineering J. G. Webster, ed. , 1st, p.-.

Bryan, K., Haugh, J. & McCune, D., 2006. Fast imaging of partially conductive linear cracks using impedance data. *Inverse problems*, 22(4), pp.1337–1358.

Cafiso, D.S. & Hubbell, W.L., 1978. Estimation of transmembrane potentials from phase equilibria of hydrophobic paramagnetic ions. *Biochemistry*, 17(1), pp.187–195.

Calder´on, A.P., 1980. On an inverse boundary value problem W. H. Meyer & M. A. Raupp, eds. , pp.65–73.

Chapman, R.A., 1966. The Repetitive Responses of Isolated Axons from the Crab, Carcinus Maenas. *Journal of Experimental Biology*, 45(3), pp.475–488. Available at: http://jeb.biologists.org/cgi/content/abstract/45/3/475.

Cheney, M.D., Isaacson, D. & Newell, J.C., 1999. Electrical Impedance Tomography. *SIAM Review*, 41(1), pp.85–101. Available at: http://epubs.siam.org/sam-bin/dbq/article/33361.

Chu, R. et al., 2004. Hunting for neuronal currents: absence of rapid MRI signal changes during visual-evoked response. *Neuroimage.*, 23(3), pp.1059–1067.

Cohen, L.B., 1968. Changes in neuron structure during action potential propagation and synaptic transmission. *Physiol Rev.*, 53(2), pp.373–418.

Cohen, L.B. & Keynes, R.D., 1973. Changes in light scattering associated with the action potential in crab nerves. *J.Physiol*, 212(1), pp.259–275.

Cole, K.S., Curtis, H.J. & Cole, S.K., 1939. Electric Impedance of the Squid Giant Axon During Activity. *The Journal of general physiology*, 22(5), pp.649–70. Available at: http://www.pubmedcentral.nih.gov/articlerender.fcgi?artid=2142006&tool=pmcentrez&rendertype=abstract.

Dale, A.M., Fischl, B. & Sereno, M.I., 2001. Cortical surface-based analysis. I. Segmentation and surface reconstruction. *Neuroimage.*, 9(2), pp.179–194.

Edwards, R.N., 1974. The magnetometeric resistivity (MMR) method and its application to the mapping of a fault. *Can.J.Earth Sci*, 11, pp.1136–1156.

Eyuboglu, B.M., Brown, B.H. & Barber, D.C., 1988. Problems of cardiac output determination from electrical impedance tomography scans. *Clin.Phys.Physiol Meas*, 9 Suppl A, pp.71–77.

Fabrizi, L. et al., 2006. A feasibility study for imaging of epileptic seizures by EIT using a realistic FEM of the head. , 14(1), pp.3733–3736.

Fabrizi, L. et al., 2007. Analysis of resting noise characteristics of three EIT systems in order to compare suitability for time difference imaging with scalp electrodes during epileptic seizures. *Physiol Meas.*, 28(7), pp.S217–S236.

Fabrizi, L. et al., 2008. Comparison of two EIT systems suitable for imaging impedance changes in epilepsy A. Hartov & E. J. Woo, eds. , pp.1–4.

Franceschini, M.A. & Boas, D.A., 2004. Noninvasive measurement of neuronal activity with near-infrared optical imaging. *Neuroimage.*, 21(1), pp.372–386.

Freeston, I.L. & Tozer, R.C., 1995. Impedance imaging using induced currents. *Physiol Meas.*, 16(3 Suppl A), pp.A257–A266.

Frerichs, I., 2000. Electrical impedance tomography (EIT) in applications related to lung and ventilation: a review of experimental and clinical activities. *Physiol Meas*, 21(2), pp.R1–21.

Frerichs, I. et al., 2002. Regional lung perfusion as determined by electrical impedance tomography in comparison with electron beam CT imaging. *IEEE Trans.Med.Imaging*, 21(6), pp.646–652.

Gencer, N.G. & Tek, M.N., 1999. Electrical conductivity imaging via contactless measurements. *IEEE Trans.Med.Imaging*, 18(7), pp.617–627.

Gibson, A.P., Bayford, R.H. & Holder, D.S., 2000. Two-dimensional finite element modelling of the neonatal head. *Physiol.Meas.*, 21(1), pp.45–52.

Gilad, O. et al., 2009. A method for recording resistance changes non-invasively during neuronal depolarization with a view to imaging brain activity with electrical impedance tomography. *Journal of neuroscience methods*, 180(1), pp.87–96. Available at: http://www.pubmedcentral.nih.gov/articlerender.fcgi?artid=2813208&tool=pmcentrez&rendertype=abstract [Accessed August 18, 2011].

Gilad, O., 2007. Preliminary studies in imaging neuronal depolarization in the brain with Electrical or Magnetic Detection Impedance Tomography. *University College London, London*.

Gilad, O. & Holder, D.S., 2009. Impedance changes recorded with scalp electrodes during visual evoked responses: Implications for Electrical Impedance Tomography of fast neural activity. *NeuroImage*, 47, pp.514–522.

Gilad, O. & Holder, D.S., 2009. Impedance changes recorded with scalp electrodes during visual evoked responses: Implications for Electrical Impedance Tomography of fast neural activity. *Neuroimage*, 47(2), pp.514–522. Available at: http://dx.doi.org/10.1016/j.neuroimage.2009.04.085.

Gratton, G. et al., 2001. Effects of measurement method, wavelength, and source-detector distance on the fast optical signal. *Neuroimage.*, 32(4), pp.1576–1590.

Grinvald, A. et al., 1992. Optical imaging of neuronal activity. *Physiol Rev.*, 68(4), pp.1285–1366.

Hagberg, G.E., Bianciardi, M. & Maraviglia, B., 2006. Challenges for detection of neuronal currents by MRI. *Magn Reson.Imaging*, 24(4), pp.483–493.

Hamalainen, M.S. et al., 1993. Magnetoencephalography-theory, instrumentation, and applications to noninvasive studies of the working human brain. *Reviews of Modern Physics*, 65(2), pp.413–497. Available at: http://link.aps.org/abstract/RMP/v65/p413.

Hamalainen, M.S., 1992. Magnetoencephalography: a tool for functional brain imaging. *Brain Topogr.*, 5(2), pp.95–102.

Hart, F.X., Berner, N.J. & McMillen, R.L., 1999. Modelling the anisotropic electrical properties of skeletal muscle. *Physics in medicine and biology*, 44, pp.413–421.

Henderson, R.P. & Webster, J.G., 1978. An impedance camera for spatially specific measurements of the thorax. *IEEE Trans.Biomed.Eng*, 25(3), pp.250–254.

Holder, D.S., 1992. Detection of cerebral ischaemia in the anaesthetised rat by impedance measurement with scalp electrodes: implications for non-invasive imaging of stroke by electrical impedance tomography. *Clin.Phys.Physiol.Meas.*, 13(1), pp.63–75.

Holder, D.S., 1987. Impedance changes during evoked nervous activity in human subjects: implications for the application of applied potential tomography (APT) to imaging neuronal discharge. *Clin.Phys.Physiol Meas.*, 10(3), pp.267–274.

Holder, D.S. & Gardner-Medwin, A.R., 1988. Some possible neurological applications of applied potential tomography. *Clin.Phys.Physiol Meas.*, 9 Suppl A, pp.111–119.

Horesh, L. et al., 2006. Multilevel preconditioning for 3D large-scale soft field medical applications modelling. *Int J Inf Syst Sci*, 2(4), pp.532–556.

Ider, Y.Z., Onart, S. & Lionheart, W.R., 2003. Uniqueness and reconstruction in magnetic resonance-electrical impedance tomography (MR-EIT). *Physiol Meas.*, 24(2), pp.591–604.

Ireland, R.H. et al., 2004. Towards magnetic detection electrical impedance tomography: data acquisition and image reconstruction of current density in phantoms and in vivo. *Physiol Meas.*, 25(3), pp.775–796.

Isaacson, D. et al., 2006. Imaging cardiac activity by the D-bar method for electrical impedance tomography. *Physiol Meas*, 27(5), pp.S43–S50.

Joy, M., Scott, G. & Henkelman, M., 1989. In vivo detection of applied electric currents by magnetic resonance imaging. *Magn Reson.Imaging*, 7(1), pp.89–94.

Joy, M.L., Lebedev, V.P. & Gati, J.S., 1999. Imaging of current density and current pathways in rabbit brain during transcranial electrostimulation. *IEEE Trans.Biomed.Eng*, 46(9), pp.1139–1149.

Jurgens, I., Rosell, J. & Riu, P.J., 1996. Electrical impedance tomography of the eye: in vitro measurements of the cornea and the lens. *Physiol Meas.*, 17 Suppl 4, pp.A187–A195.

Kamei, H. et al., 1999. Neuronal current distribution imaging using magnetic resonance. *Magnetics, IEEE Transactions on*, 35(5), pp.4109–4111.

Karbeyaz, B.U. & Gencer, N.G., Electrical conductivity imaging via contactless measurements: an experimental study. *IEEE Trans.Med.Imaging*, 22(5), pp.627–635.

Kaup, P.G., Santosa, F. & Vogelius, M., 1996. Method for imaging corrosion damage in thin plates from electrostatic data. *Inverse problems*, 12(3), pp.279–293.

Kilner, J.M. et al., 2004. Comparison of phase and magnitude of the MR signal in measuring neuronal activity. , p.TH299–.

Kim, S.G. & Ogawa, S., 2002. Insights into new techniques for high resolution functional MRI. *Curr.Opin.Neurobiol.*, 12(5), pp.607–615.

Konig, M., 2003. Brain perfusion CT in acute stroke: current status. *Eur.J.Radiol.*, 45 Suppl 1, pp.S11–S22.

Konn, D. et al., 2004. Initial attempts at directly detecting alpha wave activity in the brain using MRI. *Magn Reson.Imaging*, 22(10), pp.1413–1427.

Koretsky, A.P., 2004. New Developments in Magnetic Resonance Imaging of the Brain. *Neurorx.*, 1(1), pp.155–164.

Levy, S., Adam, D. & Bresler, Y., 2002. Electromagnetic impedance tomography (EMIT): a new method for impedance imaging. *IEEE Trans.Med Imaging*, 21(6), pp.676–687.

Lin, F.H. et al., 2006. Dynamic magnetic resonance inverse imaging of human brain function. *Magn Reson.Med*, 56(4), pp.787–802.

Liston, A.D., 2004. Models and Image Reconstruction in Electrical Impedance Tomography of Human Brain Function. , p.-.

Liston, A.D., Bayford, R. & Holder, D.S., 2012. A cable theory based biophysical model of resistance change in crab peripheral nerve and human cerebral cortex during neuronal depolarisation: implications for electrical impedance tomography of fast neural activity in the brain. *Med Biol Eng Comput.*, 50(5), pp.425–437. Available at: http://dblp.uni-trier.de/db/journals/mbec/mbec50.html#ListonBH12.

Low, K.A. et al., 2006. Fast optical imaging of frontal cortex during active and passive oddball tasks. *Psychophysiology*, 43(2), pp.127–136.

Lux, H.D., Heinemann, U. & Dietzel, I., 1986. Ionic changes and alterations in the size of the extracellular space during epileptic activity. *Adv.Neurol.*, 44, pp.619–639.

Malonek, D. et al., 1997. Vascular imprints of neuronal activity: relationships between the dynamics of cortical blood flow, oxygenation, and volume changes following sensory stimulation. *Proc.Natl.Acad.Sci U.S.A*, 94(26), pp.14826–14831.

McArdle, F.J. et al., 1988. The effect of the skull of low-birthweight neonates on applied potential tomography imaging of centralised resistivity changes. *Clin.Phys Physiol Meas.*, 9 Suppl A, pp.55–60.

McEwan, A. et al., 2006. Design and calibration of a compact multi-frequency EIT system for acute stroke imaging. *Physiol Meas*, 27(5), pp.S199–S210.

Mehta, A.D. et al., 2004. Fiber optic in vivo imaging in the mammalian nervous system. *Curr.Opin.Neurobiol.*, 14(5), pp.617–628.

Merwa, R. et al., 2004. Detection of brain oedema using magnetic induction tomography: a feasibility study of the likely sensitivity and detectability. *Physiol Meas.*, 25(1), pp.347–354.

Metherall, P. et al., 1996. Three-dimensional electrical impedance tomography. *Nature*, 380(6574), pp.509–512.

Michel, C.M. et al., 2004. EEG source imaging. *Clin.Neurophysiol.*, 115(10), pp.2195–2222.

Mueller, J.L., Isaacson, D. & Newell, J.C., 1999. A reconstruction algorithm for electrical impedance tomography data collected on rectangular electrode arrays. *IEEE Trans.Biomed.Eng*, 46(11), pp.1379–1386.

Mueller, J.L., Isaacson, D. & Newell, J.C., 2001. Reconstruction of conductivity changes due to ventilation and perfusion from EIT data collected on a rectangular electrode array. *Physiol.Meas.*, 22(1), pp.97–106.

Newell, J.C. et al., 1996. Assessment of acute pulmonary edema in dogs by electrical impedance imaging. *IEEE Trans.Biomed.Eng*, 43(2), pp.133–138.

Obrig, H. & Villringer, A., 2003. Beyond the visible--imaging the human brain with light. *J.Cereb.Blood Flow Metab*, 23(1), pp.1–18.

Oh, T. et al., 2011. A novel method for recording neuronal depolarization with recording at 125-825 Hz: implications for imaging fast neural activity in the brain with electrical impedance tomography. *Medical & biological engineering & computing*, 49(5), pp.593–604. Available at: http://www.ncbi.nlm.nih.gov/pubmed/21448692 [Accessed August 31, 2011].

Oh, T.I., Woo, E.J. & Holder, D., 2007. Multi-frequency EIT system with radially symmetric architecture: KHU Mark1. *Physiol Meas.*, 28(7), pp.S183–S196.

Ozparlak, L. & Ider, Y.Z., 2005. Induced current magnetic resonance-electrical impedance tomography. *Physiol Meas.*, 26(2), pp.S289–S305.

Packham, B.C., 2013. *Imaging fast neural activity in the brain with Electrical Impedance Tomography*. University College London.

Parkes, L.M. et al., 2006. Inability to directly detect magnetic field changes associated with neuronal activity. *Magn Reson.Med*, 57(2), pp.411–416.

Petersen, R.S. & Diamond, M.E., 2000. Spatial-temporal distribution of whisker-evoked activity in rat somatosensory cortex and the coding of stimulus location. *The Journal of neuroscience : the official journal of the Society for Neuroscience*, 20, pp.6135–6143.

Pethig, R., 1984. Phantoms for hyperthermia and impedance tomography. *Phys Med Biol*, 36(12), pp.1559–1563.

Polydorides, N. & Lionheart, W.R., 2002. A Matlab toolkit for three-dimensional electrical impedance tomography: a contribution to the Electrical Impedance and Diffuse Optical Reconstruction Software project. *Meas Sci Technol*, 13(12), pp.1871–1873.

Robinson, R.O. et al., 1999. Positron emission tomography and the central nervous system. *Arch.Dis.Child*, 81(3), pp.263–270.

Romsauerova, A., McEwan, A., Horesh, L., et al., 2006. Multi-frequency electrical impedance tomography (EIT) of the adult human head: initial findings in brain tumours, arteriovenous malformations and chronic stroke, development of an analysis method and calibration. *Physiol Meas*, 27(5), pp.S147–S161.

Romsauerova, A., McEwan, A. & Holder, D.S., 2006. Identification of a suitable current waveform for acute stroke imaging. *Physiol Meas.*, 27(5), pp.S211–S219.

Rosell-Ferrer, J. et al., 2006. A multifrequency magnetic induction tomography system using planar gradiometers: data collection and calibration. *Physiol Meas.*, 27(5), pp.S271–S280.

Schuettler, M. et al., 2008. A Flexible 29 Channel Epicortical Electrode Array. , p.-.

Seidemann, E. et al., 2002. Dynamics of depolarization and hyperpolarization in the frontal cortex and saccade goal. *Science*, 295(5556), pp.862–865.

Shanes, A.M., 1949. Electrical phenomena in nerve; crab nerve. *J Gen.Physiol*, 33(1), pp.75–102.

Shoham, D. et al., 1999. Imaging cortical dynamics at high spatial and temporal resolution with novel blue voltage-sensitive dyes. *Neuron*, 24(4), pp.791–802.

Smallwood, R.H., Mangnall, Y.F. & Leathard, A.D., 1994. Transport of gastric contents. *Physiol Meas*, 15 Suppl 2, pp.A175–A188.

Soni, N.K. et al., 2004. Multi-frequency electrical impedance tomography of the breast: new clinical results. *Physiol.Meas.*, 25(1), pp.301–314.

Soulsby, C.T. et al., 2006. Measurements of gastric emptying during continuous nasogastric infusion of liquid feed: electric impedance tomography versus gamma scintigraphy. *Clin.Nutr.*, 25(4), pp.671–680.

Steinbrink, J. et al., 2005. The fast optical signal--robust or elusive when non-invasively measured in the human adult? *Neuroimage.*, 26(4), pp.996–1008.

Stepnoski, R.A. et al., 1991. Noninvasive detection of changes in membrane potential in cultured neurons by light scattering. *Proc.Natl.Acad.Sci.U.S.A*, 88(21), pp.9382–9386.

Sun, J.J., Yang, J.W. & Shyu, B.C., 2006. Current source density analysis of laser heat-evoked intra-cortical field potentials in the primary somatosensory cortex of rats. *Neuroscience*, 140, pp.1321–1336.

Syre, F. et al., 2003. Are VEP correlated fast optical signals detectable in the human adult by non-invasive nearinfrared spectroscopy (NIRS)? *Adv.Exp.Med.Biol.*, 530, pp.421–431.

Taylor, R.E., 1963. Cable Theory. *Physical Review E - Statistical, Nonlinear and Soft Matter Physics*, 79, pp.219–262. Available at: http://www.ncbi.nlm.nih.gov/pubmed/19518253.

Tidswell, A.T. et al., 2001. Three-dimensional electrical impedance tomography of human brain activity. *Neuroimage.*, 13(2), pp.283–294.

Tozer, J.C. et al., 1999. Magnetic impedance tomography. *Ann.N.Y.Acad.Sci.*, 873, pp.353–359.

Williams, R.A. & Beck, M.S., 1995. Process Tomography, principles, techniques and applications R. A. Williams & M. S. Beck, eds. , p.-.

Wilson, A.J. et al., 2001. Mk3.5: a modular, multi-frequency successor to the Mk3a EIS/EIT system. *Physiol.Meas.*, 22(1), pp.49–54.

Wolf, M. et al., 2002. Functional frequency-domain near-infrared spectroscopy detects fast neuronal signal in the motor cortex. *Neuroimage.*, 17(4), pp.1868–1875.

Xiong, J., Fox, P.T. & Gao, J.H., 2003. Directly mapping magnetic field effects of neuronal activity by magnetic resonance imaging. *Hum.Brain Mapp.*, 20(1), pp.41–49.

Yerworth, R.J. et al., 2002. Design and performance of the UCLH mark 1b 64 channel electrical impedance tomography (EIT) system, optimized for imaging brain function. *Physiol Meas.*, 23(1), pp.149–158.

Zlochiver, S. et al., 2004. Induced current electrical impedance tomography system: experimental results and numerical simulations. *Physiol Meas.*, 25(1), pp.239–255.